Spring 2011

Numerical modeling of biomass combustion in a stoker boiler

Xinhui Zhang
University of Iowa

NUMERICAL MODELING OF BIOMASS COMBUSTION IN A STOKER BOILER

by

Xinhui Zhang

An Abstract

Of a thesis submitted in partial fulfillment
of the requirements for the Doctor of
Philosophy degree in Mechanical Engineering
in the Graduate College of
The University of Iowa

May 2012

Thesis Supervisor: Associate Professor Albert Ratner

ABSTRACT

Biomass fuel is considered a promising substitute for traditional fossil fuels. Amid a great variety of methods for converting the energy in biomass fuel into usable energy, direct combustion is still the dominant technology employed by industry. Because biomass fuel possess a much wider range of physical and chemical properties than fossil fuel, its combustion behavior is similarly diverse (and typically differs from fossil fuel), with a similar range seen in emissions characteristics. To address the variability the fuel stream imposes on the system, this work endeavors to use numerical modeling to investigate biomass combustion in a stoker boiler to provide physically insightful details while requiring minimal time and effort relative to the traditional experimental approach.

In the first part of this work, a comprehensive model was developed to investigate the co-firing of different kinds of biomass including oat hulls, wood chips and natural gas with coal in a stoker boiler located in the Power Plant of the University of Iowa. Later, this model is employed in the optimization of the air supply system and plans for efficiently injecting light weight biomass, such as oat hulls, into the stoker boiler. The other key problem is in NO_x prediction and reduction for the stoker boiler. This was by combining a standard CFD model describing the turbulent dynamics and combustion with several sub-models specifically developed for this study to model the fuel bed, fuel particle movement, and fuel gasification. To verify and baseline these sub-models, a series of experiments are performed, including a temperature measurement campaign for coal combustion in the boiler, a chemical lab analysis of oat hull chemical characteristics, an experiment measuring oat hull particles' physical properties, and a high-heating-rate gasification test of oat hulls. In particular, the stoker boiler temperature measurements are unique in the number of points measured and the range of firing conditions.

The simulation showed that for the co-firing of oat hulls with coal, the flame temperature decreased with increasing oat hull fraction. The oat hull particles follow the

flow and burn in suspension due to their light weight. The simulation showed that increasing injection velocity could slightly reduce the peak temperature and thereby reduce NO_x levels. It was also observed that there is a critical velocity above which the trend of decreasing CO_2 is reversed.

The co-firing of other types of biomass such as wood chips and natural gas in the stoker boiler were also studied. The result of co-firing wood chips shows that adding wood chips decreases the flame. The flame zone is also shortened when compared to pure coal, primarily resulting from a higher oxygen environment above the coal bed due to the high oxygen content of the wood chips. Co-firing natural gas with coal resulted in the high temperature zone shifting from the back wall closer to the front wall, significantly reducing the overall flame length.

The level of predicted NO_x agreed very well with the experimental data. The simulations showed that injecting Urea with the secondary air system on the front wall can greatly reduce the NO_x level inside the boiler for minimal cost and effort.

Abstract Approved: _____
Thesis Supervisor

_____
Title and Department

_____
Date

NUMERICAL MODELING OF BIOMASS COMBUSTION IN A STOKER BOILER

by

Xinhui Zhang

A thesis submitted in partial fulfillment
of the requirements for the Doctor of
Philosophy degree in Mechanical Engineering
in the Graduate College of
The University of Iowa

May 2012

Thesis Supervisor: Associate Professor Albert Ratner

Graduate College
The University of Iowa
Iowa City, Iowa

CERTIFICATE OF APPROVAL

PH.D. THESIS

This is to certify that the Ph.D. thesis of

Xinhui Zhang

has been approved by the Examining Committee
for the thesis requirement for the Doctor of Philosophy degree
in Mechanical Engineering at the May 2012 graduation.

Thesis Committee: _____
Albert Ratner, Thesis Supervisor

_____
James H.J. Buchholz

_____
P. Barry Butler

_____
George S. Constantinescu

_____
H.S. Udaykumar

To my family

ACKNOWLEDGMENTS

This dissertation would not have been possible without the guidance, support and cooperation of several individuals who in one way or another contributed and extended their valuable assistance in the preparation and completion of this study.

First and foremost, my utmost gratitude to my advisor, Professor Albert Ratner, whose inspirational guidance, great patience and cheerful encouragement supported me through this process and propelled me to finish this work.

A lot of my gratitude goes to Ferman Milster, Associate Director of Utilities at the University of Iowa, for the financial support which makes this work possible. I am very grateful to Joseph Schwarzhoff, Power Plant Engineer at the University of Iowa Power Plant, for his invaluable technical support. I am also grateful to Richard Webb, Senior District Engineer at Babcock Power, whose help was instrumental in the temperature measurement campaign.

I would like to thank many of my colleagues: Mohsen Ghamari, for sharing with me lots of his experience, former student Dr. Yun Huang, and senior students Yan Zhang and Majid Emadi for their encouragement and support.

Finally, I am deeply indebted to my parents: my father Dashan Zhang and mother Lihua Yang, whose unconditional love gives me the possibility and strength to pursue my dream of education. I also feel truly grateful for having my husband Feilong Liu and our son Jiahang Liu for sharing with me all the moments of life during my studies.

ABSTRACT

Biomass fuel is considered a promising substitute for traditional fossil fuels. Amid a great variety of methods for converting the energy in biomass fuel into usable energy, direct combustion is still the dominant technology employed by industry. Because biomass fuel possess a much wider range of physical and chemical properties than fossil fuel, its combustion behavior is similarly diverse (and typically differs from fossil fuel), with a similar range seen in emissions characteristics. To address the variability the fuel stream imposes on the system, this work endeavors to use numerical modeling to investigate biomass combustion in a stoker boiler to provide physically insightful details while requiring minimal time and effort relative to the traditional experimental approach.

In the first part of this work, a comprehensive model was developed to investigate the co-firing of different kinds of biomass including oat hulls, wood chips and natural gas with coal in a stoker boiler located in the Power Plant of the University of Iowa. Later, this model is employed in the optimization of the air supply system and plans for efficiently injecting light weight biomass, such as oat hulls, into the stoker boiler. The other key problem is in NO_x prediction and reduction for the stoker boiler. This was by combining a standard CFD model describing the turbulent dynamics and combustion with several sub-models specifically developed for this study to model the fuel bed, fuel particle movement, and fuel gasification. To verify and baseline these sub-models, a series of experiments are performed, including a temperature measurement campaign for coal combustion in the boiler, a chemical lab analysis of oat hull chemical characteristics, an experiment measuring oat hull particles' physical properties, and a high-heating-rate gasification test of oat hulls. In particular, the stoker boiler temperature measurements are unique in the number of points measured and the range of firing conditions.

The simulation showed that for the co-firing of oat hulls with coal, the flame temperature decreased with increasing oat hull fraction. The oat hull particles follow the

flow and burn in suspension due to their light weight. The simulation showed that increasing injection velocity could slightly reduce the peak temperature and thereby reduce NO_x levels. It was also observed that there is a critical velocity above which the trend of decreasing CO_2 is reversed.

The co-firing of other types of biomass such as wood chips and natural gas in the stoker boiler were also studied. The result of co-firing wood chips shows that adding wood chips decreases the flame. The flame zone is also shortened when compared to pure coal, primarily resulting from a higher oxygen environment above the coal bed due to the high oxygen content of the wood chips. Co-firing natural gas with coal resulted in the high temperature zone shifting from the back wall closer to the front wall, significantly reducing the overall flame length.

The level of predicted NO_x agreed very well with the experimental data. The simulations showed that injecting Urea with the secondary air system on the front wall can greatly reduce the NO_x level inside the boiler for minimal cost and effort.

TABLE OF CONTENTS

LIST OF TABLES

LIST OF FIGURES

CHAPTER 1: INTRODUCTIONS

1.1 Motivations

Expanding the use of renewable energy is a primary means of mitigating the impending energy crisis and is a way to achieve sustainable development throughout the world. As could be expected, resulting world-wide competition to develop enabling technologies has become intense. Biomass energy is a significant portion of the renewable energy employed today. Among the existing technologies for utilizing biomass energy, the most common method is direct combustion of biomass fuel in operating industrial furnaces and boilers.

Though the history of combustion technology is as long as that of civilization, the knowledge base to describe biomass combustion and that of the detailed thermal, chemical, and fluid-mechanical mechanisms is far from sufficient. This gap is primarily caused by the technical difficulties in acquiring relevant data due to the inherent features of biomass fuels' physical and chemical properties. Biomass fuel is composed of three primary components: cellulose, hemicellulose and lignin. It has a lower heating value than traditional fossil fuels (coal), typically due to a higher concentration of volatile material and lower carbon content. These differences of chemical content and physical structures significantly influence biomass's combustion behavior. In addition, biomass also comes in broader distributions of sizes and shapes, raising the hurdle for combustion facilities which were originally designed for fuel with relatively uniform properties. For these reasons and others, knowledge of biomass's combustion performance, pollutant emission, as well as coking and fouling is still quite limited.

To better understand biomass combustion and to find ways to convert biomass to energy in a thermally efficient and environmentally friendly way is the primary goal for engineers working in this area. Biomass combustion research developed significantly in

the past two decades. Though experiments were at first considered the primary method of study, it was soon realized that experiments are economically costly, time consuming and technically challenging, all the while interfering with the normal operation of a power plant. Subsequently, pilot facilities at a lab scale were widely adopted, partly solving these problems. Unfortunately, this still results in a compromise between a lab model and a full scale boiler, with simplifications and modified geometry and possibly different physics. Moreover, data collected on those facilities can only be regarded as finitely useful, due to the lack of detailed information describing the combustion process including air mixing, gaseous reactions, surface combustion, and paths of particles. Against this back drop of impending demand and inherent difficulties, numerical modeling of biomass combustion has emerged, serving as an efficient tool to bridge the gap. These models can depict the combustion phenomenon inside a boiler, predict flue gas emissions, and provide valuable information on design optimization in a cost and time efficient manner. Following the significant advances in computer technology, numerical modeling has been widely applied to simulate a broad range of facilities.

CFD models of biomass combustion have been developed on the basis of existing numerical models of coal combustion. They are commonly used to investigate biomass combustion in full scale boilers, which entails construction of a comprehensive model. This model should consist of a proper turbulent combustion model, an accurate model predicting particles' movements and reactions, and appropriately simplified sub models describing more complicated components of the combustion system. There have been some examples of CFD modeling of biomass combustion on different boilers in the literature, such as fluidized-bed and fixed-bed boilers. Though some results have successfully described the combustion of woody type of biomass, a well validated comprehensive numerical model with some efficient simplified sub-models is still needed to model biomass combustion in full scale boilers. Especially, for light weight biomass, its

combustion behavior, particle movement and optimizing design is important and rarely studied.

It is evident that stoker boilers are the most common choice of boiler for biomass combustion due to its advantages of geometric simplicity and broad tolerance of fuel types: biomass fuel with either high or medium density can be directly combusted on the coal bed. As for those with a low density, those can be blown into the furnace through a separate injecting system. Since these biomass fuels possess vastly different properties, it is critical to understand the different combustion behavior and to find an optimized system design for each one. As an example of the differences, woody biomass burns primarily on the fixed coal bed while light weight biomass follows a pattern similar to that of pulverized coal, though with a bigger diameter and irregular shape

Considering the wide range of issues related to biomass combustion in a stoker boiler, multi-scale modeling has been recognized as an efficient approach which describes these problems using different time scales (including the scales of fluid motion, chemical reaction, and particle movement). The assumption that particle's aerodynamic response time scale is the smallest time scale which is employed for heavier, denser biomass is not necessarily valid when the particles' Reynolds number and volume fraction inside the boiler are quite small, where consideration of the time scale of particle collisions is necessary and the dominating forces on the particles will be expanded to include normal and shear effects among particles, as well as the local torque, which influence the combustion behavior in the boiler.

1.2 Objectives

Propelled by the motivation described above, a comprehensive model describing biomass combustion in a stoker boiler is developed in this work. This work embraces two primary goals. The first one is investigating the co-fired combustion of different types of

biomass including oat hulls, wood chips and natural gas using a comprehensive model which is base-lined by empirical results from combustion, property, and gasification tests for these biomass fuels. More emphasis is given to the simulation of oat hulls since this work is the first one studying the combustion of this type of biomass. Driven by this goal, this work focuses on the following six objectives:

The first objective is to develop a comprehensive model for simulating the co-firing of oat hulls, wood chips and natural gas with coal in a stoker boiler. Because commercial software has been widely accepted as a tool to model biomass combustion, with a broad range of choices for turbulent combustion models and an implanted discrete phase model, a combined Lagrangian-Eulerian model implemented in Fluent was selected as the basis for this study. For this work, this model is validated by the results obtained through temperature measurements conducted on the full scale coal stoker boiler.

The second objective is to develop sub-models accurate enough to predict the movements and gasification of oat hulls. This goal is fulfilled by adjusting the CFD model parameters and adding functions derived from empirical data taking into consideration of the non-spherical and irregular in shape of oat hull particles and their unique chemical properties. Then, how oat hulls release volatiles and combust inside the boiler is analyzed. The effect of co-firing oat hulls on the flame temperature and species concentration will also be studied since these are important parameters in NO_x production (and understanding them is critical for reducing NO_x) and achieving high efficiency.

Since light weight biomass tends to follow the flow pattern, the air flow pattern inside the boiler is expected to be a dominating aspect for combustion performance. Hence, the third objective is to use the numerical model to optimize air injection in order to reduce the oxygen depletion zone inside the boiler and to enhance the turbulent mixing, and with it, the combustion efficiency by finding an optimized injection velocity. The relationship between the increased injection velocity of oat hulls and its peak temperature are also need.

Finally injecting oat hulls with increased number of nozzles are also very important since it is assumed to be able to enhanced the combustion and turbulent mixing inside the boiler

The fourth objective is to apply this fully developed comprehensive model to studying co-firing wood chips with coal. The expanded application of this numerical model can explore the changes of combustion behaviors inside the boiler and optimize the operations of the boiler. The relationships between flame temperature and wood chip fraction will be studied. The new patterns on air mixing for co-firing wood chips with coal are also needed. The fifth objective is to investigate the effect of co-firing natural gas with coal in the boiler, which is considered as an efficient way to reduce the pollutant gases emissions and to enhance the performance to the combustion. This comprehensive model will investigate the influence of co-firing natural on the turbulence and combustion mixing and on flue gas. The gas temperature at the exit will be checked at different co-firing rate of natural gas. The changes of location of high temperature zone can be the emphasis of future system optimization.

Because a relatively high emission of NO_x is a long existing problem on stoker boilers, the sixth objective of this work is to investigate NO_x concentrations in the stoker boiler and then to study methods of reducing NO_x concentrations by injecting Urea into the system. The numerical model can then predict NO_x levels for the boiler and provide the fundamental design information on utilizing Urea optimally.

The second research goal of this work is depicting biomass particle's movement by considering the collision forces on particles. This will enable a more accurate prediction of the particles' movements and hence their combustion behaviors. Driven by this goal, particle interaction theory is used to model the dynamics and combustion of the particles. This part of the work is developed through a FORTRAN code developed in the lab because of the lack of technical support in commercial software, and is carried out in two ways. The first one is to investigate the condition of cold flow inside the boiler by focusing on exploring the dynamics of the particles. The second is to analyze the effect of micro-scale

forces on the oat hull particle's movement and combustion. Due to the high cost of computation, the computational domain is further simplified in this case. The locations of particle interactions will be examined along the injecting direction. And the situation of considering particle forces will be discussed.

1.3 Organization

Chapter 1 introduces the work and the arrangement of the thesis. Research background and literature review can be found in chapter 2. Specifically, part one of chapter 2 is examines biomass properties while part two introduces the current progress in numerical modeling of biomass combustion. Chapter 3 presents the theories and equations used in this work. Chapter 4 introduces the experiments conducted to validate the CFD model and to generate a simplified particle model. The results of the comprehensive model developed in Fluent are presented in chapter 5, where the effect of co-firing oat hulls with coal, model validation, and optimization of the air flow system are all discussed. Chapter 6 includes the applications of the comprehensive model in different research areas of systematic designs including co-firing wood chips with coal in the grate boiler, co-firing natural gas with coal, base-lining the NO_x sub-model and investigating its reduction by Urea injection and in the boiler. The micro-scale study of particle movement and combustion are presented in chapter 7. The effect of particles' interactions on particle's movement and combustion are explored. Its comparison with some experimental data and prediction made by Fluent are also covered. The final chapter 8 concludes the thesis, presents all the important results and highlights their significances. It also discusses future research directions enabled by the work and talks about the opportunities for improving the numerical model.

CHAPTER 2: LITERATURE REVIEW

2.1 Biomass Combustion: The Solution

Renewable energy, together with fossil energy and fissile energy are the main energy sources on the earth. Although fossil energy sources (petroleum, coal, natural gas, bitumens, oil shales, and tar sands) still hold a dominating role in supplying over 80% of world's total energy, its availability is finite [1]. Fossil fuels also produce high quantities of greenhouse gas and pollutants. Against this backdrop of increasing energy use and a pending environmental crisis, the utilization of renewable energy is becoming more and more attractive. Despite comparatively low energy density and more requirements on technology, renewable energy has been widely recognized for its great potential for sustainability, low emissions, and low cost. For those reasons, it is regarded as one of the primary solution to the energy crisis.

Renewable energy exists in varies forms including biomass, solar, wind, geothermal, and hydro-power. It provides 14% of the total world energy demand [1]. Table 2.1, by the European Renewable Energy Council (EREC) [1], shows a global renewable energy scenario for 2040, claiming that by then nearly half of the global energy supply will come from renewable energy.

This table also shows the status of biomass among these renewable energy sources that it provided nearly 70% of the total renewable energy in 2010. This data also shows that biomass is ranked fourth as a world-wide energy source in the world. Biomass use in the USA accounts for 4% of total energy consumption [2]. In developing countries, this number increases to as high as 35% [2]. Biomass includes organic matter produced during the photosynthesis process in which green plants convert sunlight into plant material. It normally refers to all land- and water-based vegetation like wood, short rotation woody

crops, agricultural wastes, short-rotation herbaceous species, wood wastes, bagasse and all animal wastes.

Table 2.1 Global renewable energy scenario by 2040

	2001	2010	2020	2030	2040
Total consumption (Million ton oil equivalent)	10,038	10,549	11,425	12,352	13,310
Biomass	1,080	1,313	1,791	2,483	3,271
Large hydro	22.7	266	309	341	358
Geothermal	43.2	86	186	333	493
Small hydro	9.5	19	49	106	189
Wind	4.7	44	266	542	688
Solar thermal	4.1	15	66	244	480
Photovoltaic	0.2	2	24	221	784
Solar thermal electricity	0.1	0.4	3	16	68
Marine (tidal/wave/ocean)	0.05	0.1	0.4	3	20
Total renewable energy sources	1,365.5	1,745.5	2,694.4	4,289	6,351
Renewable energy contribution (%) sources	13.6	16.6	23.6	34.7	47.7

Due to its formation, biomass has a unique property in that it is neutral for carbon monoxide production, which means no additional emission of greenhouse gases involved during biomass combustion. Moreover, the content of sulfur and nitrogen in a large number

of biomass fuels is lower than fossil fuels, which can further decrease pollution which results in acid rain. These virtues make biomass fuel an attractive substitute for fossil fuels.

These various types of biomass possess significantly different forms, structures and properties, which results in a wide range of conversion technologies. These conversion processes include physical, chemical and biological conversion [3], through which biomass is converted into liquid, solid or gaseous fuels. Currently, the main technologies of biomass conversion include the following [4]:

1. Destructive carbonization of woody biomass to charcoal
2. Gasification of biomass to gaseous products
3. Pyrolysis of biomass and solid wastes to liquid, solid and gaseous products
4. Supercritical fluid extractions of biomass to liquid products
5. Liquefaction of biomass to liquid products
6. Hydrolysis of biomass to sugars and ethanol
7. Aneorobic digestion of biomass to gaseous products
8. Biomass power for generating electricity by direct combustion or gasification
9. Co-firing of biomass with coal
10. Biological conversion of biomass and waste (biogas production, wastewater treatment)
11. Biomass densification (briquetting, pelleting)
12. Domestic cook stoves and heating appliances of fuel wood
13. Biomass energy conservation in households and industry
14. Solar photovoltaic and biomass based rural electrification
15. Conversion of biomass to pyrolytic oil (biofuel) for vehicle fuel
16. Conversion of biomass to methanol and ethanol for internal combustion engines

Those technologies vary in the degree of complexity. Direct combustion of biomass is still the most convenient and economical way to utilize biomass energy. It is responsible for over 97% of the world's bio-energy production [3].

2.2 Biomass Fuels: New Properties

The development of biomass combustion technologies is principally focused on understanding the characteristics of biomass as a fuel and using it to design combustion facilities. Though having great advantage in environmental performance, biomass fuels have a wide range of different physical and chemical properties, particularly when compared with traditional fossil fuels

Table 2.2 Physical, chemical and fuel properties of biomass and coal fuels

Property	Biomass	Coal
Fuel density (kg/m3)	500	1300
Particle size (mm)	3	100
C content (wt% of dry fuel)	42–54	65–85
O content (wt% of dry fuel)	35–45	2–15
S content (wt% of dry fuel)	Max 0.5	0.5–7.5
SiO2 content (wt% of dry ash)	23–49	40–60
K2O content (wt% of dry ash)	4–48	2–6
Al2O3 content (wt% of dry ash)	2.4–9.5	15–25
Fe2O3 content (wt% of dry ash)	1.5–8.5	8–18
Ignation temperature (K)	418–426	490–595
Dry heating value (MJ/kg)	14–21	23–28

Biomass fuel generally has lower carbon content, but higher oxygen content, which means a lower heat value. In addition, biomass has a higher moisture fraction and lower density than traditional fuels. Table 2.2 [3] is a general comparison of physical, chemical and other properties for biomass and coal fuels. It shows a significant difference which will result in different combustion, deposition and emission behaviors. Those differences are discussed in more specific details in the following sections.

2.2.1 Physical Properties

Physical properties determine the suitability of biomass fuel and the type of combustion facilities employed. During the combustion process, the density, size and fracture of fuel particles will determine particle's movement and residence time inside the boiler. A poorly designed system can reduce combustion efficiency, lead to insufficient burnout and increase the number of particle in the flue gas. Biomass is composed of three main components, cellulose, hemicellulose and lignin [4], and a number of minor components, including lipids, proteins, simple sugar, starches, water and ash [5].

Cellulose is a glucose polymer, consisting of linear chains of (1,4)-D-glucopyranose units, with an average molecular weight of around 100,000. Hemicellulose is a mixture of polysaccharides, composed almost entirely of sugars, with an average molecular weight of less than 30,000. Lignin can be regarded as a group of amorphous, high molecular-weight, chemically related compounds [6]. The fractions of each class of component vary depending on species, type of plant tissue, stage of growth, and growing conditions.

The relative proportions of cellulose and lignin is one of the determining factors in identifying the suitability of plant species for subsequent processing as energy crops. Among them, cellulose is generally the largest fraction, representing about 40–50% of the biomass by weight. The second major portion is hemicellulose, representing 20–40% of

the material by weight [6]. Table 2.3 [7] is a structural analyses of some typical biomass fuels. It shows that for light weight biomass fuel such as wheat straw and olive husks, their content of cellulose is significantly lower than in heavy weight biomass fuel such as wood. More information of other physical properties is available in the literature [8-19].

Table 2.3 Structural analyses of selected biomass samples (wt. % daf)

Fuel sample	Hemicelluloses	Cellulose	Lignin	Extractive matter
Hazelnut shell	30.4	26.8	42.9	3.3
Wheat straw	39.4	28.8	18.6	
Olive husk	23.6	24.0	48.4	9.4
Beech wood	31.2	45.3	21.9	1.6
Spruce wood	20.7	49.8	27.0	2.5
Corncob	31.0	50.5	15.0	3.5
Tea waste	19.9	30.2	40.0	9.9
Walnut shell	22.7	25.6	52.3	2.8
Almond shell	28.9	50.7	20.4	2.5
Sunflower shell	34.6	48.4	17.0	2.7

2.2.2 Chemical Properties

Table 2.4 and Table 2.5 are the proximate and ultimate analysis of some typical biomass fuels [3]. They show the major portion of biomass fuel is volatile material, leaving a relatively small amount of ash. The fractional heat contribution from volatiles in biomass is of the order of around 70% of its total heat value, compared to 36% for coal. Furthermore, biomass contains more oxygen and less carbon, nitrogen and chlorine than coal, which will cause a significant change on its NO_x emission, corrosion and ash

deposition during the combustion process. For example, straw has more free alkali in its ash, which may aggravate the slagging and fouling problems in the boiler. Besides, biomass chars have higher oxidation reactivity in comparison with coal chars, probably as a result of the presence of alkalis (catalytically active) in their char matrixes [20].

The biomass samples in Table 2.4 and 2.5 are all analyzed on a dry basis, due to the great variations in individual sample moisture content. However, this doesn't decrease the importance of moisture, because the presence of moisture has a significant impact on the energy exchange and interim reactions during the process of combustion. There are two forms of moisture in biomass fuel: intrinsic moisture and extrinsic moisture [6]. The former means the moisture content devoid of the effect of the environment. The latter is moisture influenced by the prevailing environment. The moisture content often determines the form of energy conversion process that is best suited to a type of biomass. A high moisture content biomass is more desirable for biologically mediated reactions, such as fermentation, versus a biomass with lower moisture content. Additionally, the high moisture content present in some biomass fuels can cause ignition and combustion problems. The melting point of the dissolved ash tends to be low in the presence of high moisture levels, which can then cause fouling and slagging problems. The above analysis of biomass's chemical properties shows that a biomass with lower moisture content would be more appropriate for gasification, pyrolysis or combustion.

Table 2.4 Proximate analyses of typical fuel samples (wt. % of dry fuel with ash)

Fuel sample	Ash	Volatile matter	Fixed carbon
Beech wood bark	5.7	65.0	29.3
Oak wood	0.5	77.6	21.9
Wheat straw	13.7	66.3	21.4
Olive husk	4.1	77.5	18.4
Beech wood	0.5	82.5	17.0
Spruce wood	1.7	80.2	18.1
Corncob	1.1	87.4	11.5
Tea waste	1.5	85.5	13.0
Walnut shell	2.8	59.3	37.9
Almond shell	3.3	74.0	22.7
Sunflower shell	4.0	76.2	19.8
Colza seed	6.5	78.1	15.4
Pine one	1.0	77.3	21.7
Cotton refuse	6.6	81.0	12.4
Olive refuse	9.2	66.1	24.7

Table 2.5 Ultimate analyses of typical fuel samples (wt. % of dry fuel with ash)

Fuel sample	C	H	N	S	O
Hazelnut shell	52.8	5.6	1.4	0.04	42.6
Sawdust	46.9	5.2	0.1	0.04	37.8
Corn stover	42.5	5.0	0.8	0.2	42.6
Poplar	48.4	5.9	0.4	0.01	39.6
Cotton gin	42.8	5.4	1.4	0.5	35.0
Sugarcane bagasse	44.8	5.4	0.4	0.01	39.6
Peach pit	53.0	5.9	5.9	0.05	39.1
Alfafa stalk	45.4	5.8	2.1	0.09	36.5
Switchgrass	46.7	46.7	0.8	0.19	37.4

Because the combustion process for biomass with a lower heating value is often accompanied by some flame stability problems, the method of blending biomass with higher quality (heating value) coal is commonly used to achieve flame stabilization. In addition, this methodology can also minimize corrosion. Finally, the high volatile content found in most biomass means quick gasification and a subsequently fast consumption of local oxygen. Therefore, proper fuel-air mixing is crucially important in biomass combustion.

2.2.3 Thermal Properties

The phases in the biomass combustion processes include heating and drying, pyrolysis, gaseous combustion and surface reactions. During those processes, the yields of species like light hydrocarbons, carbon monoxide, carbon dioxide, hydrogen and moisture, and tars are determined by the temperature and heating rate, which vary with the local gasification environment and other factors like temperature, time and pressure. To investigate and describe these phenomena, the thermal properties of biomass are of great importance. Due to the technical complexity of testing, only a limited number of experiments are conducted to obtain the thermal properties. The majority of these are gasification tests, which provide a description of pyrolysis and gasification of biomass [21-26].

2.3 Understanding Biomass Combustion: New Issues

The advantages of using biomass energy have been described in the last chapter. It is widely recognized that the utilization of biomass energy can greatly meet the increasing demand on energy sources, vastly mitigate the emissions of greenhouse gas and successfully satisfy the requirement on the environmental performance of the combustion facilities.

From two decades ago up to the present, engineers have investigated and developed biomass combustion technologies. Though those technologies are diversified in scale, methods of combustion, and amount of co-firing, co-firing with coal is still the dominant technology to thermally convert biomass into energy at industrial scale. A lot of progresses have been achieved based on the knowledge and experience related to coal combustion. However, as shown in chapter 2, biomass deviate a lot from coal both in physical and chemical aspects and these differences will further complicates the combustion process and bring up new issues for the engineers.

First, a broader range of physical properties means system improvements. For example, the distribution of pulverized coal is quite even and the combustion facilities are normally designed on the basis of it. Therefore in the case of combustion of biomass particles on the existing facilities running for coal, in order to sustain the weight of the larger particles during combustion and to keep the rate of burnout, it is of critical significance to supply oxygen to ensure that the fixed carbon in the particles can be consumed in time.

Second, biomass contains a higher volatile content which is normally quite light both in weight and reactivity, lower carbon content, lower sulfur content and lower amount of ash. The dynamics and reactions of gaseous and granular species emitted during the progress of biomass combustion are coupled with combustions process and turbulent structure in the boiler. For instance, when biomass with rapid devolatilisation is fired into the boiler, a fast combustion will happen in a matter of very short period of time and reduce the oxygen level in the combustion zone much quicker than coal does. This fast depletion of oxygen will probably cause a reduced rate of char combustion. Therefore, the rearranging of air supply systems is becoming very necessary for achieving an efficient mixing for the combustion.

Besides, a bigger size and highly irregular shape of biomass particles can further more complicate the combustion. Because instead of only considering drag and inertia forces as

the dominating forces in the case of firing pulverized coal, other forms of forces like lift and added mass forces have to be taken into considerations as well. This introduction of new force terms will also contribute to a changed reaction rate of fixed carbon and particles' paths.

2.4 Numerical Modeling: The Solution

In biomass combustion, it is always of great importance to understand the combustion efficiency, emission of pollutants and heavy metal particles, flame stability and various issues involved in devolatilisation. However, for those reasons discussed above, the data collected on coal firing boilers can only provide limited amount of information. What is more, it is impossible to run tests on large combustions units to collect the data to address all these concerns, since those tests are timely extensive and economically costly. They will also interfere with the normal operation to the power plant. The majority of the tests reported by far on literatures of biomass combustion are only carried out on the lab scale facilities, being a compromise to those concerns. Even though, the availability of the data is still quite limited and those data are less consistent with each other as well.

Against the backdrop of huge challenge and increasing demands, computational fluid dynamics (CFD) method emerges showing its great potentials as an efficient, economic and supportive tool to investigate biomass combustion. CFD has the unparalleled advantages of revealing the detailed structure of burning process such as reaction zone, reaction thickness, combustion staging and emissions. It can also be significantly helpful in the aspect of optimizing the combustion systems. For example, it has been used for correcting the secondary air supply in the boiler system in order to enhance the mixing and reduce the ash. It has also been used to optimize particle size range of biomass to achieve the balance between grind energy and proper fuel particle size since the energy to grind

biomass (2-3% of the fuel heat value) is almost double of the percentage of coal (0.9-1.2% of the heat value).

Showing the same path of development as combustion technology, numerical modeling of biomass combustion began to develop by adopting those models used for coal combustion simulation. More sub-models focusing on solving part of the issues during combustion are subsequently created aiming at solving the specific problems such as temperature variances of irregular particles, unexpected temperature peak in combustion zone and increased pollutant emissions. The simulated scenarios vary from the micro-scale one such as the combustion of a single biomass particle, to the full scale descriptions on industrial sized boilers which mainly are grate boilers and fluidized boilers. Comparatively, grate boiler is used more often in those simulations for the reason that it asks for fewer requirements on biomass fuel's type and size. The simulated results of the numerical models have shown those prediction agrees reasonably well with the experiments and can serve as a significantly efficient tool to investigate biomass combustion.

2.5 Mathematical Models of Biomass Combustion: The Tree

In 1999, Sami et al. [27] in the first presented a three mixture fractions/Probability Density Function approach to simulate combustion of the blend of coal and manure in a swirl burner. The mixtures in this model were defined separately as primary air, coal-off gas and biomass gas. His results showed an improved combustion in terms of burnout after using biomass fuel. Following this work, the development of CFD of biomass combustion began to burgeon widely.

These numerical models are mostly based on the industrial backgrounds, therefore they are far from monolithic, being rather comprehensive by consisting of different

turbulence modeling, combustion kinetics, multiphase interactions and simplified but rational sub-models making modeling complicated components of combustion possible. Therefore, it is quite challenging to sort those models in distinct categories of mathematics. In addition to it, the research conducted by each of those major study groups are carrying a pattern of tree, growing extensively by following the time. Under all those above considerations, the following literature reviews is determined to start with the introduction of series work done by different groups in the order of time, which mainly investigated the biomass mass combustion in a fixed bed facility. They conducted their consecutive and basic investigations aiming at exploring different aspects involved in biomass combustion. After scrutinizing the groups' work, other more scattered and singled researches were presented in different categories. The aim behind this arrangement is to help the readers get a comprehensive and consistent view on how the numerical modeling of biomass combustion was developed and where the research focuses at.

2.5.1 The Work of Groups: The Path

The work of numerical modeling of biomass combustion done by different groups all last a period of time, which allows their research moving further in the depth and extending in the range. One common goal shared by all the groups is applying the numerical model to simulate biomass combustion in a full scale boiler. Commercial software is universally adopted during the research for choices of models it provides, capabilities of handling complicated computational mesh and its empirically accepted results. Instead of constructing a full scale model, those groups can be allowed to put more attention on developing different sub-models to meet their research goals.

Scharler

Scharler et al. [28-29] in 2000 used the multi-step Finite Rate Chemistry/Eddy Dissipation combustion model in commercial software Fluent to simulate a grate boiler

fired with waste wood and pellets. The coupling between the heterogeneous biomass combustion on the grate and the turbulent reacting flow in the combustion chamber was unavailable under present model. This gaseous model was only applied on the combustion above the bed, which means the mass and energy fluxes released from the fuel bed were calculated through a separate empirically derived model, and then used as the boundary conditions for the combustion model. Experiments were at the same time carried out at a pilot scale grate furnaces, where the samples were taken and analyzed through different parts for validation. The flue gas components measured in the test included CH_4, H_2, CO, CO_2, H_2O, O_2 and N_2. A linear correlation between each individual component species was found, allowing a description of the fuel consumption with only one leading parameter. This model is used to optimize the geometry of furnace, arrangements of nozzles of secondary air and flue gas and the primary air rations.

Later, they [30] combined this model with a finite cell based convective heat exchanger model to investigate the combustion of a whole boiler system composing fuel bed, furnace, evaporator, super heater tube bundles and economizer. The turbulent combustion model was chosen as Eddy Dissipation Model in this case. This expanded model allows a detailed full scale description of the flow distribution and ash formation along the path of flue gas.

Y.B.Yang

From 2003, Y.B. Yang et al. [31] also conducted serial works of numerical models of biomass combustion as well as some experimental studies in a boiler with packed bed. Different with Scharler, they used a mathematic model to describe the phenomenon on the bed. But those complicated factors inside the bed, such as a three dimensional temperature profile inside the particle and the mixing rate between under grate air and volatile gases, were all avoided under the assumption that the major bed properties only vary vertically with the bed height. The transient one dimensional transport models of gas and solid phase

were set up separately. Then the volatile hydrocarbons released from wood chips and cardboard were simplified by being treated as one single product and its oxidization products were only regarded as CO and CO_2. The impacts of the volatilization kinetic rate and moisture level on the ignition time, burning rate, reaction zone thickness, combustion process and emissions were all studied in this work. They [32] also used this model to investigate the effects of primary, and proved the significance of it. They especially claimed in their papers that the past conclusions were only applicable in the case that the particle size is small enough to be regarded as thermally thin and argued that in order to investigate the combustion of thermally thick particles, another model is needed to describe the fuel bed. They [33] further categorized the bed cells as one of the three types including void cells, boundary cells and inner cells, and used different schemes to set up three different transport equations for these cells. In this model, the particles size exerted their effects through several aspects such as two phase heat and mass transfer, the radiation heat transfer, turbulent dispersion of energy and gas species, the burning rate of volatile gaseous fuel and the non-uniform temperature distribution inside the particles. Those influences were reflected on the changes in temperature, flame propagation and residual char burnout.

It was pointed out in their work [34] that a fixed bed reactor can be used to simulate the moving bed of grate, for the reason that only the heat and mass transfer in vertical direction is regarded as the dominating factors in grate boiler. Thus, the developed model was used to investigate the ignition rate and burning rate of cardboard and waste wood on a moving grate bed with different air flow rates. The collected experimental results agree well with the predicted results and successfully supported that argument.

The bed mode was then used as a sub-model [35] for estimating the mixing between the under grate air and the volatile gases. The parametric studies in terms of fuel properties and operation parameters were all carried out where the turbulent model is chosen as $k-\varepsilon$ model. At the same time, they expanded the application of this model to study the ignition

and burning rates of segregated waste combustion [36]. Finally using all the experience, they set up a numerical model [37] for a full scale power plant furnace. The previous packed bed model was used as the bed combustion model by being expanded to a two dimension model. Like Scharler, they also chose commercial software Fluent to calculate the gaseous combustion in the chamber. But in their cases, the super heater was treated as solid surface with fixed temperature. The coupling between the bed and free board sections was achieved through interaction of boundary conditions.

Their most recent work was a preliminary study modeling the combustion of a single particle of willow coppice [38], with an intention to focus on exploring more fundamental details around and inside the particles. This model was set up as a two dimensional model and the flow around the particle was only considered as laminar flow.

Yin and Kær

Another research group lead by Yin and Kær, in the Institute of Energy Technology of Aalborg University, Denmark, also earns an international reputation for their accomplishments in modeling biomass combustions. The work was started by Yin et al. [39] as a model to simulate the motion of straw particles in a non-uniform flow. In this model, straw particles were treated as cylinders instead of spheres for the consideration that the shapes of biomass particles are more close to cylinder or disk. The motivation behind this work is that more forces terms would be used to better describe the particle track and finally combustion. Those terms included virtual mass, pressure gradient, and lift force, mainly resulting from the non-spherical property of the particles. The rotation motion of the particles was also investigated under a practically reasonable assumption that the dominating torques come from hydrodynamic forces and resistances. A different particle path was predicted by this model and agreed well with experimental data. This find signified the importance of using non spherical particle models to model the flow pattern in biomass fired boiler. Following that, they continued to test the combustion behaviors of

those cylindrical particles by co-firing straw particles with methane in a wall fired burner conducted. The calculated results once more unsurprisingly approved their original assumption as expected.

With these achievements, Yin et al. [40-44] switched their interest from conducting the micro-scale research on particle tracks to modeling the full scale boiler combustion. A baseline CFD model for the biomass fired grate boiler was developed for the purpose of design and optimization, which was proved to be reliable after being compared with experimental measurements. Two fuel bed models were developed separately to couple with the combustion model provided by commercial CFD software Fluent. The first one is using inlet boundary condition profiles obtained on the basis of experience and design of that grate boiler. The second one is a one dimensional transient fixed bed model with transport equations describing the phenomenon on the bed with some empirical corrections being used to calculate those physical properties involved in the equations.

Kær et al. [45-49], working in the same institute with Yin, made their investigations in biomass combustion from a different angle, with an interest being more focused on predicting the deposit during the full scale boiler combustion. They started with modeling the heat transfer inside the solid fuel bed by using a one dimensional bed model like what Scharler and others have done. But this model took into considerations of more details and it successfully showed that two combustion models existed on the bed. The first one is characterized by a devolatilization front moving downwards, being followed by an upward moving char oxidization front. The second one is that these two reactions both moves upwards. In their work, the first model was used to predict the phenomenon on fuel bed. The prediction obtained through this bed model was then used as the inlet boundary conditions to calculate the turbulent combustion, which was modeled by the commercial CFD code CFX. This complete CFD model was applied to analyze a straw-fired grate boiler. In this simulation, some parts of the boiler, like super heaters and tube banks were simplified as the slabs and source terms. This model was reasonably validated by the

measurements and was used to discuss the mixing conditions inside the boiler in the hope for accomplishing the reduction of the area with high concentration of CO and unburned carbon.

This fuel bed model was later combined with the commercial software Fluent to predict the ash deposition and its influence on heat transfer rates in a straw fired boiler [50]. In this quasi-transient model, the time evolution of the deposit was simulated with the deposition velocity correlation collected from the experiments. The comparison with the experiment approved that this model was capable to correctly predict the operational trends.

Leeds

For the research group in the University of Leeds, their work was more focused on investigating the effects of fuel properties on the combustion. First, Jones et al. [51] considered biomass combustion as a process consisting of three steps including devolatilisation, combustion of char and volatiles, analogous to a coal model developed in their lab. The predictions of the FG-DVC pyrolysis model for wheat straw was used in the CFD calculations in the stage of devolatilisation. The char combustion stage was modeled with measured and calculated data. Finally, a laminar combustion in a drop tube was developed basing on those models. Some significant differences of the combustion behavior from coal were illustrated by the results.

Following Jones, Backreedy et al. [52-53] developed a numerical model to simulate the co-firing of pulverized coal and pine wood. This model was set up by using a complex form of drag coefficient in order to take into account the irregularity in shape. Again, the outputs from the functional group biomass (FG-biomass sub-model) were used as an input for the devolatilisation model. The combustion of biomass char was modeled in a similar way to that for coal combustion, with a variable surface area sub-model and some modifications on the related correction factors. The results showed that the shapes and

sizes of biomass particles are more important than other factors when the property was considered as non-melting and the shape was treated as unchanged.

Ma et al. [54] further used this model to simulate the combustion of pulverized wood particles in and industrial combustion test furnace. They modeled the potassium and the overall volatile release at the same rate which was obtained through a single rate kinetic model. Their prediction on the concentrations of potassium, NO_x and other species allowed the future development of an advanced ash deposition model.

2.5.2 Singled Work: The Focus

Along with those researchers who conducted some continued work on numerical modeling of biomass combustion, other people also used CFD as a tool to solve many problems. The following content are organized according to the main features of their works to present how the problem is modeled and solved from different research angles. Besides a majority developed for fixed bed boiler fired with biomass, these investigations also include the study for other types of facilities like fluidized boiler, pulverized fuel boiler and gasifier.

Fixed bed model

Among those models, modeling the combustion on the fixed bed attracted most of the interests of people. This is because that grate boiler provides the most convenient and economical way to use biomass fuels. The success and validation of those numerical models mainly depend on how to reasonably efficiently and accurately predict the phenomenon in and close to the fuel bed. Due to the complexity of the real situations on the bed, most of the models are one dimensional ones and only very few are two dimensioned ones. How this bed model is connected with gaseous combustion simulation is also a significant issue.

Van der Lans et al. [55] developed a homogeneous two dimensional mathematical model for the combustion of straw in a grate furnace. Considering the relatively small horizontal gradients in the grate bed, they also used fixed bed model to approximate the moving bed combustion. However this model only accounted for the reactions of char with O_2, because of the unavailability of the data on the devolatilization products' kinetic models. Even with such simplification, those main processes in combustion predicted by the model were still compared well with the data.

Shin et al. [56] simulated the combustion of wooden particles in a fixed bed with a static one dimensional two phase model. A global kinetics was used to describe the wood pyrolysis, char oxidization and volatilization reactions. Three combustion models including oxygen-limited, reaction-limited and extinction by convection whose existence depended on the air supply was identified during the process.

Wei et al. [57] performed the simulation of the combustion in a grate boiler fired with bark in which an ecotube system was installed. The complicated phenomena on the grate bed were simplified as homogeneous combustion of gas phase in several well defined zones. The predicted results demonstrated a significant improvement in terms of boiler efficiency and mixing.

Zhou et al. [58] developed a one dimensional transient heterogeneous model for straw combustion in a fixed bed. The simulated processes included evaporation, pyrolysis, heterogeneous reaction of char, and homogeneous reaction of volatiles and tar. The detailed structures of the ignition flame front, gas species and temperature were described. After a parametric study, it was indicated that the effective heat conductivity, heat capacity of straw, and straw packing condition were the dominating factors influencing the combustion. A reasonable agreement between the modeling prediction and experimental data was achieved.

Goerner et al. [59] developed a mathematical sub models for the heterogeneous combustion of a solid waste/biomass bed, and defined its thermal input and concentrations

as the integral functions over the grate. Similarly, Klason et al. [60] modeled the combustion of a 50 MW grate fired furnace, injected with wet wood chips. His CFD simulation was performed only above the fuel bed, with the inflow boundary conditions being added as the inlets. The effect of turbulent structure on the NO_x reduction was proved to be important.

Yu et al. [61] modeled the combustion of rice straw in a grate fired boiler under an air and oxygen enrich operating condition, which were assumed to posse the advantages of reducing energy loss, decreasing pollutant in flue gas and minifying thermal energy in exhaust gas. This model was developed upon a model belonged to Sheffield University Waste Incineration Center.

A more detailed kinetic scheme was applied by van Kuijk et al. [62] in their work of simulation of fixed bed combustion. A multi-scale approach was used since it was argued by them that several length scales were involved in the process of combustion, where the smallest one was related to the behavior of a single particle.

Non uniform property of biomass fuel particles

One unique feature of biomass particles are the irregularity in the shape and the wide distribution in the sizes. Although in most numerical models, the particles were treated as temperature even and unique size particles which were proved to be accurate enough for modeling the combustion in the boiler, there still exists a demand for a more detailed description of the combustion around the particles.

Those factors hold a direct influence on the combustion behavior of the gas and particulate phases, which has been proved in those following works as expected.

Gera et al. [63] used commercial software to study the effect of large aspect ratio of switch grass particles on carbon burnout in a utility boiler originally fired with pulverized coal. A non-increased amount of unburned carbon was detected, which was partly explained by the high content of volatile in biomass.

Dixon et al. [64] added some new features on a CFD code, originally used for pulverized coal fired boilers, to study the bagasse combustion for sugar industry. A dual particle size distribution was used to explore the tendency of tube erosion, which consisted of larger particle as bagasse and small dense particles representing ash fraction. The tube bundle in the boiler was represented by a porous region

Thunman et al. [65] investigated the influence of size and density of wood particles on combustion in a packed bed by a one dimensional two phase combustion model. The source term in the conversion of the solid phase was treated by a separate model, which is one dimensional as well. This model can predict the temperature wave and release of moisture and volatile for the particles in the shape of sphere, cylinder and parallel piped, which made the results more accurate. However, the free room above the bed was not included in this model, making the application of this model limited. The results showed that the particle size had a significant impact on the conversion reaction, versus a relative minor influence of the density.

Venturini et al. [66] modeled the multiphase combustion and deposit formation in a biomass fed furnace. The locations of deposition were predicted, with being split up into different particle size classes.

Different with other people, Mirka et al. [67] did their work more focused on understanding the gas-solid hydrodynamics of a fluidized bed boiler fired by biomass. Their main interest was to find an appropriate drag model for the biomass particle. Therefore they only studied the cold flow cases. Particularly, two drag models were chosen to be combined with a multi-fluid Eulerian-Eulerian model: Syamlal O'Brien model and Gidaspow model. The results showed encouraging for Gidaspow model at modeling ground walnut shells, which was used to represent a Geldart type B particle

Some work also took into consideration the gradients inside a single biomass particle in order to understand the phenomenon inside and closely around the particles. Wurzhenberger et al. [68] set up a single particle model for beech particle and combined it

with a common one dimensional packed bed model. To reduce the degree of complexity, his simulation of the combustion of a single particle was decoupled from the packed bed model.

Liang et al. [69] presented a two dimensional axisymmetrical numerical model to study the pyrolysis and combustion of fibrous biomass in a thermogravimetric system. The partial differential equation for temperature, mass, and the species concentrations inside the particle and in the adjacent gas-phase were all solved with the fiber grid being assumed to be a porous medium. This model was used to define the factors which influence the pyrolysis and combustion process.

Grammelis et al. [70] used a computational code to predict the burn-out time of a single olive kernel particle in a fluidized bed boiler. The kinetic parameters used for modeling devolatilization and char combustion were determined via thermogravimetric analysis at first. Then a distributed activation energy model was applied for devolatilization and a global reaction model was employed for char combustion. The results showed that the required time for heating, drying, evolution and combustion was significantly lower for biomass versus coal due to the small volume heat capacity, the lower moister content and the higher volatile content of biomass.

Gasification model

One of the primary features of biomass fuels is its high content of volatile matters. The rate of devolatilizaton and how the volatile degrade have significant influence on combustion performance. Some works have been conducted to address this problem. Fletcher et al. [71] used commercial software to investigate the combustion of a mixture of seeds, cotton and pieces of stalk in a gasifier, with those fuel particles being represented by spherical particles assigned by an appropriate average diameter. The results showed that the gasification reactions are more sensitive to the residence time than other factors due to the fact that combustion flows resulted from that factor could cause a larger volume flow

rate. They also conducted some comparisons of different turbulent models, and concluded that the $k-\varepsilon$ turbulent model will be sufficient to model the velocity field and achieve a computational economy in the simulation of global convection in the furnace. Scala et al. [72] developed a steady state one dimensional model of a bubbling fluidized bed combustor operated with high volatile solid fuel Robinia Pseudoacacia. This combustor was treated mathematically by being divided into three sections: the bed, the splashing region and the freeboard. A unique feature of this model is that it took into account the important processes of fuel particle fragmentation and of volatile matter segregation. Marias et al. [73] modeled a biomass fired fluidized furnace which produced lime with a one dimensional two phase model as well. The kinetics of the decarbonation reaction of biomass combustion was included.

Others

The other singled works are all introduced in this section to make complete the goal of rolling out a full picture of the development of numerical models of biomass combustion. Under the assumption that volatile of biomass is released quickly when biomass enters the boiler, in some works, biomass fuels are only modeled as gaseous species.

The research interests here are more focused on the macro performance of biomass combustion. Andersen et al. [74] used commercial software to investigate the gas phase freeboard combustion which was modeled as a two dimensional axisymmetric problem. Lo et al. [75] conducted a simulation of pine wood sawdust combustion in a vortexing fluidized bed combustor, using an isothermal one dimensional model. This model was set up basing on the assumption that sawdust release out the volatiles simultaneously when being introduced into the boiler. Some works adopt Possibility Density Function (PDF) model to simulate the turbulent combustion in order to achieve a computational efficiency. Pallarés et al. [76-77] used the commercial CFD code to describe coal and cynara co-firing in a 350 Mw utility boiler. Two discrete models were used for each of the fuel particles,

along with a two beta PDF combustion model. The recommendations on improving boiler efficiency, understanding the influence of biomass injection locations and optimizing future nozzle designs were made based on the calculated results. Ghenai et al. [78] analyzed the effects of co-firing biomass with coal inside a furnace with a static mixer which was modeled by controlled vortex structures. The gas phase combustion was modeled by two mixture fractions/PDF approach. Finally, Bhaskar Dixit et al. [79] also conducted a computational investigation on a pulverized biomass fuel stove by combing a one dimensional condensed model to represent solid fuel and a gas phase model to describe the combustion.

2.6 Conclusion: Achievements and Challenges

These diverse numerical models of biomass combustion have shown their potentials to solve such issues as describing the combustion behavior, locating the deposition and optimizing the systems. They are applied to study mainly two kinds of systems: pilot lab scale furnaces, which are used to explore some fundamental phenomena and targeted to provide referenced information for the full scale furnaces, and industrial furnaces with a majority of fixed bed/grate boilers. These full scale geometries were all mathematically modeled with certain degree of simplifications.

During the process of researches, a decent amount experiments were carried out to accomplish to correct the numerical models and to valid them. Those physical properties such as shape, density and irregularity, and chemical characteristics such as chemical compositions, volatilization and inside chemical structures are regarded as the primary influencing factors during combustion.

In these works, the combustion of biomass with high or medium density is mainly modeled as two phase flow, that of biomass in the form of particles is commonly achieved by describing them as the discrete phase, where fuel particle is modeled by Lagrangian

method, experiencing several distinctive stages during the process of combustion, which include heating-up, devolatilisation, volatile combustion and char combustion. Though these above numerical modeling of biomass combustion have provided some encouraging results, there still exist some fields which are equally important and haven't be ploughed yet. It is this work's goal to make some innovative and tentative study on some of these areas.

Firstly, this work studied and compared the co-fired combustion of biomass fuels with different properties: oat hulls, wood chips and natural gas, in a stoker boiler. These works is of great significance to expand the potential of stoker boiler in utilizing biomass fuels. Especially for oat hulls, as a type of light weight biomass, oat hull particles will tend to have a shorter residence time inside the boiler, which may reduce the efficiency of burnout. Meanwhile, light weight biomass contains a high portion of volatile matter whose gasification will progress in a comparably short period. This fast gasification can further cause an instant depletion of oxygen and raise the issue of poor mixing locally. Only the method of numerical modeling can provide enough details to fully describe the combustion process.

Second, for the case of biomass particle combustion, the problem can be considered as a multi- scale problem, with the biggest one as fluid scale and smallest one as particle collision time scale. However in reality of numerical modeling, all the numerical models documented in the literature chose to use particle aerodynamic response time scale to simulate the movement of particles. The primary reason for that is adopting the particle collision time scale will hugely increase the cost of computation. In the case of a small particles' Reynolds number and their volume fractions, the time scale of particle collisions will thus be more appropriate to be used in the simulations. Accordingly, the dominating forces on the particles will then be expanded to include normal and shear effects among particles, so does the torques influencing particles' rotations. The particles will show a different pattern of projection, the combustion behavior such as temperature, species

concentration and particle surface combustion are worthy to be reconsidered as well. Therefore this work will adopt particle collision time scale to investigate light weight biomass combustion. A multi time step computation method is used to efficiently solve the problem of high computing demand on the computer.

CHAPTER 3: METHODOLOGY

The research subject of this work is the combustion of gaseous flow with particles. The comprehensive numerical model developed in this investigation is based on governing equations that describe the dynamics of fluid flow with heat transfer, species transportation with chemical reaction and particle movement with surface combustion. The equations describing the continuous phases are derived using the Euler Method, and those for discrete phase are described by a Lagrangian Method. Finally, these analytical equations are discretized by a Finite Volume Method. The model can capture the details of the combustion process, evaluating the interactions of solid fuel particles with the continuous phase through the exchanges of mass, momentum and energy. It can also describe the movement and combustion of biomass particles at the micro time scale.

These sections will first introduce the general equations describing the continuous phase in a Langrangian frame both in single mixture form and in multi species form. Following that, equations describing the different turbulence models and different turbulent combustion models are presented. The equations for the discrete phase are also presented, with all the fluid forces, collision forces and heating stage models being discussed.

3.1 Model of Continuous Phase

3.1.1. General Forms of Conversation Equations of Fluid

The continuous phase is modeled by conservation equations of mass, momentum and energy. The general forms are written as Equation (1) to (4):

$$\frac{\partial \rho}{\partial t} + \nabla \cdot (\rho \vec{v}) = S_m \tag{1}$$

$$\frac{\partial}{\partial t}(\rho\vec{v}) + \nabla\cdot(\rho\vec{v}\vec{v}) = -\nabla p + \nabla\cdot(\bar{\bar{\tau}}) + \vec{F} \tag{2}$$

$$\bar{\bar{\tau}} = \mu[(\nabla\vec{v} + \nabla\vec{v}^T) - \frac{2}{3}\nabla\cdot\vec{v}I] \tag{3}$$

$$\frac{\partial}{\partial t}(\rho E) + \nabla\cdot[\vec{v}(\rho E + p)] = \nabla\cdot(k\nabla T + \bar{\bar{\tau}}\cdot\vec{v}) + S_E \tag{4}$$

In the mass conservation Equation (1), S_m is the source term of mass, which is contributed by the mass loss of biomass fuel particles in this work. In Equation (2) which describes the momentum transportation in fluid by neglecting the effect of gravity, p is the static pressure, $\bar{\bar{\tau}}$ is the stress tensor and $\vec{F}$ is the force exerted by the particles on the fluid. The complete formula of stress tensor is illustrated in Equation (3), where μ is the molecular viscosity, I is the unite tensor.

The energy Equation (4) is written in the form of total energy, whose expression is shown in Equation (5), with body force being neglected. The first term on the right side of Equation (5) is the heat flux due to conduction, and the third term is heat sources including radiation and chemical reactions.

$$E = H - \frac{p}{\rho} + \frac{v^2}{2} = i + \frac{v^2}{2} \tag{5}$$

Substituting Equation (5) into Equation (4), expanding, rearranging this obtained equation and using the continuity equation can give the conservation equations of internal energy i and enthalpy H separately, shown in Equation (6) and (7):

$$\frac{\partial}{\partial t}(\rho i) + \nabla\cdot(\rho\vec{v}i) = -p\nabla\cdot\vec{v} + \nabla\cdot(k\nabla T + \bar{\bar{\tau}}\cdot\vec{v}) + S_i \tag{6}$$

$$\frac{\partial}{\partial t}(\rho H) + \nabla\cdot(\rho\vec{v}H) = \nabla\cdot(k\nabla T + \bar{\bar{\tau}}\cdot\vec{v}) + S_H \tag{7}$$

In these two energy equations, S is the energy source term caused by chemical reactions. Its subscript indicates the exact form of energy.

3.1.2 Equations for Species

The equations above show the property of the mixture consisting of some gaseous species. The phenomena of mixing, transporting and reacting of different those species are described in Equation (8) and (9).

$$\frac{\partial}{\partial t}(\rho Y_j) + \nabla \cdot (\rho \vec{v} v Y_j) = -\nabla \cdot \vec{J}_j + R_j + S_j \tag{8}$$

$$\vec{J}_j = -\rho D_{j,m} \nabla Y_j \tag{9}$$

Equation (8) is the transportation equation of j species, where Y_j is its mass fraction. The first term on the right side of this equation represents mass diffusion flux which is calculated through Equation (9), where $D_{j,m}$ is the mass diffusion coefficient for species j in the mixture. The term R_j is source term of specie production/reduction resulting from gaseous chemical reaction, whose expression is explained in the following section. The other source term S_j is due to the releasing/absorbing of gaseous species by solid fuel particles.

Correspondingly, the total energy, internal energy and enthalpy energy in Equations (4), (6) and (7) are expressed as the summation of each species in Equation (10), (11) and (12). Among those equations, enthalpy equation is most commonly used, which is calculated by Equation (13).

$$E = \sum_j Y_j E_j \tag{10}$$

$$i = \sum_j Y_j i_j \tag{11}$$

$$H = \sum_j Y_j H_j \tag{12}$$

$$H_j = \int_{T_{ref}}^{T} c_{p,j} dT \tag{13}$$

The energy equation is then adjusted to the form of Equation (14):

$$\frac{\partial}{\partial t}(\rho E) + \nabla \cdot [\vec{v}(\rho E + p)] = \nabla \cdot (k\nabla T + \overline{\overline{\tau}} \cdot \vec{v} - \sum_j H_j \vec{J}_j) + S_E \quad (14)$$

3.1.3 State Equation

Under the assumption that all the gaseous species will obey the ideal gas law, state equation and ideal gas mixing law are enabled to be used in the model, as the equations below:

$$p = \rho \frac{R}{M} T \quad (15)$$

$$\rho = \frac{1}{\sum_i \frac{Y}{\rho_i}} \quad (16)$$

In Equation (15), R is the universal gas constant, M is molecular weight. Equation (16) is used to obtain the mixture density. The relationship between heat capacity at constant pressure and heat capacity at constant volume is expressed in Equation (17), where n is the number of moles of the gas mixture.

$$C_p - C_V = nR \quad (17)$$

3.2 Turbulence

The phenomenon studied in this research is a typical problem of turbulent combustion. To capture the character of chaotic and random state of motion in turbulence, where velocity, pressure and other parameters vary continuously with time, static techniques are

used. In this method, all properties ϕ are decomposed into a steady mean value $\bar{\phi}$ and fluctuation component ϕ', written in Equation (18). This assumption is considered sufficiently rational in the field of engineering. The results obtained after its application can provide adequate information about turbulent flow progresses, while avoiding the high expense of computation time.

$$\phi = \bar{\phi} + \phi' \tag{18}$$

The averaging method is usually based on time averaging flow properties. After the application of averaging rules on the flow equations, the Reynolds averaged form of Navier –Stokes equations are derived with the additions of several unknown terms like Reynolds stresses for the Navier-Stokes equations and other extra terms of turbulent transport, shown in Equation (19) to (21), where the mean properties are represented by the letter without the bar for the reason of simplification.

$$\frac{\partial \rho}{\partial t} + \nabla \cdot (\rho \vec{v}) = S_m \tag{19}$$

$$\frac{\partial}{\partial t}(\rho u_i) + \frac{\partial}{\partial x_i}(\rho u_i u_j) = -\frac{\partial p}{\partial x_i} + \frac{\partial}{\partial x_j}[\mu(\frac{\partial u_i}{\partial x_j} + \frac{\partial u_j}{\partial x_i} - \frac{2}{3}\delta_{ij}\frac{\partial u_l}{\partial x_l})] + \frac{\partial}{\partial x_j}(-\rho\overline{u'_i u'_j}) \tag{20}$$

$$\frac{\partial}{\partial t}(\rho E) + \nabla \cdot [\vec{v}(\rho E + p)] = \nabla \cdot (k_{eff}\nabla T - \sum_j H_j \vec{J}_j + (\overline{\overline{\tau_{eff}}} \cdot \vec{v})) + S_E \tag{21}$$

In Equation (21), $k_{eff} = k + k_T$ is the effective conductivity, where k_T is the turbulent thermal conductivity, defined according to the turbulent model being used.

It is a main task of turbulence to derive expressions and to develop computational schemes of a sufficient accuracy to calculate the Reynolds stresses and the turbulence transport term. Some most classical turbulence models are based on the time-averaged Reynolds equations, like mixing length model and the $k-\varepsilon$ model. In those models, it is assumed that there exist an analogy between the action form of viscous and Reynolds

stresses, i.e. Reynolds stresses are treated as being proportional to the deformation rate of the fluid element. Specifically, standard and other types of $k-\varepsilon$ model are employed in this research to study the problem.

3.2.1 Standard $k-\varepsilon$ Model

More than hundred years ago, Boussinesq (1877) proposed the following expression for Reynolds stresses which is denoted as the eddy viscosity principle, show in Equation (22) and (23).

$$-\overline{u_i'u_j'} = \upsilon_t\left(\frac{\partial \overline{u_i}}{\partial x_j} + \frac{\partial \overline{u_j}}{\partial x_i}\right) = 2\upsilon_t \overline{D} \tag{22}$$

$$\tau_{ij} = -\rho\overline{u_i'u_j'} = 2\mu_t \overline{D} \tag{23}$$

In Equation (22), $2\upsilon_t = \mu_t / \rho$ is the kinematic turbulent viscosity and μ_t is the dynamic turbulent viscosity. The $k-\varepsilon$ model was one way to determine the turbulent viscosity, by defining that $\upsilon_t \approx v^* L^*$, where v^* and L^* are expressed by turbulent kinetic energy k and dissipation ε, with $k = (\overline{(u_1')^2} + \overline{(u_2')^2} + \overline{(u_3')^2})/2$.

Proposed by Launder and Spalding (1972), the standard $k-\varepsilon$ model has become universally general in the field of practical engineering with its robustness, economy and a rational accuracy. It is a semi-empirical model and its derivation relies on phenomenological considerations and empiricism.

$$\frac{\partial}{\partial t}(\rho k) + \frac{\partial}{\partial x_j}(\rho u_j k) = \frac{\partial}{\partial x_j}\left[(\mu + \frac{\mu_t}{\sigma_k})\frac{\partial k}{\partial x_j}\right] + G_k + G_b - \rho\varepsilon + S_k \tag{24}$$

$$\frac{\partial}{\partial t}(\rho\varepsilon) + \frac{\partial}{\partial x_j}(\rho u_j \varepsilon) = \frac{\partial}{\partial x_j}\left[(\mu + \frac{\mu_t}{\sigma_\varepsilon})\frac{\partial \varepsilon}{\partial x_j}\right] + C_{1\varepsilon}\frac{\varepsilon}{k}(G_k + C_{3\varepsilon}G_b) - C_{2\varepsilon}\rho\frac{\varepsilon^2}{k} + S_\varepsilon \tag{25}$$

$$C_{1\varepsilon} = 1.44, C_{2\varepsilon} = 1.92, C_{\mu} = 0.09, \sigma_k = 1.0, \sigma_{\varepsilon} = 1.3$$

Equation (24) and (25) are the transport equations for standard $k-\varepsilon$ model, where $\mu_t = \rho C_{\mu} k^2 / \varepsilon$. In Equation (24), G_k represents the generation of turbulent kinetic energy due to the mean velocity gradients, and G_b is the generation of turbulence kinetic energy due to buoyancy. These values are calculated through Equation (26) and (27).

$$G_k = -\rho \overline{u_i' u_j'} \frac{\partial u_j}{\partial x_i} \tag{26}$$

$$G_b = -g_i \frac{\mu_t}{\rho \mathrm{Pr}_t} \frac{\partial \rho}{\partial x_i} \tag{27}$$

3.2.2 Realizable $k-\varepsilon$ Model

It was recognized that combining the Boussinesq relationship and the eddy viscosity definition, a new form of expression of normal Reynolds stress in an incompressible strained mean flow is obtained, shown in Equation (28).

$$\overline{u^2} = \frac{2}{3} k - 2\upsilon_t \frac{\partial U}{\partial x} \tag{28}$$

Therefore the truth that the normal stress in a positive quantity is violated when the strain is large enough to satisfy the condition in Equation (29).

$$\frac{k}{\varepsilon} \frac{\partial U}{\partial x} > \frac{1}{3C_{\mu}} \approx 3.7 \tag{29}$$

This conflicting issue causes the birth of realizable $k-\varepsilon$ equation. The term 'realizable' means that the model satisfies certain mathematical constraints on the Reynolds stresses, consistent with the physics of turbulent flows. It is a relatively recent development and differs from the standard $k-\varepsilon$ model in two ways: the first one is that it

contains a new formulation of turbulent viscosity, the second is that a new transportation equation for the dissipation rate has been derived from an exact equation for the transport of the mean square vorticity fluctuation.

The new features adopted in Realizable $k-\varepsilon$ model, shown in Equation (30) and (31) were intended to address the above deficiency and to improve the prediction of the spreading rate for axisymmetric jets by other $k-\varepsilon$ models. Some substantial improvements by using this new model are significant in the flows including strong streamline curvature, vortices, and rotations.

$$\frac{\partial}{\partial t}(\rho k)+\frac{\partial}{\partial x_j}(\rho u_j k)=\frac{\partial}{\partial x_j}[(\mu+\frac{\mu_t}{\sigma_k})\frac{\partial k}{\partial x_j}]+G_k+G_b-\rho\varepsilon+S_k \tag{30}$$

$$\frac{\partial}{\partial t}(\rho\varepsilon)+\frac{\partial}{\partial x_j}(\rho u_j \varepsilon)=\frac{\partial}{\partial x_j}[(\mu+\frac{\mu_t}{\sigma_\varepsilon})\frac{\partial \varepsilon}{\partial x_j}]+\rho C_1 S_\varepsilon-\rho C_2\frac{\varepsilon^2}{k+\sqrt{\upsilon\varepsilon}}+C_{1\varepsilon}\frac{\varepsilon}{k}C_{3\varepsilon}G_b+S_\varepsilon \tag{31}$$

$$C_1=\max[0.43,\frac{\eta}{\eta+5}],\eta=S\frac{k}{\varepsilon},S=\sqrt{2S_{ij}S_{ij}}$$

In this model, C_μ, used to obtain the eddy viscosity, is computed from Equation (32), instead of being treated as constant in other models.

$$C_\mu=\frac{1}{A_0+A_s\frac{kU^*}{\varepsilon}} \tag{32}$$

In this equation, $U^*\equiv\sqrt{S_{ij}S_{ij}+\tilde{\Omega}_{ij}\tilde{\Omega}_{ij}}$, where $\tilde{\Omega}_{ij}=\Omega_{ij}-2\varepsilon_{ijk}\omega_k$ and $\Omega_{ij}=\overline{\Omega}_{ij}-\varepsilon_{ijk}\omega_k$. The model constants are given by the expression $A_0=4.04, A_s=\sqrt{6}\cos\phi$, where $\phi=\cos^{-1}(\sqrt{6}W)/3, W=S_{ij}S_{jk}S_{ki}/\tilde{S}^3, \tilde{S}=\sqrt{S_{ij}S_{ij}}, S_{ij}=(\partial u_j/\partial x_i+\partial u_i/\partial x_j)/2$.

3.3 Finite Rate Chemistry

In the problem of turbulent combustion, an important part of the research interests is always focused on describing these details such as how the mixture changes from its initial state to the final stage and how long it takes to reach this state. In this research, the turbulent chemistry is explored through three methods separately: reaction kinetics, eddy dissipation model and Possibility Density Function (PDF) model.

3.3.1 Reaction Kinetics

Equation (33) represents a single forward chemical reaction, with the subscript f designating the direction of the reaction.

$$\sum_{i=1}^{N} \nu_i' M_i \xrightarrow{k_f} \sum_{i=1}^{N} \nu_i'' M_i \tag{33}$$

Equation (34) is to calculate the rate of change of molar concentration C_i of specie i. The rates of change of each species all obey a unique relation shown in Equation (35), indicating that the reaction rate ω in this equation is species independent.

$$\hat{\omega}_i = \frac{dc_i}{dt} \tag{34}$$

$$\frac{\hat{\omega}_i}{\upsilon_i'' - \upsilon_i'} = \frac{\hat{\omega}_j}{\upsilon_j'' - \upsilon_j'} = \omega \tag{35}$$

The phenomenological law of mass action states that ω is proportional to the product of the concentrations of the reactants, shown in Equation (36).

$$\omega = k_f(T) \prod_{i=1}^{N} c_i^{\upsilon_i'} \tag{36}$$

The term $k_f(T)$ is called the specific reaction rate constant and is primarily a function of temperature.

Associated with every forward reaction, there also exists a backward reaction, represented by Equation (37).

$$\sum_{i=1}^{N} \nu_i'' M_i \xrightarrow{k_b} \sum_{i=1}^{N} \nu_i' M_i \tag{37}$$

Therefore the net reaction rate in the presence of both forward and backward reaction is written as $\hat{\omega}_i = \hat{\omega}_{i,f} + \hat{\omega}_{i,b} = (\upsilon_i'' - \upsilon_i')(\omega_f - \omega_b) = (\upsilon_i'' - \upsilon_i')\omega$. Here ω is given by Equation (38):

$$\omega = k_f(T)\prod_{i=1}^{N} c_i^{\upsilon_i'} - k_b(T)\prod_{i=1}^{N} c_i^{\upsilon_i''} \tag{38}$$

The Arrhenius law gives the functional dependence of the reaction rate on temperature, which is shown in Equation (39), where A is a constant, β is temperature exponent and E_a is the activation energy of the reaction.

$$k(T) = AT^{\beta} e^{-E_a/RT} \tag{39}$$

The net source of chemical specie i in Equation (8) can hence be calculated through Equation (40), derived through manipulating those chemical kinetic equations. In this equation, $M_{w,j}$ is the molecular weight of specie i, N_R is the number of reactions.

$$R_j = M_{w,j}\sum_{r=1}^{N_R} \hat{R}_{j,r} \tag{40}$$

$$\hat{R}_{j,r} = (\nu_{j,r}'' - \nu_{j,r}'')(k_{f,r}\prod_{i=1}^{N}[C_{i,r}]^{\eta_{i,r}'} - k_{b,r}\prod_{i=1}^{N}[C_{i,r}]^{\upsilon_{i,r}''}) \tag{41}$$

The source of energy of every reaction is shown in

(42), where h_i^0 is the standard state enthalpy or heat of formation.

$$\frac{\Delta H_r^0}{RT} = \sum_{i=1}^{N}(\nu_{i,r}'' - \nu_{i,r}')\frac{h_i^0}{RT} \tag{42}$$

3.3.2 Eddy Dissipation Model

In some conditions, when the fuel is fast burning, the overall reaction is controlled primarily by turbulent mixing. Therefore, the combustion is said to be mixing limited and the chemical kinetic rate can be safely neglected.

In Eddy dissipation model, the net rate of production of specie i is given by Equation (43), where $Y_{\Re}$ is the mass fraction of a particular reactant, A and B are the empirical constants, $A = 4.0$, and $B = 0.5$.

$$R_{j,r} = \nu'_{j,r} M_{w,i} A \rho \frac{\varepsilon}{k} \min_{\Re} \left(\frac{Y_{\Re}}{\upsilon'_{\Re,r} M_{w,\Re}} \right) \tag{43}$$

3.3.3 PDF Model

The theory of non-premixed combustion is based on that the mixing is not sufficiently fast before the initiation of chemical reaction, therefore the mixing and reaction will take place only in thin reaction zones that separate them. Since an infinitely fast reaction rate is assumed here, the relevant factors controlling the combustion phenomena are the stoichiometric rats of transport of fuel and oxidizer.

In this model, the transport equations for one or two conserved scalars which are called mixture fractions are solved. Species concentrations are derived from the predicted mixture fraction fields through thermodynamic equilibrium calculation instead of solving each individual species transport equation. The interaction of turbulence and chemistry is therefore accounted for with an assumed shape PDF.

The mixture fraction can be written in the form shown in Equation (44).

$$f = \frac{Z_i - Z_{i,OX}}{Z_{i,\,fuel} - Z_{i,OX}} \tag{44}$$

Equation (45) and (46) are the transport equation for the Favre mean mixture fraction and mixture fraction variance, where σ_t, C_g and C_d is 0.85, 2.86 and 2.0 respectively.

$$\frac{\partial}{\partial t}(\rho\bar{f}) + \nabla\cdot(\rho\vec{v}\bar{f}) = \nabla\cdot(\frac{\mu_t}{\sigma_t}\nabla\bar{f}) + S_m \tag{45}$$

$$\frac{\partial}{\partial t}(\rho\overline{f'^2}) + \nabla\cdot(\rho\vec{v}\overline{f'^2}) = \nabla\cdot(\frac{\mu_t}{\sigma_t}\nabla\overline{f'^2}) + C_g\mu_t(\nabla\bar{f})^2 - C_d\rho\frac{\varepsilon}{k}\overline{f'^2} \tag{46}$$

For a single mixture faction system, the instantaneous values of mass fraction, density and temperature are calculated from Equation (47), where H is the instantaneous enthalpy.

$$\phi_i = \phi_i(f, H) \tag{47}$$

Then the probability density function p_f, which describes the temporal fluctuations of mixture mass fraction, can be used to compute averaged values of variables that depend on it. Equation (48) and (49) are to calculate the mean scalars and mean enthalpy.

$$\overline{\phi_i} = \int_0^1 \phi_i(f, \overline{H})p(f)df \tag{48}$$

$$\frac{\partial}{\partial t}(\rho\overline{H}) + \nabla\cdot(\rho\vec{v}\overline{H}) = \nabla\cdot(\frac{k_t}{c_p}\nabla\overline{H}) + S_H \tag{49}$$

The function p_f can be described by either double delta function or the β function.

3.3.4 NO_x model

NO_x emission consists of mostly nitric oxide, to a lesser degree nitrogen dioxide and nitrous oxide. It is a precursor for photochemical smog, contributes to acid rain, and caused ozone depletion. It is why it becomes one important problem in biomass combustion. Since its concentration is generally low, the NO_x chemistry has negligible influence on the

predicted flow field, temperature and major combustion product concentration. Therefore, the most efficient way is using NO_x model as a postprocessor after the main combustion calculation.

The transport equations for NO species are shown in Equation (50) to (53), where D is the effective diffusion coefficient.

$$\frac{\partial}{\partial t}(\rho Y_{NO}) + \nabla \cdot (\rho \vec{v} Y_{NO}) = \nabla \cdot (\rho D \nabla Y_{NO}) + S_{NO} \tag{50}$$

$$\frac{\partial}{\partial t}(\rho Y_{HCN}) + \nabla \cdot (\rho \vec{v} Y_{HCN}) = \nabla \cdot (\rho D \nabla Y_{HCN}) + S_{HCN} \tag{51}$$

$$\frac{\partial}{\partial t}(\rho Y_{NH_3}) + \nabla \cdot (\rho \vec{v} Y_{NH_3}) = \nabla \cdot (\rho D \nabla Y_{NH_3}) + S_{NH_3} \tag{52}$$

$$\frac{\partial}{\partial t}(\rho Y_{N_2O}) + \nabla \cdot (\rho \vec{v} Y_{N_2O}) = \nabla \cdot (\rho D \nabla Y_{N_2O}) + S_{N_2O} \tag{53}$$

The mechanism of NO_x production during the process of combustion is quite complicated, and can be categorized as thermal NO_x formation, prompt NO_x formation, Fuel NO_x formation and Intermediate formation. In this study, only first three mechanisms are considered.

Thermal NO_x formation

The principal reactions governing this formation mechanism are shown below in by Equation (54) to (56). They are a set of highly temperature dependent chemical reactions.

$$O + N_2 \leftrightarrow N + NO \tag{54}$$

$$N + O_2 \leftrightarrow NO + O \tag{55}$$

$$N + OH \leftrightarrow NO + H \tag{56}$$

The expressions for the rate coefficients for those equations are as follows.

$$k_{f,1} = 1.8\times10^{8} e^{-38370/T} \quad k_{r,1} = 3.8\times10^{7} e^{-425/T}$$

$$k_{f,2} = 1.8\times10^{4} T e^{-4680/T} \quad k_{r,2} = 3.81\times10^{3} T e^{-20820/T}$$

$$k_{f,3} = 7.1\times10^{7} e^{-450/T} \quad k_{f,1} = 1.7\times10^{8} e^{-24560/T}$$

Prompt NO_x formation

The amount of NO_x produced by prompt NO_x formation mechanism can be significant in some combustion environments, such as in low temperature, fuel rich conditions and where the residence times are short. The mechanism is given in Equation (57) to (61).

$$CH + N_2 \leftrightarrow HCN + N \tag{57}$$

$$N + O_2 \leftrightarrow NO + O \tag{58}$$

$$HCN + OH \leftrightarrow CN + H_2O \tag{59}$$

$$CN + O_2 \leftrightarrow NO + CO \tag{60}$$

$$CH_2 + N_2 \leftrightarrow HCN + NH \tag{61}$$

Fuel NO_x formation

The nitrogen containing organic compounds in biomass particles can contributed to the overall NO_x formation during the combustion process. Figure 3.1 shows a simplified model of the route leading to fuel NO_x formation.

In the case of biomass fuel, both HCN and NH_3 can be used as the intermediate species, each of which has different mechanisms.

Figure 3.1 Mechanism of fuel NO_x

NO_x Reduction

It has been well understood that a successful reduction of NO_x requires the control of a range of parameters including local stoichiometry, chemical concentration, residence time, velocity field and mixing pattern.

The most common methods employed by the industry are reburning NO_x and selective non-catalytic reduction of NO_x (SNCR).

When NO_x is considered to get re-burnt, two models are used, called instantaneous approach and partial equilibrium approach. The first model is shown in Equation (62), and the second model is shown in Equation (63) to (65).

$$CH_i + NO \rightarrow HCN + products \tag{62}$$

$$CH_2 + NO \rightarrow HCN + OH \tag{63}$$

$$CH + NO \rightarrow HCN + O \tag{64}$$

$$C + NO \rightarrow CN + O \tag{65}$$

SNCR is a method to reduce the emission of NO_x from combustion by injecting a selective reactant such as ammonia or urea into the furnace. Since those reactants can be oxidized as well to form NO_x, which decrease their selectivity with temperature increasing, the SNCR process is limited to a narrow temperature interval.

In this research, Urea in injected into the boiler as NO_x reduction reagent. The mechanism is shown in Equation (66) to (72).

$$NH_3 + NO \rightarrow N_2 + H_2O + H \tag{66}$$

$$NH_3 + O_2 \rightarrow NO + H_2O + H \tag{67}$$

$$HNCO + M \rightarrow NCO + M + H \tag{68}$$

$$NCO + NO \rightarrow N_2O + CO \tag{69}$$

$$NCO + OH \rightarrow NO + CO + H \tag{70}$$

$$N_2O + OH \rightarrow N_2 + O_2 + H \tag{71}$$

$$N_2O + M \rightarrow N_2 + O + M \tag{72}$$

3.4 Radiation

Equation (73) is the radiation heat transfer equation for an absorbing, emitting, and scattering medium at position $\vec{r}$ in the direction $\vec{s}$.

$$\frac{dI(\vec{r},\vec{s})}{ds} + (a+\sigma_s)I(\vec{r},\vec{s}) = an^2\frac{\sigma T^4}{\pi} + \frac{\sigma_s}{4\pi}\int_0^{4\pi} I(\vec{r},\vec{s})\Phi(\vec{s},\vec{s}')d\Omega' \tag{73}$$

In this research, P-1 radiation model is chosen, which is based on the expansion of the radiation intensity I into an orthogonal series of spherical harmonics. In this model, the

radiation flux q_r is calculated using Equation (74), where a is the absorbing coefficient, σ_s is the scattering coefficient, G is the incident radiation, and C is the linear-anisotropic phase function coefficient.

$$q_r = -\frac{1}{3(a+\sigma_s)-C\sigma_s}\nabla G \tag{74}$$

With the expression that $\Gamma = 1/(3(a+\sigma_s)-C\sigma_s)$, Equation (74) is transformed into Equation (75).

$$q_r = -\Gamma \nabla G \tag{75}$$

Therefore the transport equation for G is expressed as Equation (76),

$$-\nabla \cdot q_r = aG - 4a\sigma T^4 \tag{76}$$

3.5 Discrete Phase Model

The discrete phase (solid fuel particles) in this research is modeled using Lagrangian approach, which tracks a large number of particles through the flow field. During this process, the dispersed phase can exchange momentum, mass and energy with the fluid phase.

The fundamental assumption behind this model is that the discrete phase only occupies a low volume fraction of the fluid field, which is automatically satisfied in the case of biomass combustion inside the boiler.

3.5.1 Lagrange Equation of Translation

Equation (77) is the general equation used to calculate the trajectory of a particle, whose theory is based on Newton's second Law.

$$m_p \frac{du_p}{dt} = F_{g+} F_p + F_a + F_d + F_l + F_v + F_A \tag{77}$$

In this equation, F_g is the reduced gravity force, F_p is the pressure gradient force, F_a is the added mass force, which is also called virtual mass force, representing the force required to accelerate the fluid surrounding the particle, F_v is volume change force and a is the radius of the particle. The equations to calculate those terms are shown in Equation (78) to (81) separately.

$$F_g = (\rho_p - \rho_f) m_p \vec{g} \tag{78}$$

$$F_p = -\frac{m_p}{\rho_p} \nabla p \tag{79}$$

$$F_a = -\frac{1}{2} \rho_f \frac{m_p}{\rho_p} \left(\frac{du}{dt} - \frac{du_p}{dt}\right) \tag{80}$$

$$F_v = 2\pi a^2 \rho_f (u - u_p) \frac{da}{dt} \tag{81}$$

In those equations, F_d is drag force, F_l is lift force and F_A is the sum of particle forces including elastic collision forces, which are introduced in the following individual sections.

3.5.2 Fluid Forces

The other two terms on the right side of Equation (77) are F_d and F_l, representing the drag force and lift fore separately, which are called fluid forces.Generally, drag fore is the dominant fluid force for small particles, its general expression of drag force is shown as Equation (82), where C_D is the drag coefficient, whose value varies depending on the problem and the type of particles.

$$F_d = \frac{1}{2} C_D \pi a^2 \rho_f |u - u_p| (u - u_p) \tag{82}$$

Schiller used Equation (83) to calculate the drag coefficient of a solid sphere is a dilute fluid field, where Re_p is Reynolds number of particle, calculated through Equation (84).

$$C_D = \frac{24}{\mathrm{Re}_p}(1 + 0.15\,\mathrm{Re}_p^{0.687}) \tag{83}$$

$$\mathrm{Re}_p = \frac{2\rho_f |u - u_p| a}{\mu} \tag{84}$$

Later Moris and Alexander chose Equation (85) to obtain drag coefficient, where a_1, a_2 and a_3 are constants that apply over several ranges of Re_p.

$$C_D = a_1 + \frac{a_2}{\mathrm{Re}_p} + \frac{a_3}{\mathrm{Re}_p^2} \tag{85}$$

In 1989, Haider and Leverspiel developed another correlation, shown in Equation (86) to calculate the drag force for non-spherical particles.

$$C_D = \frac{24}{\mathrm{Re}_{sph}}(1 + b_1 \mathrm{Re}_{sph}^{b^2}) + \frac{b_3 \mathrm{Re}_{sph}}{b_4 + \mathrm{Re}_{sph}} \tag{86}$$

The constant in this equation are as follows, where $\phi = s/S$ is the shaper factor with s as the surface area of a sphere having the same volume as the particle and S as the actual surface area of the particle, and Re_{sph} is computed with the diameter of a sphere having the same value.

$$\begin{cases} b_1 = \exp(2.3288 - 6.4581\phi + 2.4486\phi^2) \\ b_2 = 0.0964 + 0.5565\phi \\ b_3 = \exp(4.905 - 13.8944\phi + 18.4222\phi^2 - 10.2599\phi^3) \\ b_4 = \exp(1.4681 + 12.2584\phi - 20.7322\phi^2 + 15.8855\phi^3) \end{cases} \tag{87}$$

In the case of dense particle flow, the drag coefficient is expressed as Equation (88), where f is the friction factor, calculated from Equation (89).

$$C_D = \frac{24}{\mathrm{Re}_p} f \tag{88}$$

$$f = (1-c)^{-\beta} \tag{89}$$

In Equation (89), c is the local particle concentration (i.e., the ratio of the particle volume to the fluid volume in a small region around the particle) and β is given by

$$\beta = 3.7 - 0.65 \exp\left[-\frac{1}{2}\left[1.5 - \ln(\mathrm{Re}_p)\right]^2\right] \tag{90}$$

When a particle is placed in a shear flow, the fluid exhibits a lift force in the direction normal to the direction of the flow. If the particle is assumed to rotate at the same rate as the local rotation rate of fluid particles, the lift force solution of Saffman (1965) is shown in Equation (91).

$$F_l = \frac{1}{2} C_L \rho_f \pi a^2 \left|u - u_p\right| (u - u_p) = \frac{3}{8} \rho_f \frac{m_p}{\rho_p} C_L \left(\frac{(u - u_p) \times \omega}{\alpha}\right) \tag{91}$$

In this equation, $\alpha = \left|\omega\right| a / \left|u - u_p\right|$, and the lift coefficient is calculated by Saffman model (1965) shown in Equation (92) .

$$C_L = 5.82\, \mathrm{Re}_p^{-1/2} \alpha^{1/2} \tag{92}$$

3.5.3 The Collision Forces of Particles

The collision forces acting on the particles are decomposed into four parts: that acting along the line normal to the particle centers and the resisting from sliding, twisting, and rolling of one particle over another, as shown in Figure 3.2 [80]. Therefore the total collision and adhesion forces on particle can be written as Equation (93), where the unit vector n is pointing tangent two the line connecting the center of two particles, t_s is the direction of relative motion of the particle surfaces at the contact point projected onto the contact plane.

$$F_A = F_n n + F_s t_s \tag{93}$$

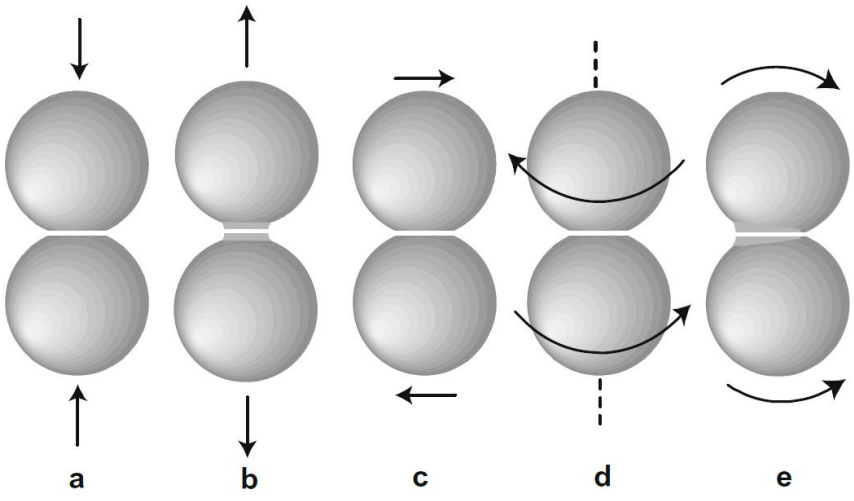

Figure 3.2 Models of particle interactions: (a) normal impact, (b) necking in normal extension, (c) shearing, (d) twisting, and (e) rolling

Normal forces

The normal forces mainly consist of two parts: one is due to the elastic deformation of the particles and the other one is caused by the energy losses during of normal particle impact.

Considering two particles with the radii r_i and r_j, elastic moduli E_i and E_j, and shear moduli $G_i = E_i / 2(1+\sigma_i)$ and $G_j = E_j / 2(1+\sigma_j)$. An effective particle radius R, effective elastic E and effective shear moduli G are defined in Equation (94) to (96).

$$\frac{1}{R} = \frac{1}{r_i} + \frac{1}{r_j} \tag{94}$$

$$\frac{1}{E} = \frac{1-\sigma_i^2}{E_i} + \frac{1-\sigma_j^2}{E_j} \tag{95}$$

$$\frac{1}{G} = \frac{2-\sigma_i}{G_i} + \frac{2-\sigma_j}{G_j} \tag{96}$$

The particle normal overlapping distance δ_N is defined by Equation (97), where x_i and x_j denote the centroid positions of two particles.

$$\delta_N = r_i + r_j - \left| x_i - x_j \right| \tag{97}$$

The elastic response F_{ne} is obtained by Hertz et al. [81] in Equation (98), where the stiffness coefficient $K = 4E\sqrt{R}/3$.

$$F_{ne} = -k_N \delta_N = -K \delta_N^{3/2} \tag{98}$$

The dissipation force F_{nd} is given by Equation (99), where $v_R = v_{Ci} - v_{Cj}$ ($v_{Ci} = v_i + \Omega_i \times r_i$).

$$F_{nd} = -\eta_N v_R \cdot n \tag{99}$$

Sliding resistance

The model proposed by Cundal et al. [82] is adopted to calculate the sliding resistance, shown in Equation (100) and (101), where the critical value $F_{crit} = \mu_f |F_n|, \mu_f = 0.3$.

$$F_s = -k_T(\int_{t_0}^{t} v_S(\xi)d\xi) \cdot t_S - \eta_T v_S \cdot t_S \ , |F_s| < F_{crit}, \tag{100}$$

$$F_s = -F_{crit}, \ |F_s| \geq F_{crit} \tag{101}$$

The slip velocity $v_S = v_R - (v_R \cdot n)n$ is the tangent projection of v_R to the particle surface at the contact point. K_T is derived by Mindlin et al. [83], shown in Equation (102), and $\eta_T = \eta_N$, assumed by Tsuji et al. [84].

$$k_T = 8Ga(t) \ , \ a(t)^2 = R\delta_N \tag{102}$$

3.5.4 Lagrange Equation of Rotation

The angular momentum is described by Equation (103), where $I_p = md^2/10$ is the particle momentum of inertia, M_F denotes the fluid torques and M_A is the sum of other types of torques exerted on the particle. The torque is calculated by using the forces obtained at last section.

$$I_p \frac{d\Omega}{dt} = M_F + M_A \tag{103}$$

3.5.5 Modifications Due to Van der Waals Adhesion

In Johnson's model [85], there is van der Waals adhesive force will acts within the flattened contact region between particles. The normal forces are modified in the presence

of van der Waals force, as shown in Equation (104), where $F_C = 3\pi\gamma R$, $a_0 = (9\pi\gamma R^2 / E)^{1/3}$.

$$\frac{F_{ne}}{F_C} = 4\left(\frac{a}{a_0}\right)^3 - 4\left(\frac{a}{a_0}\right)^{3/2} \tag{104}$$

The effect of van der Waals adhesion on tangential sliding force was modeled a simplified model provided by Thornton [86]. This simplified approach uses the same expressions developed for the case with no adhesive force, but replace the critical sliding force by Equation (105).

$$F_{crit} = \mu_f \left| F_{ne} + 2F_C \right| \tag{105}$$

3.5.6 Time Scale

The simulation of fluid with particle phase involves a number of different time scales: the largest one T_F associated with the fluid flow, the particle aerodynamic response time scale T_P and the particle collision time scale T_C, expressed in Equation (106) to (108).

$$T_F = \frac{L}{U} \tag{106}$$

$$T_P = \min(T_{CP}, T_{AP}), T_{CP} = \frac{d}{U}, \; T_{AP} = T_F \frac{\rho_p d^2 U}{18\mu L} \tag{107}$$

$$T_C = d(\rho_p{}^2 / E_p{}^2 U)^{1/5} \tag{108}$$

A computational algorithm developed by Marshall [80] is developed to study the fluid with particle phase under these three different time scale, shown in Figure 3.3, which is not only true to the physics of particle movement, but also consisted with the demands of rapid computation for large number of particles.

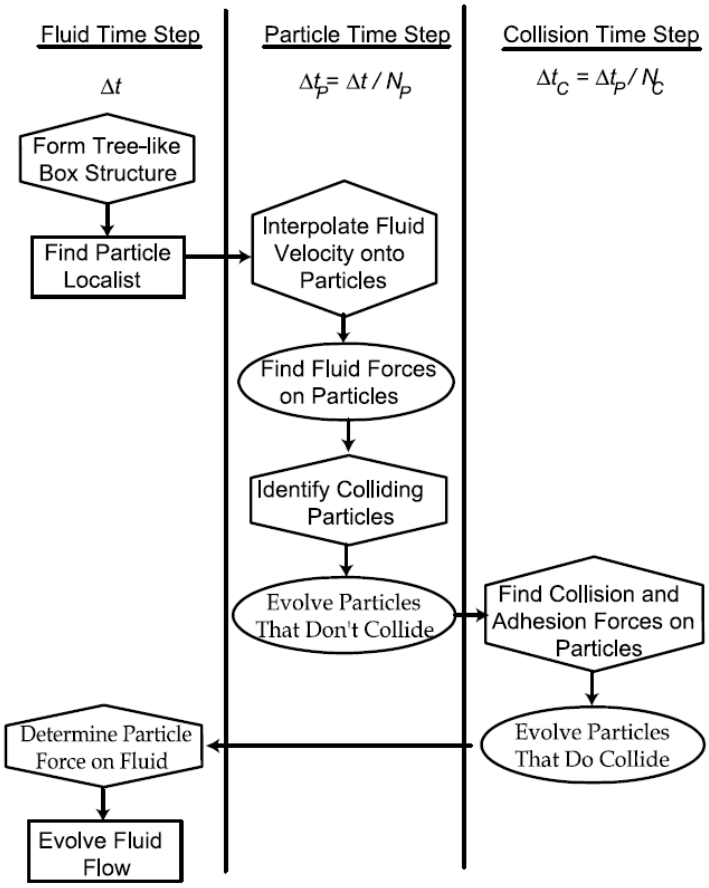

Figure 3.3 Algorithm

3.5.7 Particle Stages in Fluid

During the process of combustion, the biomass particle experiences three stages in the fluid after being injected into the boiler: initial heating, releasing volatile species and char combustion.

Heating

At this first stage, biomass particle is heated rapidly by both the convective heat and absorption of radiation at the surface. This progress is represented by Equation (109),

where A_P is the surface area of particle, T_∞ is the local temperature of the continuous phase, h is the convective heat transfer coefficient, ε_P is the particle emissivity and θ_R us the radiation temperature.

$$m_p c_p \frac{dT_p}{dt} = hA_p(T_\infty - T_p) + \varepsilon_p A_p \sigma(\theta_R{}^4 - T_p{}^4), \quad T_p < T_{vap} \tag{109}$$

Devoltalization

When $T_p \geq T_{vap}$, the devolatilization process begins, which are described by two models. In the first model, the devolatilization of biomass particle is considered as a single rate reaction with one compound volatile matter, therefore the reaction rate is given in Equation (110) with a reaction coefficient $k = A_1 e^{-(E/RT)}$, and the particle temperature is described in Equation (111), where $f_{w,0}$ is the mass fraction of the volatile matte, h_{fg} is the latent heat.

$$-\frac{dm_p}{dt} = k[m_p - (1 - f_{v,0})m_{p,0}] \tag{110}$$

$$m_p c_p \frac{dT_p}{dt} = hA_p(T_\infty - T_p) + \varepsilon_p A_p \sigma(\theta_R{}^4 - T_p{}^4) + \frac{dm_p}{dt} h_{fg} \tag{111}$$

In the second model, the major species released are modeled separately, which enable a more accurate physics of devolatilization. Equation (112) shows the mass change of each species.

$$-\frac{dm_{p,i}}{dt} = k[m_p - (1 - f_{v,0})m_{p,0}] \tag{112}$$

Char surface combustion

For the surface combustion of biomass particle: $char(C) + S_b O2 \rightarrow products$, the diffusion limited surface reaction rate model is used in this study, shown as Equation (113),

where $D_{i,m}$ is the diffusion coefficient for oxidant in the bulk, Y_{OX} is the local mass fraction of oxidant in the gas and S_b is the stoichiometry of oxidization equation of char.

$$\frac{dm_p}{dt} = -4\pi d_p D_{i,m} \frac{Y_{OX} T_\infty \rho}{S_b (T_p + T_\infty)} \tag{113}$$

3.5.8 Coupling

The interaction between particle and continuous phase is achieved through coupled method, like shown in Figure 3.4.

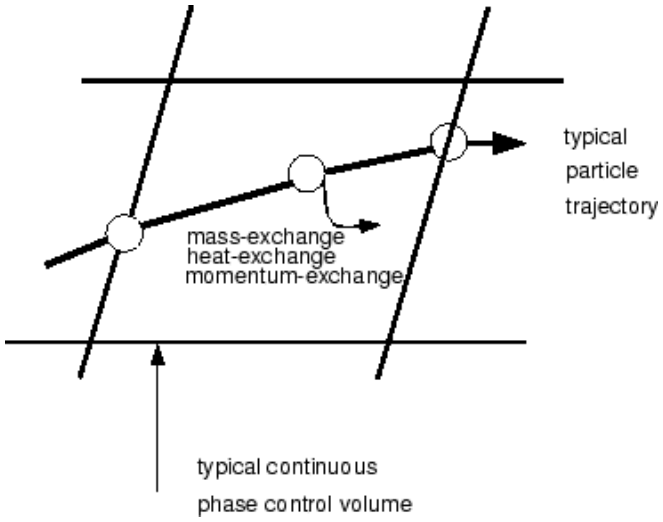

Figure 3.4 Interactions between discrete and continuous phases

Equations (114) to (117) show separately the mass, momentum and heat exchanges between the phases.

$$M = \frac{\Delta m_p}{m_{p,0}} \dot{m}_{p,0} \tag{114}$$

$$F = \sum (\frac{18\mu C_D \,\mathrm{Re}}{\rho_p d_p^2 24})(u_p - u) + F_{other})\dot{m}_p \Delta t \tag{115}$$

$$Q = \frac{\dot{m}_{p,0}}{m_{p,0}}[(m_{pin} - m_{pout})(-H_{lat,ref}) - m_{pout}\int_{T_{pout}}^{T_{pout}} cp_p dT + m_{pin}\int_{T_{ref}}^{T_{pin}} cp_p dT] \tag{116}$$

$$H_{latref} = H_{lat} - \int_{T_{ref}}^{T_{p,init}} cp_g dT + \int_{T_{ref}}^{T_{p,init}} cp_p dT \tag{117}$$

CHAPTER 4: EXPERIMENTS AND DATA PROCESSING

Experimental method holds an important role in numerical modeling of biomass combustion in many aspects. It provides those critical parameters needed for modeling boundary conditions. It is also used to correct the sub-models describing the physics and gasification process of biomass particle. More important, it serves to verify and validate the CFD model and makes its predications fundamentally convincing. For those reasons above, some necessary experiments have been designed and conducted in this work. Those experiments include a temperature measurement campaign employed in the Power Plant of the University of Iowa, the lab researches on oat hulls' chemical and physical properties and an oat hulls gasification induced by high heat flux. The validation and correction made through those experiments enable this CFD model's predictions physically correct and rationally instructive for engineering optimum design.

4.1 Temperature Measurement of Unit10

Figure 4.1 is the scheme of the University of Iowa Power Plant's stoke boiler Unit 10, which is the prototype of the CFD model in this work. During the past several years, it has been the test bed for a range of innovative biomass combustion experiments. Unit 10 consists of three major sections as shown in Figure 4.1 and 4.2: the coal bed section including the primary air injection system under the grate and a moving grate, the free board section consisting of the air above the grate and the secondary air injecting system, and the heat exchanger section made of the heat exchanger and a drum system.

A few works introduced in chapter 3 include some measurement plans carried out on some full scale grate boilers and fluidized boilers. These plans, some of whom are shown in Figure 4.3, are all sharing a common feature that the measurement should be conducted on

different horizontal planes crossing the boiler. This kind of arrangement is aimed at getting a fuller view of temperature field and species concentration inside the boilers.

However due to technical constrains, most of those experiments only collect a limited amount of data, providing scant information for the purpose of validation. Moreover, most of the tests are carried out on just one working case. This then raises questions on the applicability of the validated model. Therefore the primary goal of the temperature measurement test in this work is to enhance the effect of validation of the CFD model. In the final plan, more than 60 test locations are picked under different working conditions, aiming at drawing a more complete picture of the temperature inside the furnace.

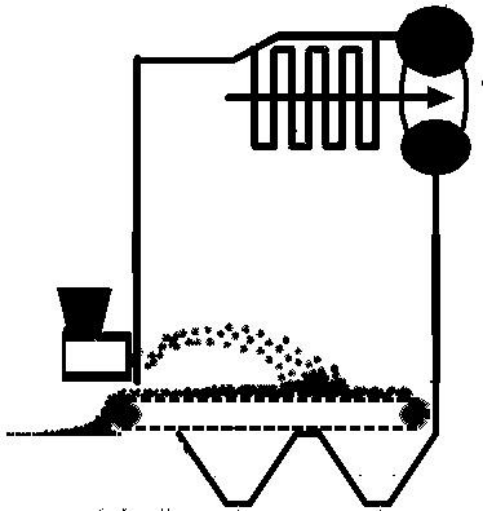

Figure 4.1 Boiler

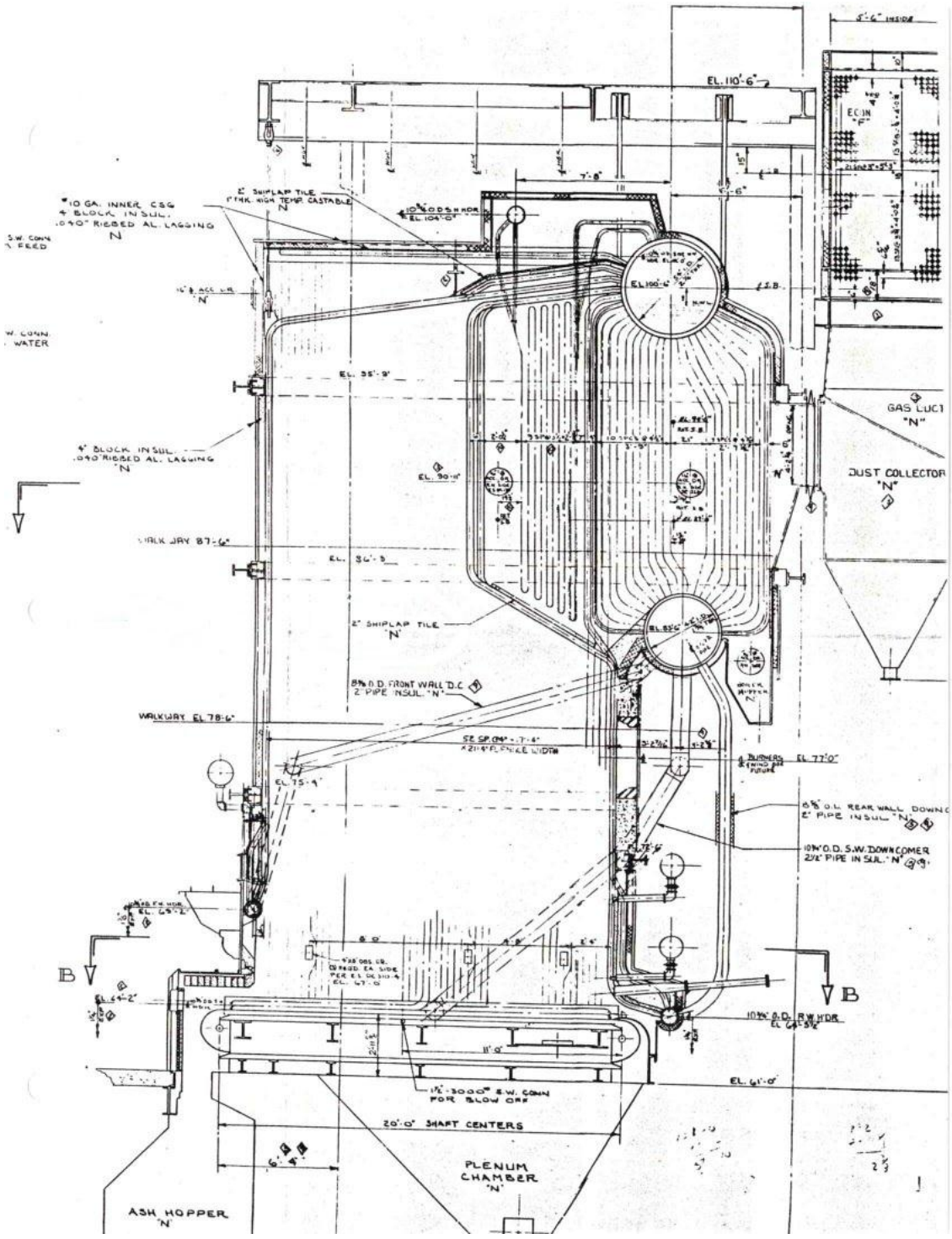

Figure 4.2 Cross section of Unit 10

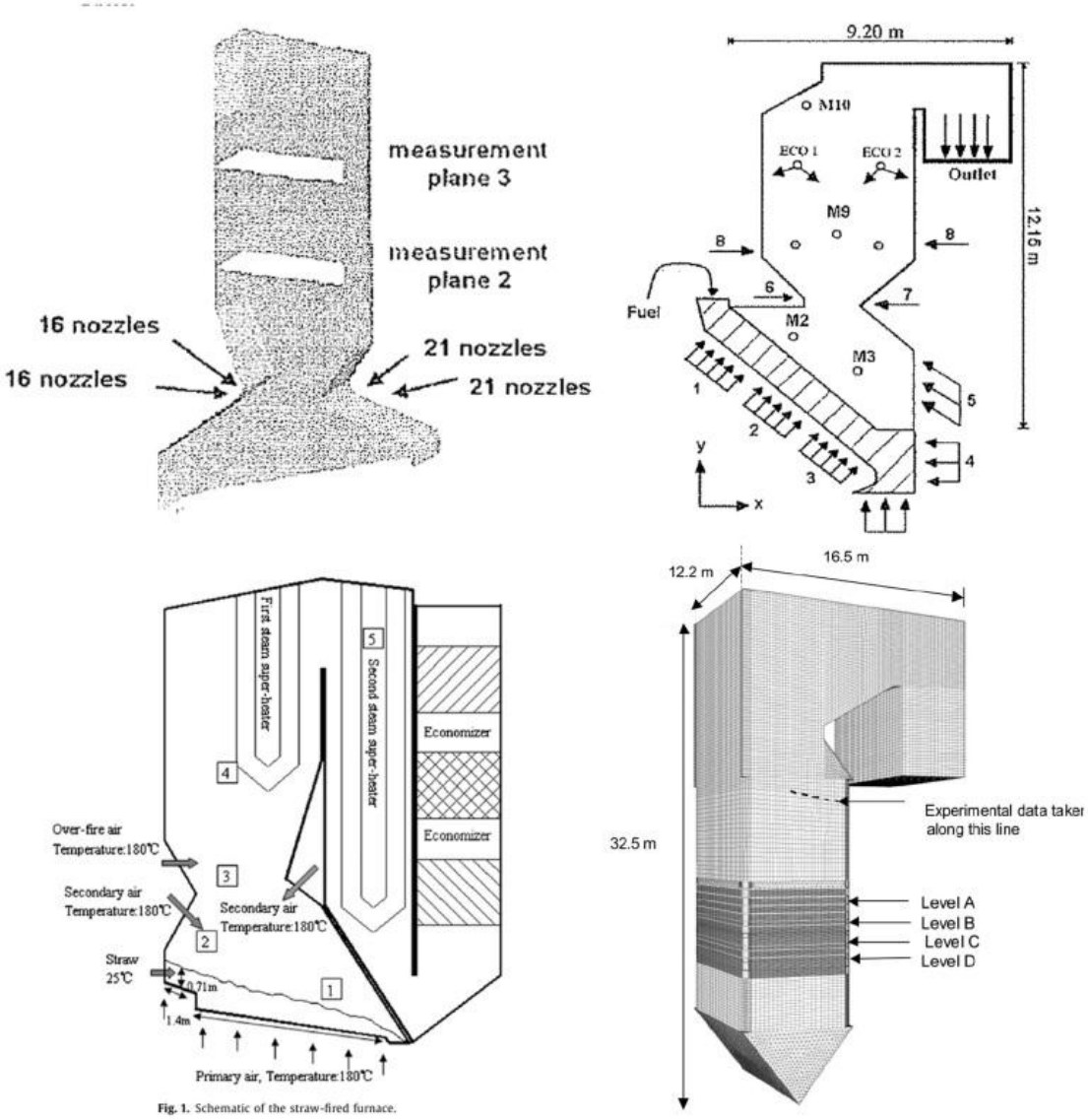

Fig. 1. Schematic of the straw-fired furnace.

Figure 4.3 Examples of temperature measurement plans

4.1.1 Test Scheme

Unit 10 is a closed combustion facility, having a rough dimension of $7 \times 7 \times 12.5$ m. Its chamber is located in the first floor of University of Iowa Power Plant, surrounded by another two fluidized boilers and some facilities like pump, monitors and supporting frames.After a careful on-site inspection, the measurement scheme is finalized as what is shown in Figure 4.4. In this test plan, the observation windows on the north and south walls of Unit 10 are engaged. Because of the confined space and the premise of avoiding the interference with Unit 10's normal operation, there are four windows considered as available for the test, among which three locate on the north side (N1, N2 and N3) and one locates on the south side (S2). A 3.65 m long HVT (high velocity thermocouple) probe with a stainless steel sheathed "type C" thermocouple at the front end will be gradually put through those windows with an angle. The temperature value will be read at every 0.3 m interval crossing the horizontal plane the observation windows belong to.

The inspection also shows that readings of temperatures with angles other than zero are significantly challenging for several reasons. The primary reason is the compacted space near these windows, which causes the 3.65 m long port hitting the nearby steel stairs when it is poised with angles. The second main reason results from the small coal particles flowing around the test area. The particle tends to flow into the probe shield when the port is upward or downward erected, causing the test failure due to the blockade of the shield. Therefore in the real test, the total number of data collected with angles other than zero is just five.

Since Unit 10 is running in full load of coal to provide electric power for the university campus, it makes the test of co-firing oat hulls with coal not available. Therefore this test is conducted merely on coal combustion of Unit 10. As for co-firing oat hulls in the grate boiler at different percentage, it is important for this comprehensive model to correctly predict the coal bed combustions at different load of coal. So two working conditions: 19.5

kg/s and 15.1 kg/s steam flows were measured separately during the test. The data for the first working condition is for validating the simulation results and that for the second condition is for examining the capability of the numerical model of calculating the problem at different working load. The data collected is then used to validate the simulation of pure coal combustions which serves as a baseline model. Below is the procedure of the test at one observation window.

1. Configuring the probe

The middle of the probe was put on a metal brace, with both its front end and back end supported by members of the test team.

2. Inserting the probe into the boiler

The people carrying the front end of the probe, where the thermal couple is located (which has a ceramic shield surround), opened the observation window and inserted the probe into the boiler to the depth specified.

3. Reading the temperature

The thermal couple was connected with a digital meter which displayed the reading. The temperature value was recorded when the probe temperature was stabilized, which was taken as a period of several seconds with no change in the value.

4. Monitoring the temperature of the cooling water

During the above processes, the temperature of the cooling water in the probe was monitored to ensure it wasn't above the critical value (which would indicate damage to the thermocouple).

5. Repeating step 3 and 4 until the test at the observation window is finished

The thermocouple grade is between 473 K and 1523 K. The standard error is ±0.75 % above freezing point. The thermocouple reader is the Multi-Type Calibrator Thermometer (115V) of EXTECH with a maximum accuracy to ±0.15%. Taking into consideration of the procedure of the test, the overall test accuracy is about ±1.5%.

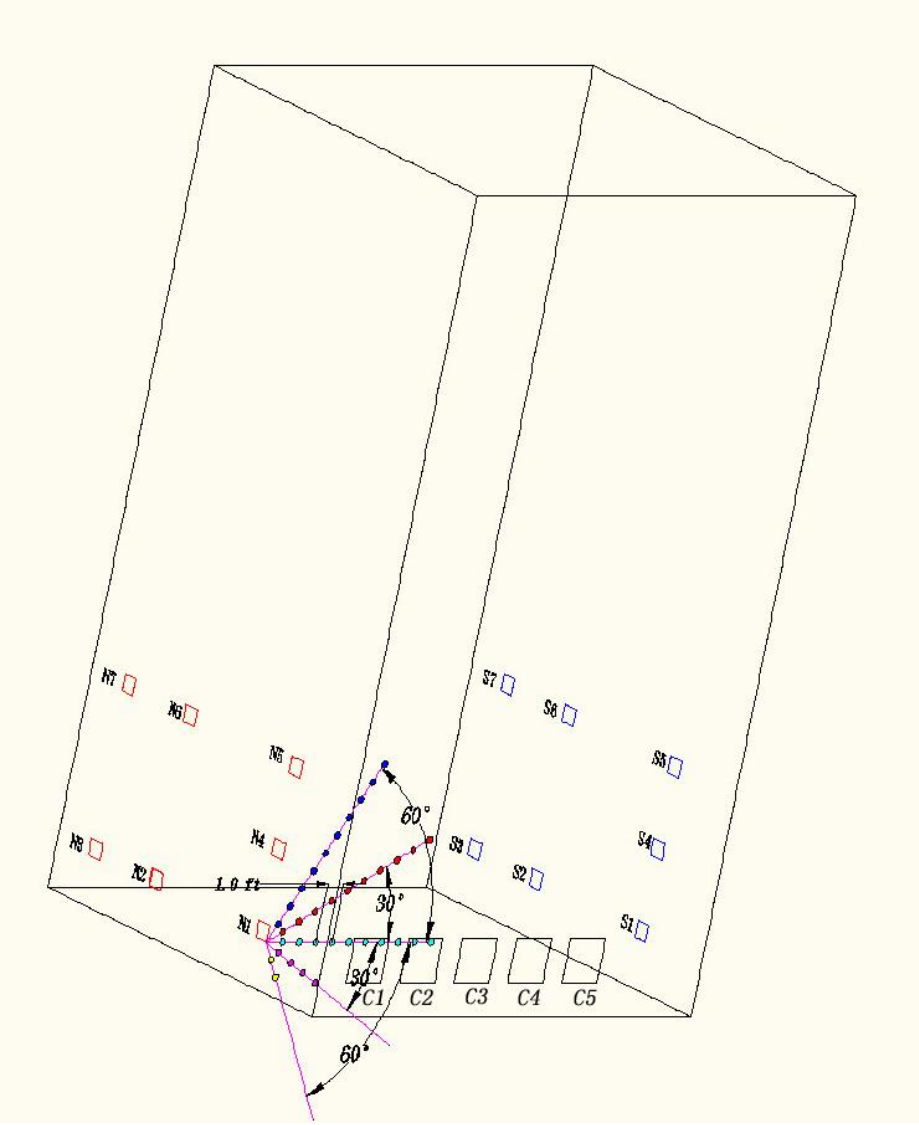

Figure 4.4 Measurement scheme for the N1 window.

Note:

N1 – N7: Windows on north wall.

S1 – S7: Windows on south wall.

C1 – C5: Coal feeders

4.1.2 Measurement Results

This test campaign was conducted in two working days, some scenes of which are shown by the following figures. Figure 4.5 is the front view of Unit 10, showing five coal feeders with air flow systems. Figure 4.6 is the view of north wall, with three observation window shown. Figure 4.7 is one photo showing how the test is conducted. Figure 4.8 is front end of the probe after being pulled out from the window.

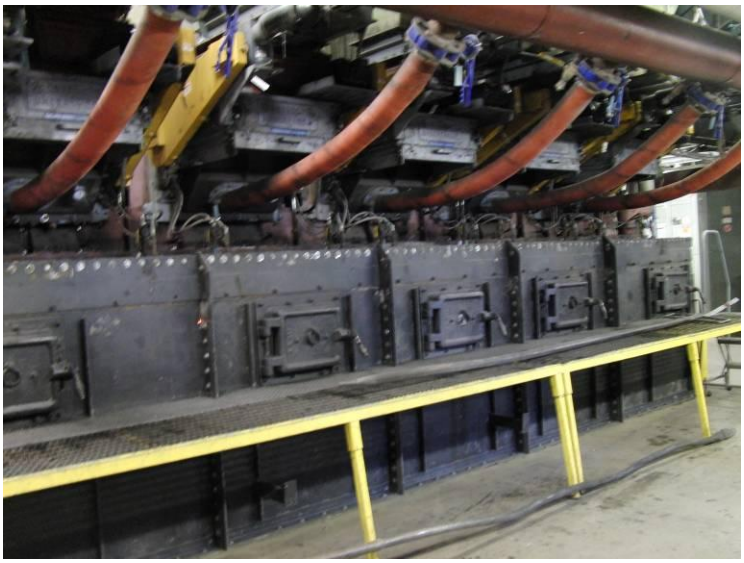

Figure 4.5 The front view of Unit 10

Figure 4.6 The view of north wall, with three observation windows shown

Figure 4.7 The test being conducted

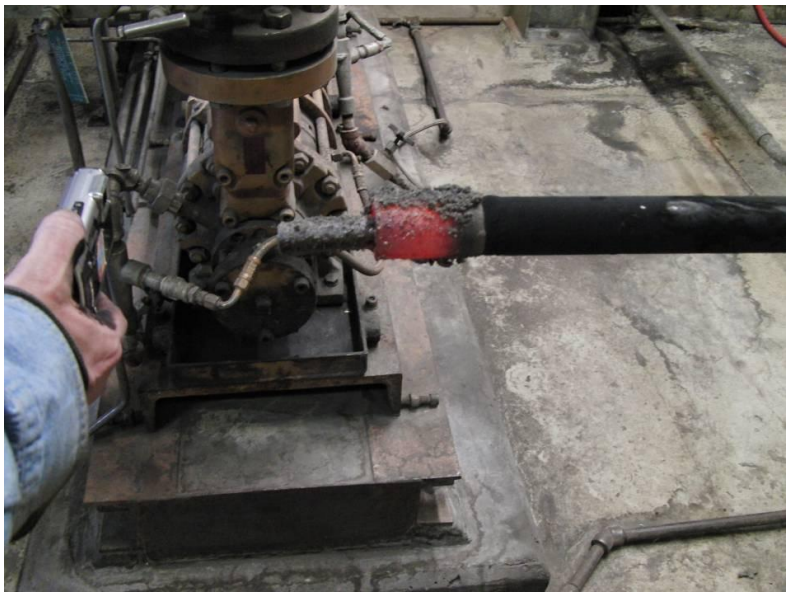

Figure 4.8 The front end of the probe is pulled out from the window

The facilities involved in this test include a type ‘C’ thermal couple inserted into the probe, a ceramic shield used to compensate the heat loss due to radiation, an air flow gun for sucking flue gas into the probe, a water cooling system for the probe, and a portable thermal meter managing the temperature of cooling water.

4.1.3 Date Analysis

For the reason of technical convenience, the majority of the test locations are on the plane of observation windows. The temperature measurements under the working condition of 2.58 kg/min are firstly applied in all the four windows, shown in Table 4.1. Then the measurements of working condition of 2 kg/min are deployed in window N2 and N3, shown in Table 4.2, being prepared for further comparisons. Some temperature values at scattered locations are also measured, shown in Table 4.3. Those locations at different heights are chosen to depict a fuller view of the temperature field above grate.

Table 4.1 Temperatures (K) for a the steam flow rate of 2.58 kg/min steam

Points	1	2	3	4	5	6	7	8	9	10
N1	650	652	678	906.48	1175	872.59	899.82	1134.26	1065.93	839.817
N2	1554.8	1531.5	1542	1529.3	1512	1510.4	1514.3	1540.9	1555.9	N/A
N3	1088.7	1175.9	1177	1369.3	1402	1346.5	1374.8	1374.8	1328.7	1370.4
S2	1366.5	1422	1422	1366.5	1416.4	1535.9	1491.5	1549.8	1548.2	1537.6

Table 4.2 Temperatures (K) for a the steam flow rate of 2 kg/min steam

Points.	1	2	3	4	5	6	7	8	9	10
N2	1229.3	1287.6	1288.7	1272	1269.8	1268.7	1282	1290.4	1298.7	1414.8
N3	1255	1222	1250	1319	1402	1440	1469	1612	1690	1890

Table 4.3 Temperatures (K) in different heights

	2.58 kg/min steam			2 kg/min steam	
No.	1	2	3	4	5
Temperature (K)	944.3	1052.6	1249.8	1040.9	1133.7
X (m)	1.45	1.45	1.45	1.45	1.45
Y (m)	2.21	2.97	0.92	3.01	2.67
Z (m)	-5.69	-4.37	-4.01	-5.56	-4.90

The fact that the readings at symmetric locations from window N2 and S3 shows a significant difference of temperature implicate that Unit 10 is not working according to the symmetric design for some reasons. One possibility is that under the current operation condition, Unit 10 is running asymmetrically. Another explanation is that the sampling procedure like opening the window will also interfere with the temperature field. Also the temperature readings from window N1 show an intense variance due to the fact that this window locates closely to the coal feeders. All these factors need to be taken into considerations in the process of comparisons.

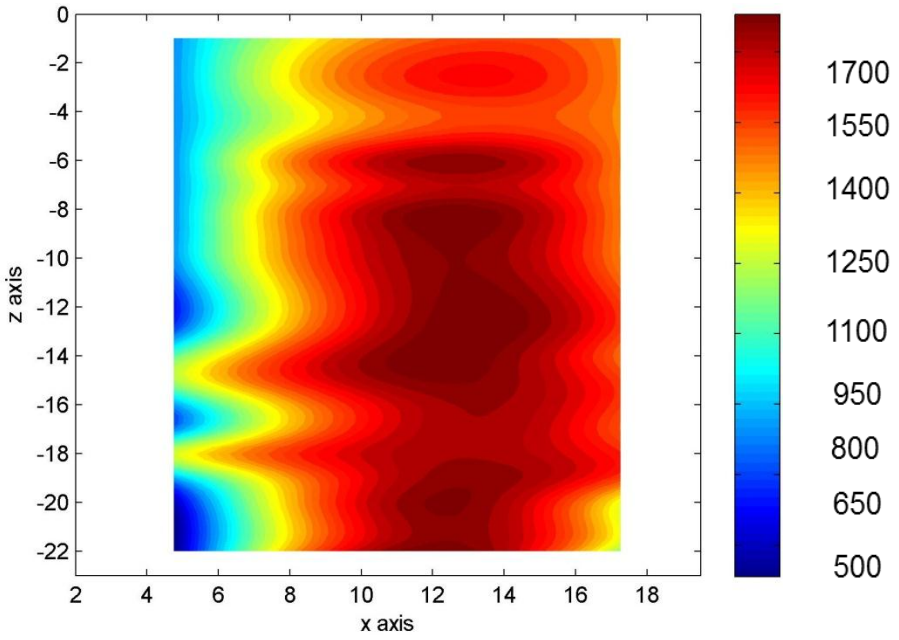

Figure 4.9 The temperature contour (K) in the measuring plane

Two dimensional plot of the temperature contour of that plane for the working condition of 2.58 kg/min is obtained, shown in Figure 4.9. Due to the uneven distribution of coal along the grate, the peak temperature area is expected to be about in the middle of

the grate. The highest temperature readings from window N2 and S2 convincingly prove this assumption. A similar pattern of variance is further adopted to model the coal bed in the numerical model developed in this work

4.2 Biomass Physical Property Test

The biomass fuel studied in this research is oat hulls, whose photo is shown in Figure 4.10. It is a granular agricultural waste product in a minimally processed form (not ground). The usage of it is propelled by a project of co-firing oat hulls with coal in the stoke boiler Unit 10 conducted by The University of Power Plant. It is estimated that through this project the University can decrease carbon dioxide emissions by 72 million kilograms (72,000 tons) annually [87] and reduce SO_2, NO_2, CO and particulate emissions. Meanwhile, the food company producing oat hulls as the by-product during its manufacturing procedure can avoid the landfill disposal fees and make profit by selling it. Therefore it becomes necessary to conduct series of lab analysis about oat hulls

Figure 4.10 Photo of oat hulls

4.2.1 Chemical Analysis

The primary lab analysis of oat hulls has been done by Babcock Power in its engineering study required by the University Power Plant, whose results are shown in Table 4.4 and Table 4.5. For the purpose of comparison, the chemical and physical properties of Eastern Bituminous coal and oat hulls are both presented in it. The lab chemical analysis shows that different with coal, oat hulls contain a higher moisture and volatile matter, while processing a significantly lower density. Those variances will thus results in changed patterns of combustion performance on Unit 10 in the aspects such as pollutant emissions, combustion mixing, and the overall efficiency.

Table 4.4 Proximate analysis of oat hulls

	Oat Hulls Proximate Analysis wt%	Coal Proximate Analysis wt%
Moisture	10.43	5.85
Volatile matter	67.8	35.61
Fixed Carbon	16.55	47.94
Ash	5.22	10.6
Total	100.0	100
HHV [KJ/Kg]	16118	28470
Density [Kg/m3]	143.69 (ungrounded)	1346

Table 4.5 Ultimate analysis of oat hulls

	Oat Hulls Ultimate Analysis wt%	Coal Ultimate Analysis wt%
Moisture	10.43	5.85
Carbon	43.51	68.16
Hydrogen	4.71	4.77
Nitrogen	0.65	1.54
Oxygen	35.44	7.78
Sulfur	0.04	1.3
Ash	5.22	10.6
Total	100.0	100

4.2.2 Oat Hulls Physical Property

Unlike pulverized coal particles, which can be regarded as a group of uniform spheres or spheres with a distribution of radius, biomass particle are mainly cylinder or slab and furthermore holds a wide range of shape and size. In this specific case of oat hulls particles, it is more appropriate to consider them as groups of cylinders or hollowed cylinders. The volatile matter released from the oat hulls' particle and the its surface char combustion will carry out a significantly different pattern from that of pulverized coal particles, since the fluid forces acted on the particle will be different and its larger relative surface will cause an increased reaction rate. Those differences will further couple with the turbulent mixing and combustion inside the boiler. Correctly and properly describing the shape and size of

oat hulls particle therefore becomes critically important during the process of developing the CFD model.

Motivated by this goal, a measurement of oat hull particle's physical properties is deployed. In this test, oat hulls particles are treated as cylindrical particles with different radius and length which are considered as the major characters to describe the particles.

A sample group of oat hulls particles (141 pieces) was chosen by random, on each of which the measurement of particle length and radius is applied. After the measurement was finish, those oat hulls particles were then categorized under three criteria: length, shape factor and equivalent shape diameter. Table 4.6 presents the results of measurement of oat hulls particles, showing a wide distribution of particles under each category.

In order to take into consideration these irregularities, the values of shape factor and equivalent sphere diameter of oat hulls particles are used in the sub-model depicting the discrete phase. The corrected sub-model then can allow a more rational and correct prediction on the fluid force exerted on oat hulls particles.

Table 4.6 Physical property of oat hulls particles

							Total
Count based on length (mm)							
	7.0 - 8.0	**8.0 - 9.0**	**9.0 - 10.0**	**10.0 - 11.0**	**11.0 -12.0**	**12.0-12.9**	
Quantity distribution (%)	2.1%	17.7%	28.4%	31.2%	17.7%	2.8%	100.0%
Weight distribution (%)	1.1%	12.2%	26.2%	34.3%	22.7%	3.4%	100.0%
Count based on Shape Factor							
	0.70 - 0.75	**0.75 - 0.80**	**0.80 - 0.85**	**0.85 - 0.90**	**0.90 - 0.95**		
Quantity distribution (%)	6.4%	19.9%	51.8%	20.6%	1.4%		100.0%
Weight distribution (%)	4.5%	16.1%	55.3%	21.8%	2.3%		100.0%
Count based on equivalent sphere diameter (mm)							
	3.0 - 3.5	**3.5 - 4.0**	**4.0 - 4.5**	**4.5 – 5.0**	**5.0 - 5.5**		
Quantity distribution (%)	2.9%	12.9%	36.7%	35.3%	12.2%		100.0%
Weight distribution (%)	3.9%	10.6%	34.5%	38.7%	12.3%		100.0%

4.3 Biomass Devolatilization

When biomass particle is released into boiler, it is quickly heated up and enters the next stage: devolatilization. This is a complicated phase mainly consisting of three overlapped stages: pyrolysis, char gasification and char oxidation. In the phase of pyrolysis, the majority of the biomass is decomposed into solid char, volatiles (condensable hydrocarbon or tar) and gases, which normally takes a matter of few minutes. In the phase of char gasification, char continues to release gaseous species with a spontaneous oxidation. As for oat hulls, the dominating majority of its weight is released out during the stage of pyrolysis. Therefore, pyrolysis of oat hulls is considered as the primary phase of its devolatilization. A rationally accurate prediction of it is then significantly important and becomes one of the major goals of the numerical model in this work.

4.3.1 Oat Hulls Pyrolysis Experiment

The devolatilization model developed in this research is based on the pyrolysis experiment employed in the University of Iowa Industrial and Engineering department. An updraft gasifier was used to represent Unit 10 where oat hulls particles are injected. This experiment set up carries the features of short-residence time, non-steady state, and high heating rate, which are true in industrial boilers. The oat hull sample is stationary in a chamber and is heated by an inert gas flow coming through from an industrial heater. The hot gas that leaves the gasification chamber passes through cooling tubes and a Parker finite particulate filter, then finally, is split into different tubes, each leading to a specific gas sensor to detect the concentration of O_2, H_2, CO, CO_2, and CH_4, temperature and humidity. This experiment can predict the evolution of volatiles during the devolatilization of oat hulls at various temperatures.

Categorized by the temperature of the reaction and the speed at which it occurs, there are mainly three types of pyrolysis, shown in Table 4.7.The effect of the heating rate and the final pyrolysis temperature has been found to predominantly influence the composition and relative yield of the produced syngas. For example, it was found that H_2 production from pyrolysis was 20% higher at lower heating rates (~9 K/s) than at a rapid heating rate (~17 K/s).

Table 4.7 Pyrolysis Types

Pyrolysis Type	Heating Rate	Gas Residence Time	Average Temperature
Slow Pyrolysis	0.1 - 2°C/s	>5 seconds	500°C
Flash Pyrolysis	>2°C/s	<2 seconds	400 - 600°C
Fast Pyrolysis	200 – 10^5 °C/s	<2 seconds	>550°C

Specifically in this research, fast pyrolysis with a rapid heating rate was explored because its mechanism is similar to what fuel experiences in the combustion facilities. Because most modern industrial combustion facilities have a heating rate as rapid as 100 to 500 K/s, thus the particular heating rate for this work was determined to be 100 K/s.

4.3.2 Data Analysis

In the field of engineering, the simulation of a combustion facility is aimed at rationally predicting the combustion behavior while avoiding an increased time cost, which requires a reasonable simplification of the chemical reaction mechanism.

As chapter 3 shows, the majority of the reaction mechanism used to describe fuel particle devolatilization is the single step reaction. This work follows the past work by adopting a single step reaction mechanism for oat hulls' devolatilization.

Single step reaction of devolatilization

The single step reaction of devolatilization model has been introduced in chapter 4, as shown in Equation (111). Here, the pre-exponential factor $A_1 = 1.02 \times 10^3 s^{-1}$ and the kinetic energy $E = 99.5 kJ/mol$ are obtained by applying the Least Squares Fitting method to the experimental result mentioned above. Those values are with a fitting error NRMSD (Normalized Root Mean Squared Deviation) equaling 4.26%. Since those experiments were conducted at temperatures ranging from 700 K to1000 K, there the interpolation prediction method is used to calculate devolatilization mechanism ranging until 1500 K. This is considered as available method since the temperature range doesn't departure far from the experimental temperature range.

CHAPTER 5: APPLYING A COMPREHENSIVE MODEL ON CO-FIRING OAT HULLS WITH COAL IN UNIT 10

A standard comprehensive model in Fluent 6.12 is adopted in this work to study the phenomenon of co-firing oat hulls with coal in Unit 10. For engineering applications, the majority of the CFD models used to simulate the full scale combustion facilities are based on commercial software. The dominating role of commercial software in CFD modeling of biomass combustion roots in its empirically accepted predictions and those flexible models supported by it. After constructing a standard general model in Fluent by defining the proper turbulent model, radiation model, kinetic reaction model and discrete phase model, a tremendous amount of efforts then has been dedicated to empirically and theoretically correcting those models to investigate co-firing oat hulls with coal in the stock boiler Unit 10. The first section of this chapter is spent to introduce the standard comprehensive model, thus follows the part describing the coal bed of Unit 10. A pure coal combustion case is then presented and has been compared with the experimental results. The satisfying agreement between the prediction and the measurement shows its credibility as the baseline model. Then series researches are conducted based on this baseline model. At first, the co-firing of oat hulls with coal at varied percentage of total heat value input is simulated. The combustion performances of co-firing are investigated and the relationship between the percentage of oat hulls and the peak temperature is discussed. The turbulent mixings of different cases have also been discussed through examining the oxygen and CO_2 concentration in the boiler. Then the optimizations of injection plans of oat hulls are discussed. Different injection velocity of oat hulls, the utilization of different numbers of injection nozzle and the nozzle spreading are all investigated and compared.

5.1 The Standard Comprehensive Model

The standard comprehensive model is set up in Fluent 6.12. Since this model is applied on an industrial furnace whose combustion is complicated in the aspect of geometry, phenomenon and research scales, some assumptions have to be made to rationally simplify the problem and to reduce the computational cost. The following sections introduce each specific model adopted in this comprehensive model and the reasons behind these choices.

5.1.1 Grid

The geometry of Unit 10 has been introduced in last chapter. As it shows, Unit 10 consists of several geometrically and thermodynamically complicated components including grate, water tube system, drums and super heaters. Therefore, it is of great importance to apply some rational assumptions on Unit 10 when transforming it into mathematically computable grid while reserving enough features to make it correctly predict the combustion performance of Unit 10.

Several grids of Unit 10 have been created in Gambit to address different requirements of research. The final version of the grid is shown as Figure 5.1, composing of a heat source volume representing grate bed, five square coal feeders on the front wall, oat hulls injection nozzles among the coal feeders, second air systems and a heat sink zone representing water tubes. Figure 5.2 shows the enlarged picture of the front wall of Unit 10, providing a better view of the fuel feeding system. It shows four nozzles among five coal feeders, which are considered as the place where oat hulls fuel is injected through.

Under the current situations, the two nozzles locating closet to the center of Unit 10 are considered as the primary nozzles to inject oat hulls. Most of the co-firing oat hulls with coal simulations in this work are conducted using these two nozzles. The other two nozzles

are then considered and investigated in the section of optimizing the air and fuel injection systems in Unit 10.

The amount of cells investigated for industrial boilers varies from about 0.5 million to about 4 millions. After applying all these assumption and simplification, three final grids are created, consisting of 634,568, 842, 961 and 1137,842 tetrahedral cells individually. After the grid sensitivity analysis, the second grid is considered to provide rationally accurate precision while achieving a reasonable computational efficiency.

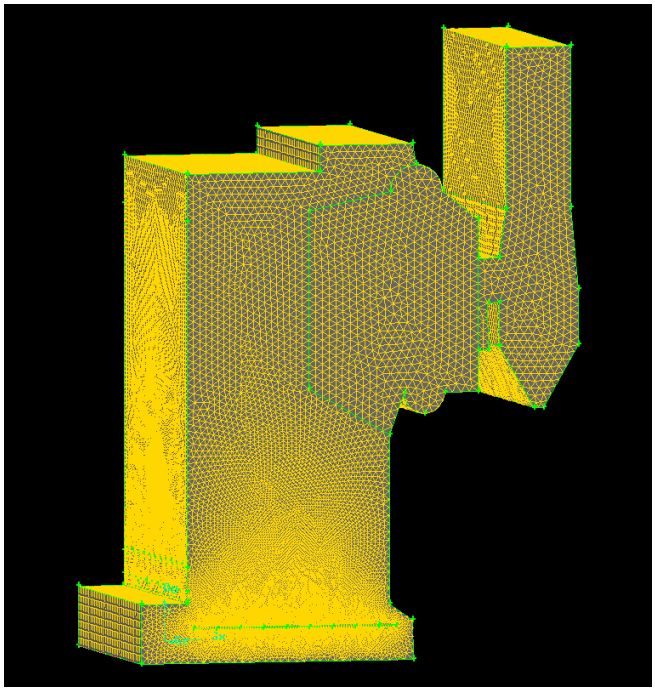

Figure 5.1 Grid of Unit 10

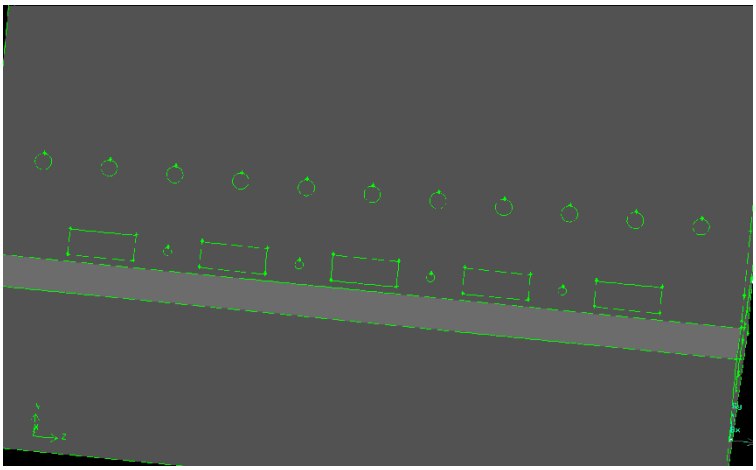

Figure 5.2 Fuel injecting scheme

5.1.2 Turbulent Model

Both the standard $k-\varepsilon$ model and realizable $k-\varepsilon$ model have been applied to describe the fluid dynamics of Unit 10. Due to the complexity of the inside geometry and air flow systems, the streamline curvature and the rotation of mixing are significantly intense in the boiler. As mentioned in chapter 3, the realizable $k-\varepsilon$ turbulent model shows its advantage of describing such kinds of problems and has been widely applied on the numerical modeling of combustion of boiler recently. Therefore this latter turbulent model is adopted in this work. The detailed expression of realizable $k-\varepsilon$ turbulent model can be found in chapter 3 for reference.

5.1.3 Turbulent Combustion Model

Several turbulent combustion models have been considered and adopted separately in the comprehensive model. These models include: finite rate/Eddy Dissipation model, Eddy Dissipation model and possibility density function models. The equations of these models have been clearly presented in Chapter 3.

In the first method, both the reaction rate determined by Arrhenius kinetic expression and the eddy dissipation reaction rates are calculated. By taking the net reaction rate as the minimum of these two rates, the instantaneous combustion in the premixed flame can be better described. In Eddy-Dissipation Model, it is assumed the reaction is dominantly controlled by turbulent mixing, therefor only eddy dissipation reaction rate is calculated.

On the contrary to last two methods, the individual specie equation is not solved in PDF method. Instead, the concentration of each species will be derived from a predicted mixture fraction fields. This mixture fracture is obtained after the application of a set of simplifying assumptions. The instantaneous relationships between mixture fraction and species fractions, density, and temperature are built up under the assumption of chemical equilibrium.

Because of the quickness of gasification and burning of biomass fuel, the simulations results show that the last two turbulent combustion models perform better to describe co-firing of oat hulls with coal in Unit 10. Though PDF model provides a higher computational efficiency, it has several inherent restrictions over EDM. First, the Lewis number must be unity, implying equal diffusion coefficients for all the species. Second, a maximum of two mixture fraction can be used PDF, which thus reduces the number of fuels the comprehensive model can investigate. Therefore, the EDM is finalized as the model to describe the turbulent combustion in Unit 10.

5.1.4 Discrete Phase Model

In this comprehensive model, Euler-Lagrange approach is used. The dispersed phase is solved by the Lagrangian discrete phase model. A large amount of particles is tracked in this method, exchanging momentum, mass and energy with the fluid phase treated as a continuum by solving the Navier-Stokes equations.

Those specific equations describing the status of particles have been presented in Chapter 3. In this comprehensive model, drag force is considered as the dominating fluid forces acted on oat hulls particles. Because oat hulls particle bears a significant irregularity of shape, Haider and Leverspiel Model is used to calculated the drag coefficient for these particles. For this method has been tested to efficiently describe the drag coefficient for nun-sphere particles. The value of shape factor is obtained through the analysis of the experimental data of oat hulls physical property introduced in Chapter 3. In this discrete model, oat hulls particles are injected in either the form of uniformed diameter and shape factor, or a group of particles with a distributed sizes and shape factors.

In Chapter 3, it shows that oat hulls particle will experience three stages when it passes through the boiler. These stages include initial heating, devolatilizing and char surface combustion separately. Two methods are used to describe the gasification of oat hulls. First, due to the complexity of the gasification products, one representative species is chosen as the overall gasification product. Following it, this work finally uses single rate kinetic model as the specific model describing oat hulls' devolatilization. These related equations are shown by Equation (110) and (111) in Chapter 3. The Arrhenius kinetic rate in Equation (110) is calculated with the pre-exponential factor $A_1=1.02\times10^3 s^{-1}$, and the kinetic energy E=99.5 kj/mol. These values are obtained by applying the Least Squares Fitting method to the experimental result mentioned in Chapter 3. The fitting error NRMSD (Normalized Root Mean Squared Deviation) is 4.26%. The second the method is a simpler one by choosing CO as the main devolatilization species of oat hulls based on the

results of the gasification test which shows a dominating role of CO as the gasification products.

5.2 Coal Bed Modeling

In numerical modeling of grate boilers, a rationally accurate coal bed model is of great importance. Because it is where the combustion happens, exchanging heat flux and species intensively with the combustion area above it. However, achieving the coal bed model precisely describing these above phenomena is extremely challenging. This tremendous difficulty results from the complicated situations existing on the coal bed, which include a series of physical processes occur on the grate including absorption of incoming radiation (thermal) from the surrounding, the heating and drying of the coal chunks, their subsequent pyrolysis and volatilization, the interactions between gas phase and solid phase fuel, and the combustion of both near zone gases and solid char.

Some of the numerical models applied on the grate boilers have been introduced in Chapter 3. It is clear that a decent amount of efforts has been attributed to modeling the coal bed. These past models include modeling coal bed as porous medium, a one dimension or two dimension functions of temperature, heat flux and species flux, used as the input of boundary in the comprehensive model. And the latter one has become the most common method accepted by the researchers. These functions are either set up through two phase combustion theory under proper assumptions or being corrected by the experimental measurement.

For the subject of Unit 10 in this work, it has a horizontally moving grate with the primary air coming through from below, with the whole operation being considered as at steady state. Due to the intense flow and combustion on the bed, collecting data on the coal bed of Unit 10 is tremendously difficult. Therefore, a two dimensional model of the coal bed and a two-step reaction kinetic are chosen in this work to model the combustion of coal

bed. The predicted results are then compared with the temperature measurement test deployed in Unit 10, shown in Chapter 3. A satisfying agreement between the calculation and the measurement is shown in the follow section.

Since Unit 10 is operating under a steady state, it is reasonable to consider the distribution of the gases and energy released from the bed as series of constant values on the bed. Based on this assumption, the grate bed is divided into 9 zones, with each being treated as having evenly distributed heat flux and species flux shown as Figure 5.3. By doing this, it becomes possible to assign different values of heat flux and species flux at each zone to obtain a thermally accurate description on the grate. It should be made clear that in the real coal bed, the coal chunks don't distributed along the coal bed evenly. There will be some areas on the bed where no chucks or only very few chunks exist. Due to the complexity of this issue, this uneven distribution pattern of coal on the bed is neglected in the numerical model.

During the phase of coal combustion on the grate, the coal is heated by the radiation and begins to release volatile into the freeboard. The volatile matter will join the gaseous combustion above the grate, and the fixed carbon will combust on the bed. To describe the volatile flux released from the coal bed, the ultimate and proximate analysis of coal in last chapter is used. By subtracting the amount of fixed carbon in proximate analysis from the carbon content in ultimate analysis, the carbon content in the volatile of coal is obtained. Then a representative species of volatile is calculated using this value with other species contents in the ultimate analysis. This volatile will experience two-step reaction mechanism shown in Equation (118) and (119) after being discharged to the free board above the bed.

$$C_{2.25}H_{4.71}N_{0.05}O_{2.22} + 2.3525O_2 \rightarrow 2.25CO + 2.355H_2O + 0.025N_2 \quad (118)$$

$$CO + 0.5O2 \rightarrow CO_2 \quad (119)$$

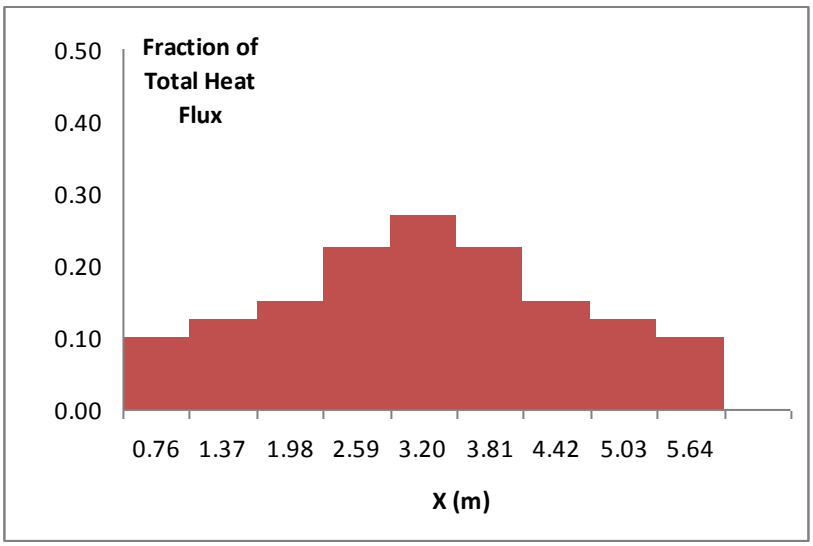

Figure 5.3 Scheme of coal bed

Besides the volatile, the species released from the coal bed also include CO_2 produced during the process of carbon combustion, the moisture content of the coal and a negative flux of O_2 resulting from the combustion on the bed. The amounts of them are calculated through Equation (120) and (121).

$$\dot{m}_{CO2} = 11/(3\dot{m}_{Carbon}) \quad (120)$$

$$\dot{m}_{O2} = 8/(3\dot{m}_{Carbon}) \quad (121)$$

By modeling the coal bed combustion in this mechanism, the heat value of coal needs to be distributed between the reaction heat of the carbon on the bed and the volatile. This process is in a similar way of the way calculating the composition of volatile matter.

5.3 Baseline Model: Coal Combustion

A baseline model is developed in this work to validate this comprehensive model. After evaluation of the technical difficulties, the pure coal combustion case is chosen as the baseline model. This model includes all the features introduced earlier in this chapter. The predicted results are then compared with the measurement data introduced in Chapter 3. The good agreement between the data and the results proves the credibility of this baseline model.

First this baseline model is used to simulate the full load of coal combustion in Unit 10, whose working capacity is 2.58 kg/min steam with a thermal efficiency of 82%. It has become a commonly accepted consensus that for the numerical model as complicated as the one simulating the combustion in the furnace, it is barely impossible to end up with a converged results. Therefore other criteria have to be adopted to judge the convergence for this kind of numerical models instead of using the definitions of residual.

In this work, there are two criterion used to decide the convergence of the simulation. First, the temperature field is nearly constant following the increasing of the iterations. Second, the overall balance of mass and energy are obtained. After applying these two criteria, the iteration is evolved up to 14000 steps. It is found that after 9000 iteration, the temperature field shows a constant pattern and the overall heat and mass balance are both satisfied. Therefore, the 9000 interaction is considered as the amount of iterations required for a converged result. Figure 5.4 shows the temperature contour of this baseline case. And Figure 5.5 and 5.6 are the concentrations of O_2 and CO_2. It is shown that the high temperature zone is sitting on the coal bed, with a peak temperature as high as 1790 K. This zone rises from the bed and tails down before passing through the heat exchanger. Because the coal chunks are thrown on the middle of the bed, where it is assumed exist the area with the highest averaged temperature. The temperature pattern along the bed shows an identical trend like it

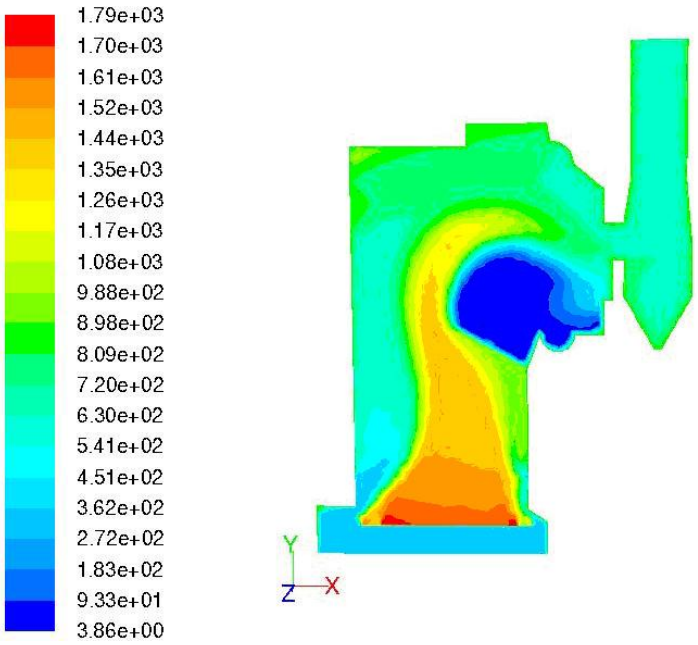

Figure 5.4 Temperature contour in the symmetric plane (2.58 kg/min steam, K)

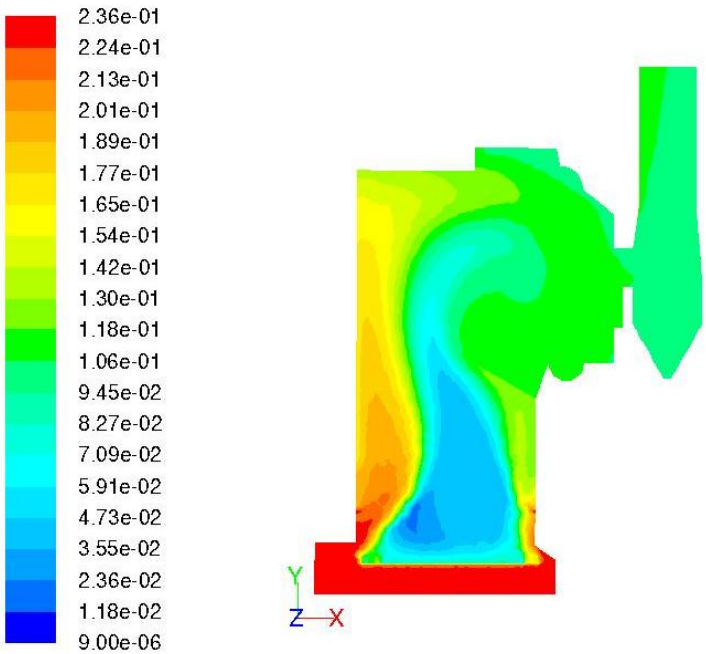

Figure 5.5 Mass fraction of O_2 (2.58 kg/min steam)

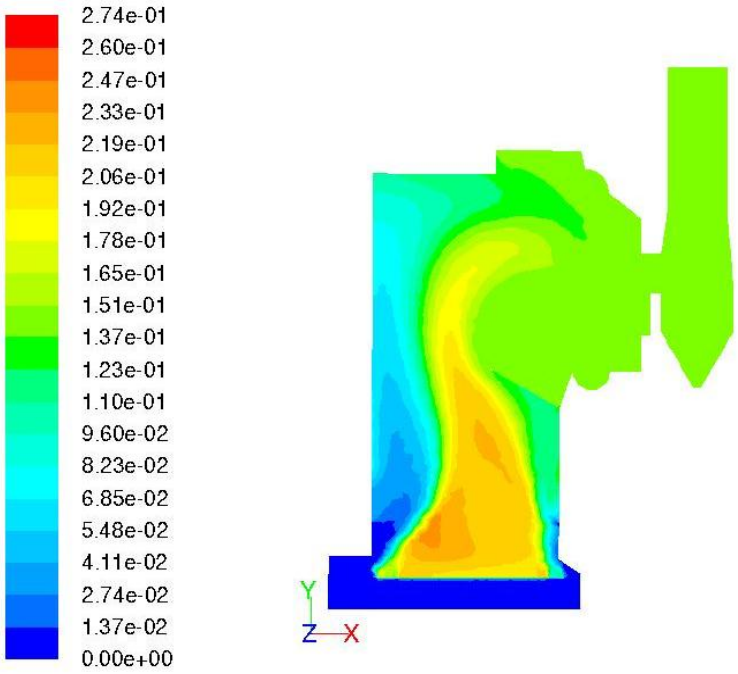

Figure 5.6 Mass fraction of CO_2 (2.58 kg/min steam)

Corresponding to the variance of temperature, the oxygen depletion zone is above the bed as well, which means the volatile matter of coal will began to combust quickly after being released. The turbulent mixing condition in Unit 10 satisfies the requirement of combustion without causing a significantly large zone of fuel lean area. The CO_2 mass fraction also reaches its peak value above the bed and continues to reduce due to the ending of combustion and dilution from secondary air systems.

Figure 5.7 shows the cross section of measurement plane, passing the centerlines of the observation windows. After analyzing the data, it is shown that the first two measurements points through window S2 and N3 are not trustful. This is caused by the wall effect and the air flow interruptions caused by opening windows. Therefore, the first two data points closest to the windows are neglected during the process of data comparison.

Meanwhile, the data collected in N1 shows an intense fluctuation, due to its close distance to the coal feeder. This strongly interaction between flow field and temperature field makes a correct prediction along the measuring path extremely challenging. Though the predicted results show a similar pattern of temperature variance and agree well at some locations, the role of N1 window measurement data as the validation data is considered being negligible. Another point needed to be made clear is that Unit 10 is theoretically designed and technically operated as symmetric grate boiler. A symmetric pattern of temperature of the data collected from window N2 and S2 is then expected to show in the measurement data. However, the results show a significant temperature difference between N2 window and S2 window for the data collected close to the window. It can be derived from this fact that there exist some physical problems inside Unit 10 causing an unsymmetrical operation of the facility. So the validity of the first part of the data set of S2 window raises the doubt and should be taken into consideration during the process of data comparison. In the final comparison, the first five data collected through S2 window are obsolete and replaced by the temperature value in the symmetric place collected from N2 window. After all these considerations, finally the comparison is conducted and the results are presented by Figure 5.8, 5.9 and 5.10, where the bar represents a precision of the experimental data.

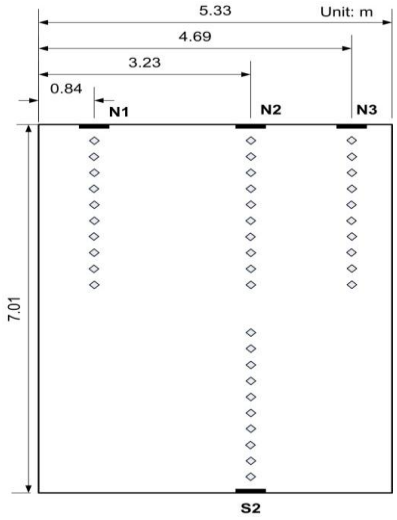

Figure 5.7 Data measurement scheme in window plane

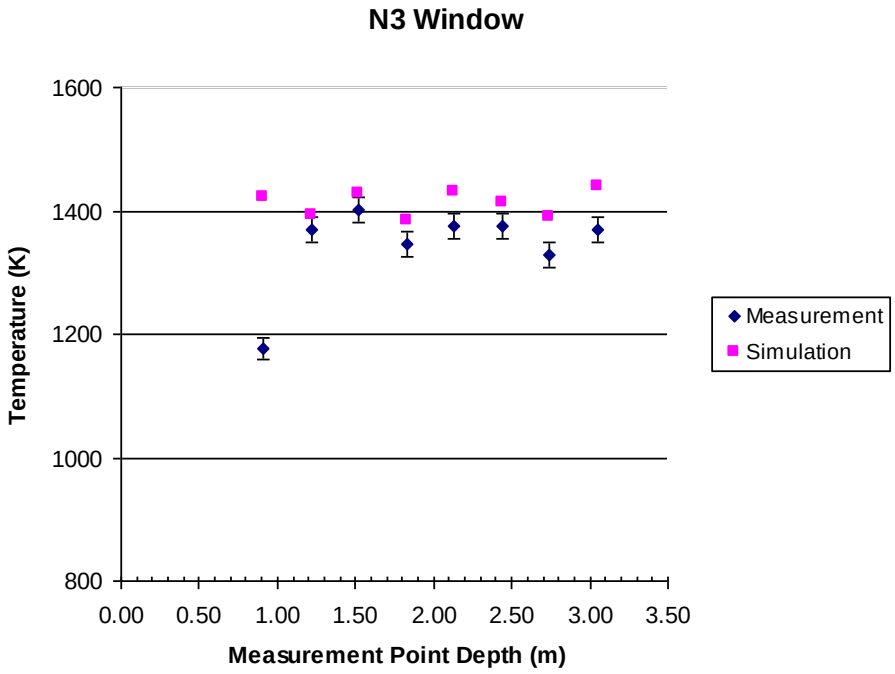

Figure 5.8 Comparison of predicted results with measurement data of window N2

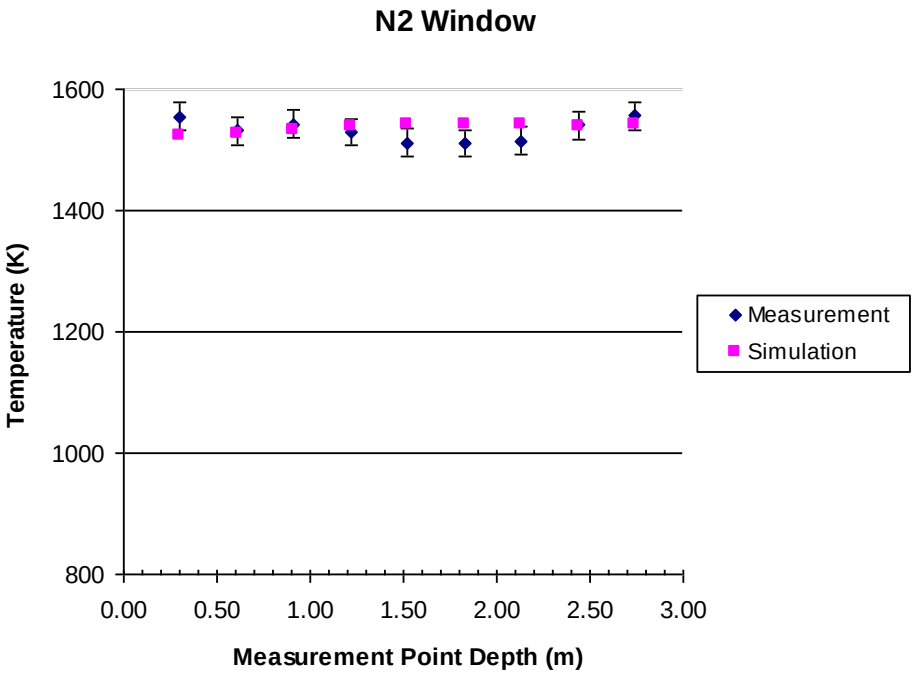

Figure 5.9 Comparison of predicted results with measurement data of window N3

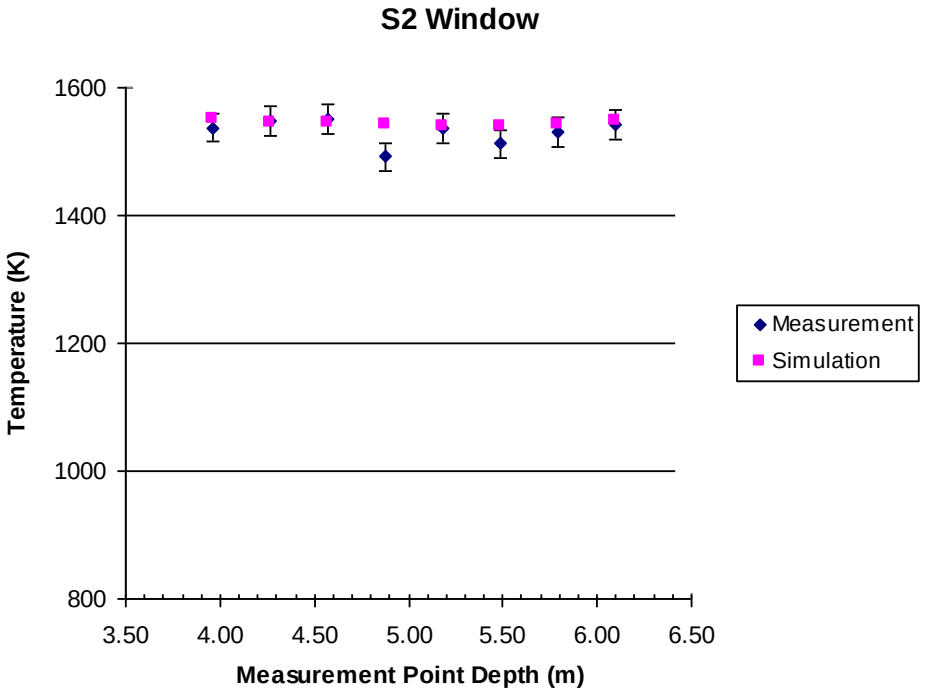

Figure 5.10 Comparison of predicted results with measurement data of window S2

It is shown that this coal combustion models works satisfyingly well to predict the temperature field of the observation plane in the area several inches from the wall. Particularly, the good coincidence with the measurement data in N2 and S2 windows shows this model can precisely predict the high temperature in Unit 10, which is an importance index to decide the combustion efficiency and NO_x emissions. The prediction on the data location through N2 window has the averaged deviation of 1.1%. Symmetrically in S2, the averaged deviation is 0.9%. This value for N3 window is about 3.6%. This difference can be explained by the difference of the numerical model of coal bed and the real phenomenon on the grate. The real coal bed is a two dimensional plane with an uneven distribution of coal along the direction paralleling to the front wall of Unit 10. The heat flux released at the end stage of the combustion on the bed then shows a value lower than the prediction of the CFD model.

As mentioned before, oat hulls will be co-firing with coal at different percentage of heat. Therefore it is important to ensure this comprehensive model can still make a reasonable prediction when coal load on be grate deceases. To further validate this model, this model is used to simulate another working condition with a steam flow rate of 2.0 kg/min steam flow. In this case, the only change applied on the comprehensive model is the steam and air loads. Comparing the data with the simulation results can test how accurate this comprehensive model can be to prediction the coal combustion in Unit 10. Due to the time and cost constrains, the measurements are only conducted through N2 and N3 windows 20 minutes after applying the changes on the system. The stabilization of Unit 10 is first achieved at the center where respond to the coal feeding the quickest. Also the pattern of variance of temperature data of N3 window indicates an intense fluctuation and unstable state. Therefore the data collected through N2 window is considered valid and the comparison is shown in Figure 5.11.

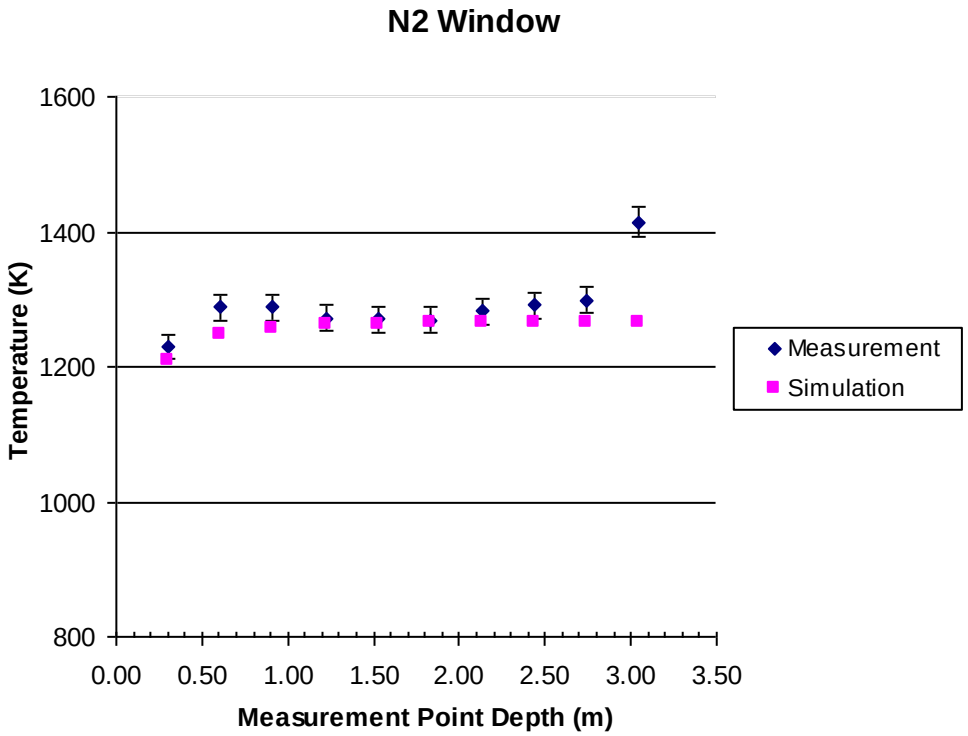

Figure 5.11 Comparison of predicted results with measurement data of window N2

Again, good agreement has been achieved when applying this comprehensive model to investigate another working condition, with an averaged deviation of 1.2%. The predictions on the high temperature zone in the middle of Unit 10 matches with the measurement except the last data point very well thus ensures the validity of this comprehensive model as the baseline model. The big temperature difference at the last data point can be explained by the longer response time to coal flow change required by this point which tends to be the where the peak temperature in the middle zone in Unit 10 is.

5.4 Investigations on Co-Firing Oat Hulls with Coal

This baseline model is then applied to simulate series scenarios on Unit 10, which includes co-firing oat hulls with coal in Unit 10 with varied percentage of heat values, optimizing fuel injection system, exploring the effect of particles' irregularity, and investigation on NO_x reduction in Unit 10.

5.4.1 Effect of Percentage of Heat Value

The University of Iowa is planning to co-fire oat hull with coal in Unit 10. The maximum percentage of total heat value input of oat hulls is about 30%. Therefore a series simulation is carried out to investigate the effect of co-firing oat hulls in Unit 10 at a varied percentage of total heat value input from 5% to 30%. Because of its light density and small size, it is assumed that oat hulls will show a flow following pattern after entering the boiler. Based on this assumption, the interaction between particles and fluid field isn't taken into account here.

In these simulations, the discrete phase model (DPM) is used to describe the projection and combustion of oat hulls particles in this particular research. Besides DPM, other features of the numerical models are kept as the baseline model. In DPM, oat hulls particles are set up with a uniformed radius and a shape factor which were obtained based on the physical property test introduced in last chapter to count for the non-sphere property of oat hull particles. Because the main gasification species measured in the gasification experiment are CO and CO_2, and the latter one doesn't take part in the gaseous reactions happening in the boiler. Thus the devolatilizaton species chosen at the DPM is CO and its releasing process was described by a one-step reaction model based on the gasification data where reaction coefficient A_1=1020/s, the activation energy E=99.5 kj/mol. The injecting velocity nozzle is chosen as 17.78 m/s to satisfy the technical requirement.

Because coal is still the dominating heat source, therefore the temperature contour of co-firing oat hulls with coal presents a similar pattern to that of pure combustion, but with a decreased temperature. Figure 5.12 shows the relationship between oat hulls' percentage of total heat value input and the peak temperature. This figure shows a linear relation between these two factors. The temperature can be reduced to as much as to 1460 K when 30% of the total heat is provided from oat hulls. This temperature reduction can be explained by two reasons. First, the decreased amount of coal on the grate will directly reduce the peak temperature above the coal bed where the high temperature zone exists. The second reason is oat hulls will combustion in the area above the high temperature zone close to the coal bed, where the air flow from the second air systems will cause a strong mixing and reduce the temperature quickly. Therefore, though the substituted amount of heat is released by the oat hull, it will not produce a peak temperature as high as pure coal combustion.

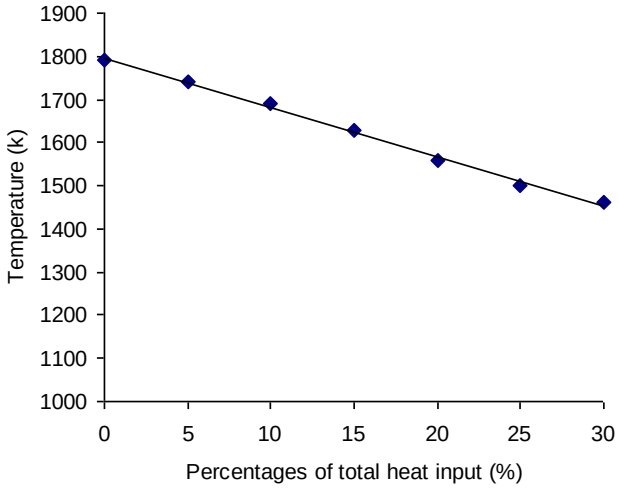

Figure 5.12 Change of the temperatures with oat hulls' percentages

Figure 5.13 is one example of the concentrations of oat hulls' gasification species, showing the location of gasification is close to the front wall of Unit 10. This means oat hulls start to gasify quite quickly after entering the boiler and the span of this progress is quick short.

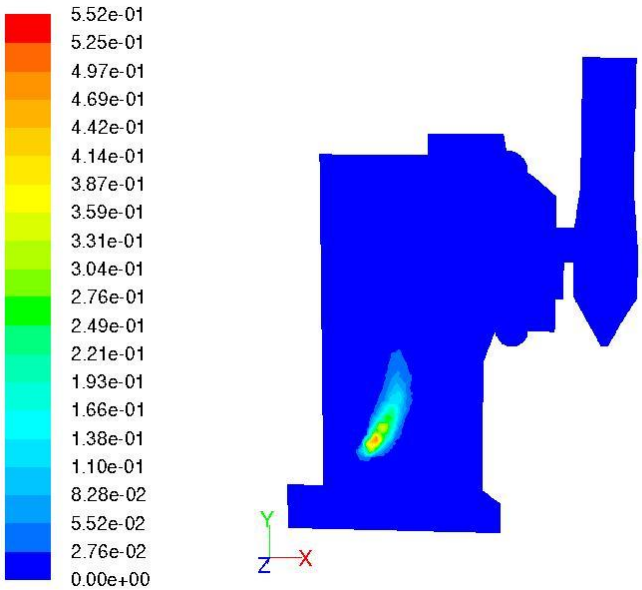

Figure 5.13 Concentration of oat hulls develatilization species (15% of total heat)

Figure 5.14 is the corresponding oat hull particle trajectory colored by temperature. The temperature variance shows a three staged pattern: heating, devolatilizing and surface combusting.

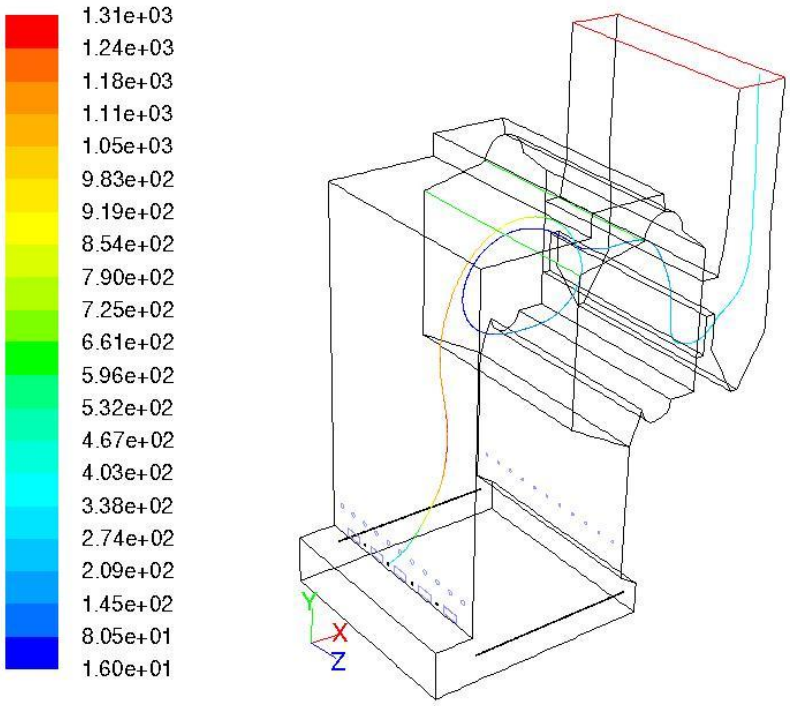

Figure 5.14 Particle trajectory colored by temperature (15% of total heat)

As Figure 5.5 shows, for the case of pure coal combustion, the oxygen depletion zone is right above the coal bed. However in the case of co-firing oat hulls, the oxygen depletion zone is shifted upward and narrowed down following the increasing of percentage of total heat input of oat hulls. For example, Figure 5.15, 5.16 and 5.17 show the concentrations of O_2 at the percentage of 5%, 15% and 25%. Due to the smaller content of carbon in oat hulls, the amount of the oxygen for the combustion is lower than pure coal combustion. Therefore these figures show an increased oxygen concentration inside the boiler. It is concluded that the depletion of oxygen is improved in Unit 10 by co-firing oat hulls with coal.

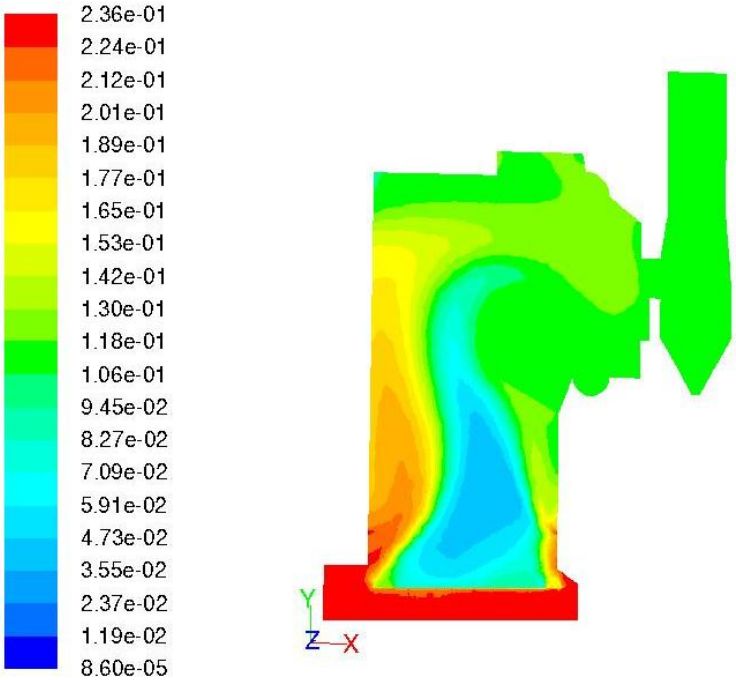

Figure 5.15 Oxygen mass fraction (5% oat hulls)

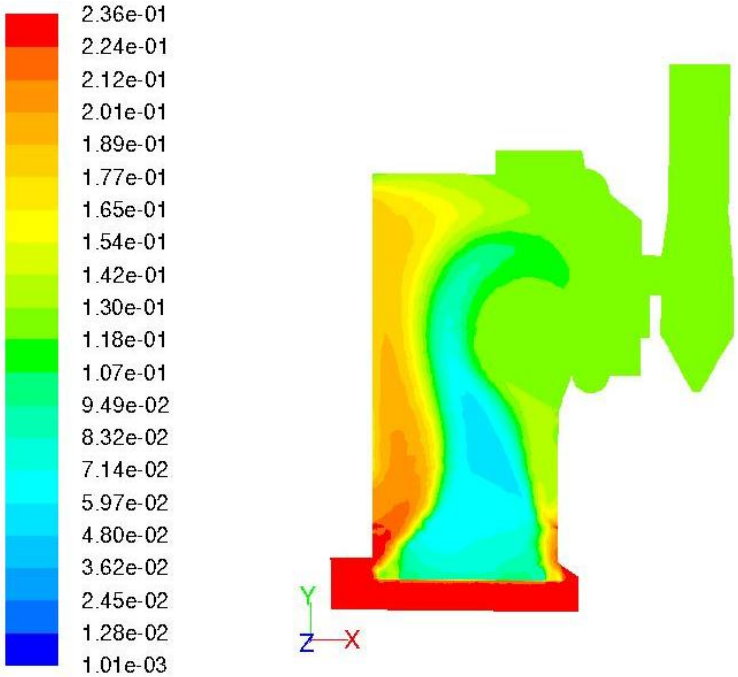

Figure 5.16 Oxygen mass fraction (15% oat hulls)

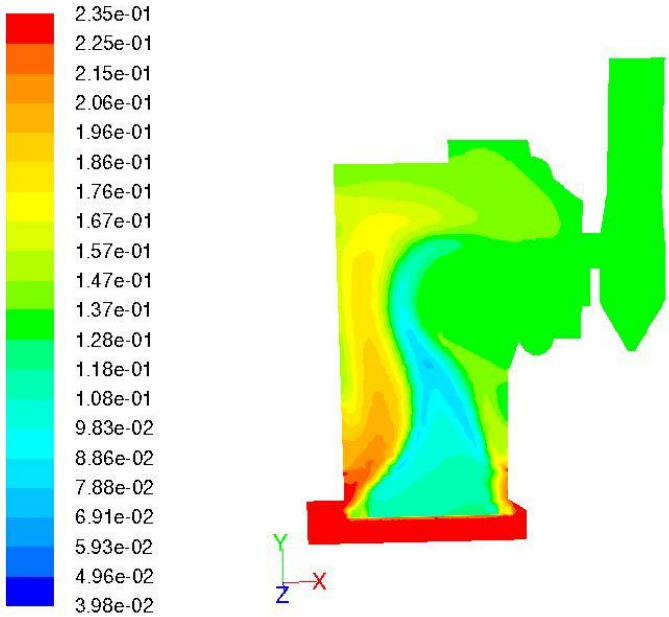

Figure 5.17 Oxygen mass fraction (25% oat hulls)

5.4.2 Effect of the Air Velocity of Nozzles Injecting Oat Hulls

The injecting nozzles of oat hulls used to inject oat hulls are designed to have a velocity ranging from 17.78 to 25.4 m/s. The knowledge of the effect of the injecting velocity on the general behavior inside the boiler will be beneficial for finding the optimized velocity to the combustion system.

This section introduces the simulations on co-firing oat hulls with coal with a varied injection velocity from 17.78, 20.32, 22.86 and 25.4 m/s with the same injecting angle. Since each percentage may require different optimizing injecting velocity, every oat hulls' percentage weight of total heat input is simulated for every injecting velocity in order to sufficiently explore the relationships between these two important parameters.

Figure 5.18 are the trends of temperature decreasing for each injecting velocity. It shows the peak temperature of the boiler varies as a linear function of percentage of oat hulls. It also indicates that by increasing the injecting velocity, the peak temperature can be further slightly reduced due to the adding of increased amount of air except in the case of injecting 5% oat hulls. The reason for undetectable temperature drop at 5% of oat hulls may be that in this case the heat contributed by the oat hull are not significant and the injecting air mainly impact on the second combustion zone where oat hulls' combustion happens and has less influence on the coal bed combustion.

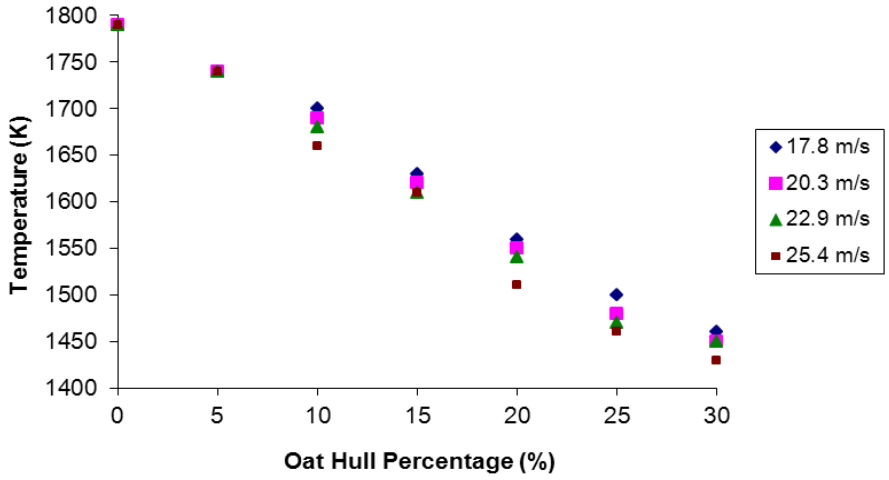

Figure 5.18 Change of the peak temperatures with oat hulls' percentages of total heat input at every injecting velocity

It is also detected from the particle's trajectory that the increased injecting velocity will not cause a significant change the path of particle and shows no obvious pattern on the

variance of particle residence time. Therefore it can be derived that the value of inject velocity will not have a significant impact on the particle's path line inside the boiler.

Beside the temperature, the turbulent mixing inside the boiler is also an important factor used to describe the general combustion behavior. Like being discussed in the last section, co-firing oat hulls with coal can enhance the mixing on the combustion area thus improve the combustion efficiency. And it is expected that by increasing the injecting velocity the mixing can be further improved. Figure 5.19 shows the peak concentration of CO_2 at different velocity and percentage. This figure shows a common trend of change of CO_2 in the boiler with the injecting velocity at every percentage of oat hulls: the CO_2 emission is at first decreasing with the increasing of oat hulls and begins to ascend after reaching a critical velocity between 22.86 m/s and 25.4 m/s. One explanation for this phenomenon is that the locations of oat hulls particles after gasification are gradually shifting upward in the boiler, driven by the air with an increasing injecting. Therefore the surface combustion of the carbon tends to happen on the upper part of the boiler above the second air system, causing an increased concentration of CO_2.

The conclusions conducted from the simulations are strongly helpful to determine a proper injecting velocity for oat hulls of certain percentage of heat by showing the details of the variance of combustion behavior inside the boiler. It is shown that increasing injecting velocity impacts less effect on the peak temperature in the case of co-firing a low percentage of oat hulls than in the case of injecting oat hulls with a high percentage. Moreover, the velocity should be kept under the critical value to improve the combustion and reduce the greenhouse gas CO_2's emission. Therefore the balance between air velocity and percentage should be addressed in the optimizing design of oat hull injecting system in the future.

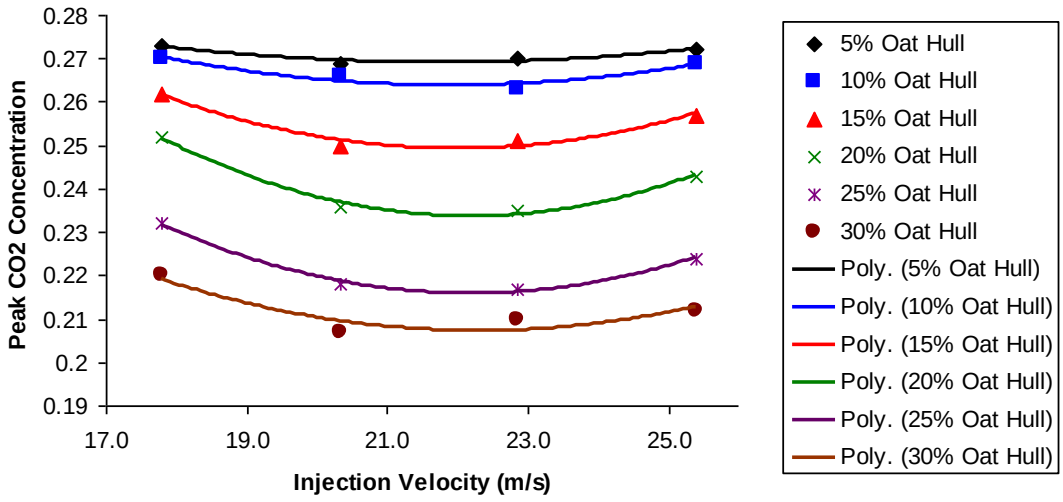

Figure 5.19 Peak mass fraction of CO_2

5.4.3 Spreading Injection of Oat Hulls

To further spread oat hulls inside the boiler for an improved combustion, the University of Iowa Power Plant is considering increase the number of oat hulls injecting nozzles to four, which means the two outer sides of nozzles in Figure 15.

The simulation of using four injecting nozzles is carried out in this section. This inject plan is employed on co-firing 30% oat hulls in Unit 10. A peak temperature of 1430 K is predicted by the CFD model, which is 30 K lower than using only two front nozzles for oat hulls. It is coincided with the assumption that spreading the fuel and reduce local temperature. The concentration of CO_2 is also reduced in this case, shown as Figure 5.20.

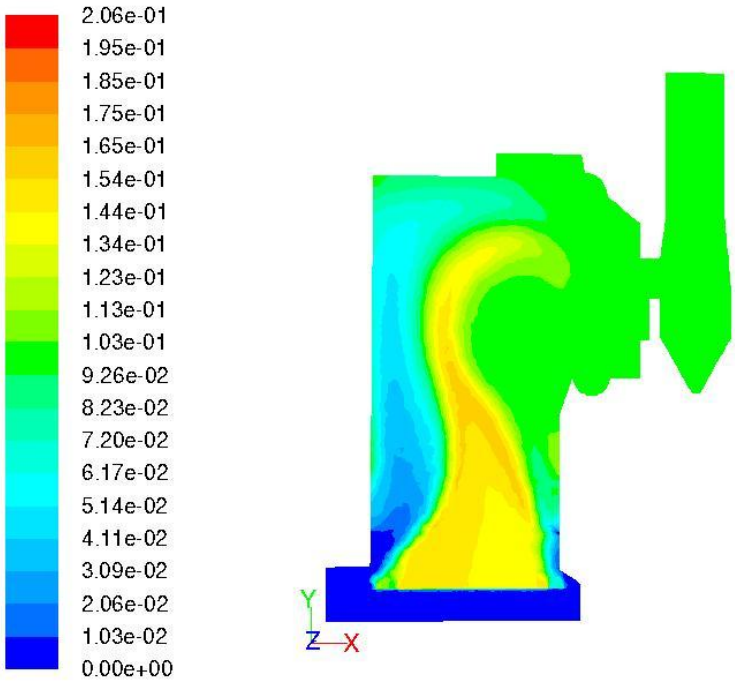

Figure 5.20 Mass fraction of CO_2

For the convenience, each oat hulls injector is assigned a number, show as Figure 5.21. Because of its light weight, oat hulls particle begin to gasify right after it enters the boiler no matter the changes of the injecting nozzles. And there is no significant difference of particle path among these four nozzles. However the peak temperatures of particle entering from different nozzle are not all the same. Table 5.1 shows that the temperatures of particles injected from A2 and A3nozzles are about 20 K higher than the particles coming through A1 and A4. This temperature variance means the arrangement of coal on the bed result in a higher temperature in the middle, therefore though increasing number of injecting nozzles can even the combustion, the heating of particles is more complete in the middle.

Table 5.1 Peak temperature of particle

Nozzle	A1	A2	A3	A4
Temperature (K)	937	975	974	935

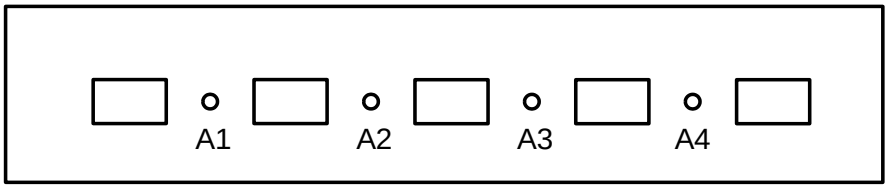

Figure 5.21 Injection nozzle scheme

CHAPTER 6: DESIGN INVESTIGATION OF UNIT 10

In this chapter, the benchmarked comprehensive model was applied in several areas, the first of which is co-firing woodchips with coal in Unit 10, driven by the motivation of broadening the range of biomass Unit 10 can use. A new two-step coal bed model was created to model the combustion of wood chunk. The results showed some important details of combustion of wood chips on the coal bed with coal, unknown but needed for the design. The second task conducted through applying the comprehensive model is reducing NO_x level in Unit 10. As the old fashioned grate boiler, Unit 10 keeps a relatively high NO_x level which is challenging the University of Iowa power plant to satisfy an increasingly strict environmental standard. After the on-site investigation and screening the possible design plans, it was decided that the most efficient and convenient way is to inject Urea in Unit 10 through the second air injecting system. The simulated results supported the feasibility of this plan by showing a significant reduction of NO_x level in Unit 10. Finally, this comprehensive model was employed to study the effect of installing two natural gas burners in the back wall for enhancing the combustion. The results showed an improved mixing of gases and combustion after co-firing natural gas with wood chips in Unit 10.

6.1 Co-firing Wood Chips

As one of the most common sources of biomass for power plant, the UI power plant is investigating the feasibility of using wood chips in Unit 10. In general, wood chips can be regarded as a biomass fuel with great potential in US Midwest since it can be received in abundant quantities. With current technology, the primary method of using wood chips is by co-firing them with coal. However, due to significantly different material properties between wood chips and coal, a strongly changed and varied pattern of combustion

behavior is reasonably expected. This dictates some necessary technical improvement and process revisions for existing facilities.

6.1.1 Properties of wood chips

Wood can be continually replenished, which leads to a sustainable and dependable supply. It also contains minimal heavy metals and extremely low levels of sulfur which means that wood fuel is no threat to acid rain pollution. Usually, wood ash is less than 1% of the weight of the wood, and sometimes ash may be used as a fertilizer.

Table 6.1 and Table 6.2 show the proximate and ultimate chemical analysis for wood chips individually, alongside that for coal. These are the chemical properties used in the numerical model to describe wood chip and coal fuel properties. They show wood chips contain a much lower content of fixed carbon than coal, meaning most of the carbon in wood chip exists in the form of volatiles. The oxygen content of wood chips is on the other side much higher than coal, indicating a more oxygen rich atmosphere inside the boiler. Due to the high content of moisture, wood chip has a relatively lower heat value as much as 12.84 Mj/kg. Its sizes range from approximately 8 to 22 mm with a density of 440 kg/m3.

Table 6.1 Proximate analysis of wood chip

	Wood Chips Proximate Analysis wt%	Coal Proximate Analysis wt%
Moisture	29.41	5.85
Volatile matter	56.70	35.61
Fixed carbon	11.65	47.94
Ash	2.24	10.6
Total	100	100
HHV [kj/kg]	12840	28470

Table 6.2 Ultimate analysis of wood chip

	Wood Chips Ultimate Analysis (daf) wt%	Coal Ultimate Analysis (daf) wt%
Carbon	49.76	72.4
Hydrogen	5.6	5.07
Nitrogen	0.23	1.64
Oxygen	44.39	8.26
Total	100	100

6.1.2 Coal bed model of co-firing wood chips with coal in Unit 10

The University of Iowa Power Plant is considering mixing the wood chips with coal through the coal feeders on the front wall and throwing them altogether on the grate. Both coal and wood chip will burn along the slowing moving grate. Another two-step coal bed model was developed to model the combustion of wood chips on the bed, where wood chip releases volatile and char combusts with air. Based on the published literature [88-89], the composition of volatile gases released from the wood chips was taken to be C_2H_4, CO_2, and H_2O, shown by Equation (122).

$$Volatile_{wood} \rightarrow 22.81\%C_2H_4 + 38.2\%CO_2 + 38.99\%H_2O \quad (122)$$

To simplify the problem, the physical and chemical interactions between the coal chunk and wood chips were neglected and the distributions of mass and heat fluxes were assumed similar to that of coal. Under these assumptions, the mass and heat fluxes released

from the coal bed represent an accumulated effect resulted from the wood chip and coal chunk combustion on the bed.

6.1.3 Co-firing wood chips with coal

The common amount of biomass co-fired with coal in the industrial boiler is about 10%. In this research, the wood chips are co-fed with coal at various percentages of the total heating value from 5%, 10%, 15%, up to 20%, in the hope to which explored the feasibility of co-firing biomass under a larger co-firing amount. Since the overall heat source on the bed was kept unchanged, no significant change of the flame temperature was expected. However, due to a big difference in fuel properties, co-firing wood chips in Unit 10 is assumed to have a significant impact on the species left inside the boiler.

The results were consistent with these above assumptions, showing only a small drop in the peak temperature, whose value gently decreased with the co-firing ratio of wood chip, shown by Fig. 6.1. Since the nitrogen content of wood chip is only slightly higher than that in coal, this small temperature reduction will cause a friendly environment for reducing the NO_x level inside the. Fig. 6.2 showed temperature profile of co-firing wood chips at the heat ratio of 15%. It also showed a shortened flame zone above the coal bed, which can be explained by the significant amount of oxygen content carried by wood chips, making most of the combustion species completely combust right above the bed. This feature of co-firing wood chips means a more complete combustion of fuels and a higher overall/economic efficiency.

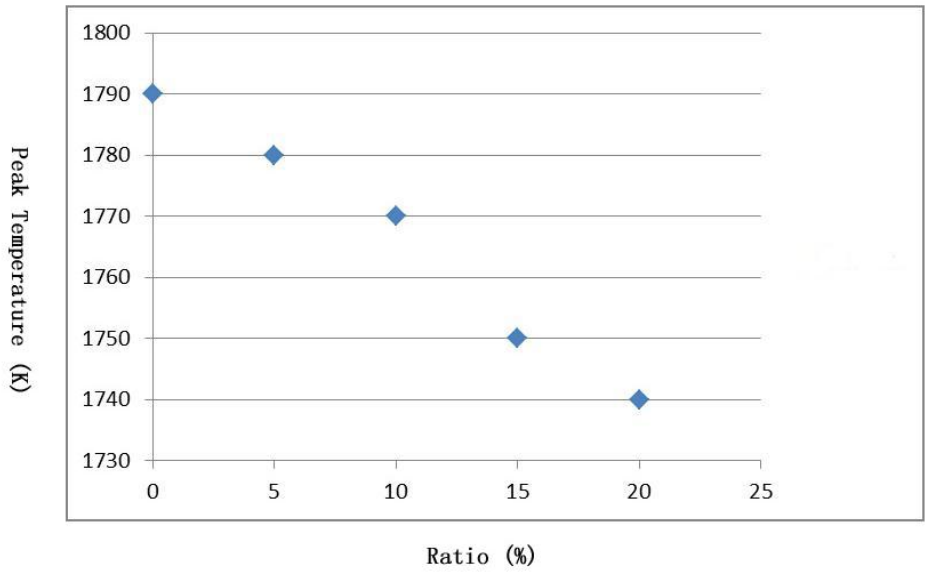

Figure 6.1 Peak temperatures vs. co-firing ratios

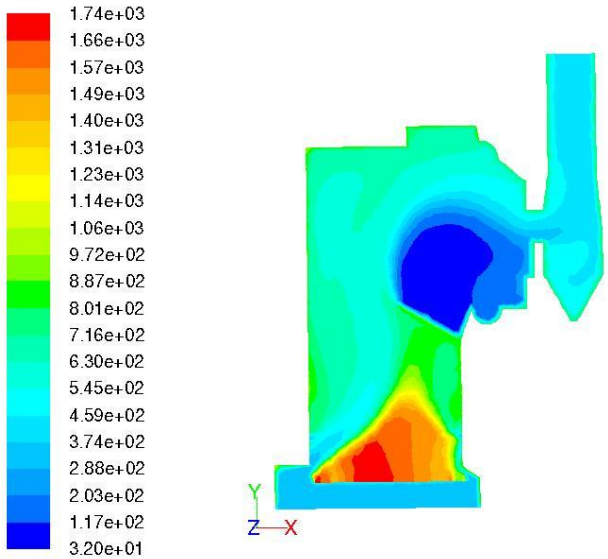

Figure 6.2 Temperature (15% wood chips, K)

Figures 6.3 showed how the O_2 concentrations inside the boiler changed with increasing wood chip use. It showed that the average level of oxygen left inside the boiler is greatly increased compared with the pure coal combustion. The temperature depletion zone (represented by the blue area) stayed above the bed as expected but with a much smaller area than coal and it kept the shape regardless the amount of wood chips co-fired. This oxygen rich environment was resulted from the combined effect of high oxygen content in wood chip and the ample amount of primary air coming through the grate bed. The more oxygen-rich environment is not only beneficial for achieving higher combustion efficiencies, but also aids overall efficiency through the smaller working load on air system.

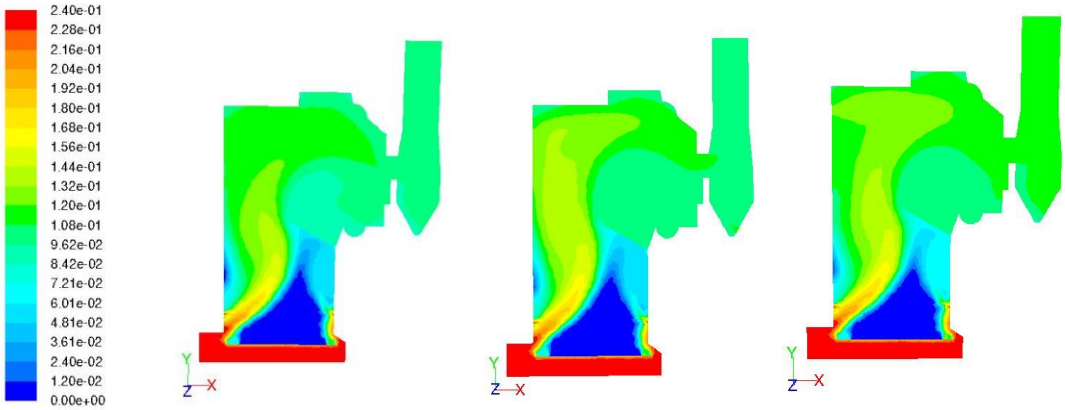

Figure 6.3 Mass fractions of O_2 (5%, 10%, and 20%)

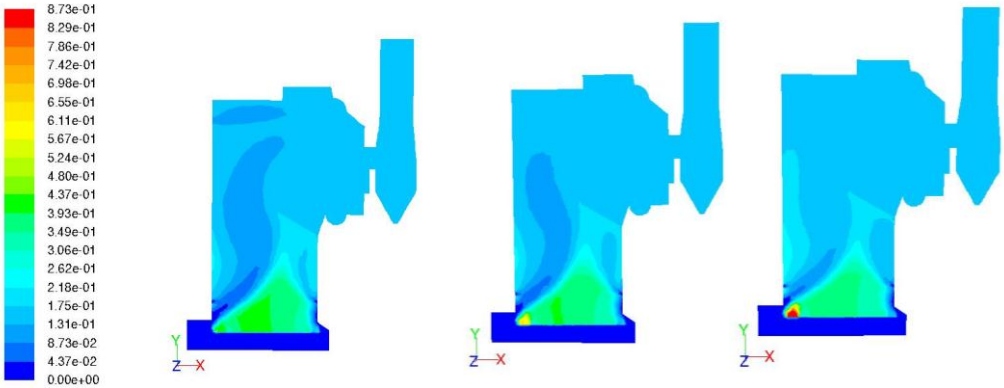

Figure 6.4 Mass fractions of CO_2 (5%, 10%, and 20%)

Figure 6.4 showed the mass concentration of CO_2 inside the boiler. Since the volatile of wood chips contains a decent amount of CO_2, it significantly attributed to the increase of CO_2 level in addition to the CO_2 produced during the combustion. This raises the possibility of a higher overall CO_2 level than coal combustion.

6.2 NO_x Level and Its Reduction

In the normal operation of stoker boiler Unit 10, fuel is combusted in the fuel bed releasing heat. Because the air of the boiler is mainly provided by the primary air coming through the grate, peak combustion temperature occurs in the fuel bed with excessive oxygen which peaks NO_x formation. Following the increasingly strict NO_x standard, it is of great significance to reduce the NO_x level for Unit 10.

Driven by this goal, the comprehensive model was employed to predict the NO_x level inside the boiler, which showed a very good match results with the power plant operation

data. Then the simulation of injecting Urea at different mass ratio was conducted in the hope of finding a most efficient way to reduce the NO_x level in Unit 10.

6.2.1 NO_x level of coal combustion

As introduced in chapter 3, NO_x is produced through three mechanisms during combustion, which are fuel NO_x, thermal NO_x, and prompt NO_x. Thermal NO_x is the most significant NO_x mechanism in boiler combustion. The rate of conversion is controlled by both excess O_2 in the flame and the temperature of the flame. In general, NO_x levels increase with higher flame temperatures that are typical in the fuel burning zone. Fuel NO_x is formed by the oxidation of nitrogen and nitrogen complexes in the fuel. In general, approximately 60 percent of fuel nitrogen is converted to NO_x. The resulting NO_x emission is primarily affected by the nitrogen content of fuel and excess O_2 in the flame. "Prompt NO_x" is a term applied to the formation of NO_x in the flame surface during luminous oxidation. The formation is instantaneous and does not depend on flame temperature or excess air. Compared with the first two mechanisms, the amount of prompt NO_x is normally significantly smaller and was neglected during this study. The detailed reaction equations can be found in chapter 3.

Fig. 6.5 showed the predicted NO_x level inside the boiler in the case of pure coal combustion, represented by the form of mole fraction. Since the common unit used to describe NO_x level in the industry is PPM, therefore equation (123) was employed to convert the unit. The converted final result showed that the present NO_x level at the exit of the boiler is 241 PPM, which agreed with the data (varying between 238 and 243) provided by the power plant very well. The sensor collecting NO_x sample in the Power Plant is installed at the exit of the flue gas pipe, which is a NO-NO_2-NO_x analyzer of Thermal Fisher Scientific. The accuracy is the lower detectable limit of 0.40 ppb. The continuous sample for the NO_x analyzer is drawn from the ductwork located after the induced draft

fan, which means it is collected immediately ahead of the stack. In this simulation, the NO_x level was chosen according to this location. This agreement between the data and the simulation provide the solid foundation to conduct the simulation for NO_x reduction.

$$PPM_{NO} = \frac{x_{NO} \times 10^6}{1 - x_{H_2O}} \tag{123}$$

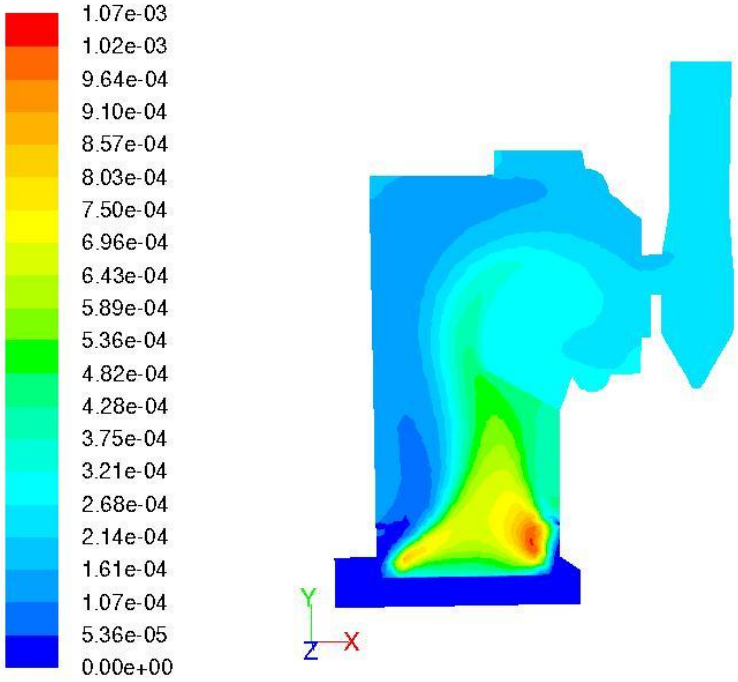

Figure 6.5 Mole fraction of NO

6.2.2 NO_x reduction

These findings and future stringent air quality standards necessitate finding new ways to remove NO_x from the exhaust of the industrial boilers. One possible way is to use a more efficient and selective reducing agent. For example, ammonia has been known to be a highly selective and efficient reducing agent to remove NO_x from the flue gas streams of power plants. Urea as ammonia source is an organic compound with the chemical formula $(NH_2)_2CO$. The molecule has two amide (—NH_2) groups joined by a carbonyl (C=O) functional group. It may be the best choice because it is not toxic and also can be easily transported. The exact NO_x reduction kinetics used in the simulations can be found in chapter 3.

After the onsite inspection and screening the design options, the present plan to reduce NO_x level inside the boiler is to inject Urea from the second air system on the front wall, shown as Fig. 6.6. To simplify the problem, the Urea used in the simulation was assumed to be injected in the form of gaseous phase pollutant with air through the nozzles of second air system instead of using a separate nozzle for it. The density of urea vapor is 2.454 kg/m^3.

The simulations showed a very promising result of using U2rea to reduce the NO_x level in Unit 10. Fig. 6.7 showed the NO_x level reduced to 180 PPM after injecting. When the ratio increased to, the level then could be reduced to 135 PPM, shown as Fig. 6.8. These results showed Urea can work well in the area of second air system and can be able to reduce the NO_x level effectively. These results can be regarded as some important preliminary results. However to further investigate the effect of injecting Urea, a more precise model of Urea should be involved.

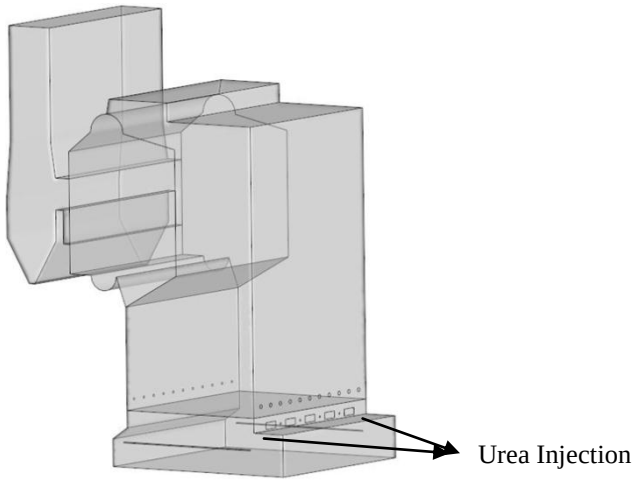

Figure 6.6 Injection plan of Urea

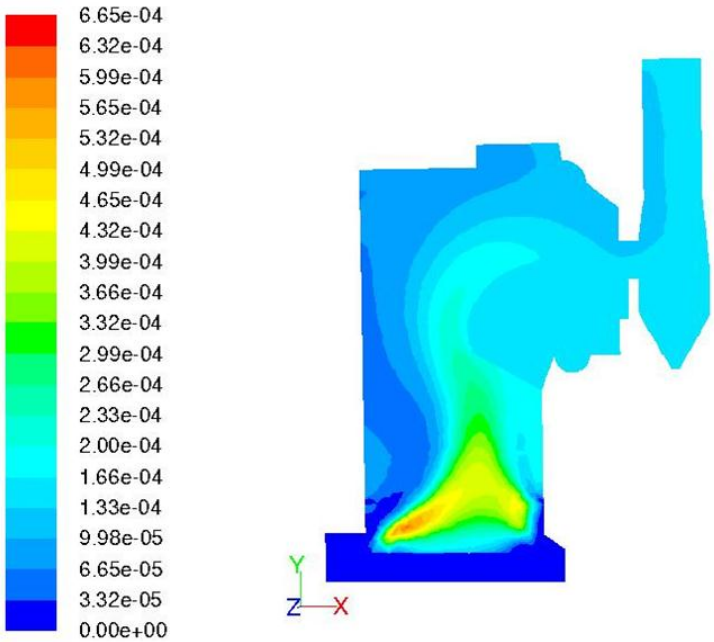

Figure 6.7 NO mole fraction (0.15 kg/s Urea)

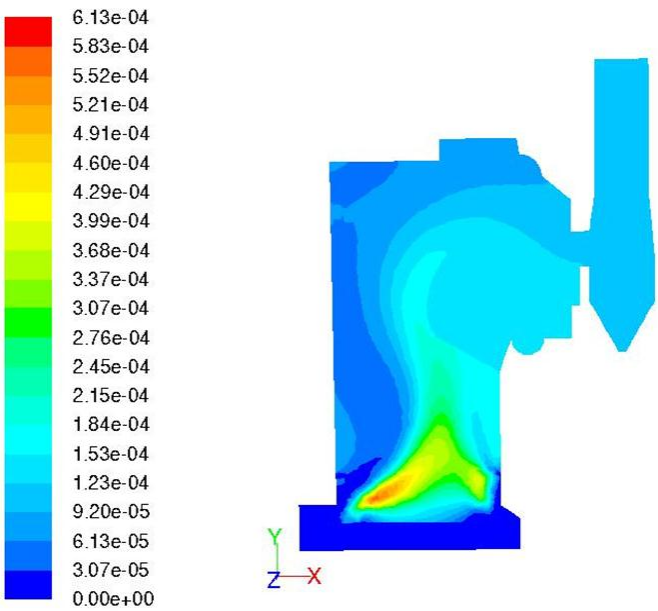

Figure 6.8 NO mole fraction (0.3 kg/s Urea)

6.3 Co-firing Natural Gas with Coal in Unit 10

Natural gas co-firing technologies can be helpful in the aspect of increasing industrial energy efficiency, and reducing harmful atmospheric emissions. During the process of co-firing, natural gas is used as a supplemental fuel in the combustion of other fuels, such as coal, wood, and biomass energy. For example, there exist a significant amount of energy lose and high harmful emissions in a traditional industrial wood boiler which simply burns wood to generate energy. Adding natural gas to the combustion mix can have a two-fold effect. Natural gas emits fewer harmful substances into the air than a fuel such as wood. Since the energy needed to power the natural gas boiler remains constant, adding natural gas to the combustion mix can reduce harmful emissions. Natural gas, which has a relatively low price in recent months, produces approximately 40 to 50 % lower carbon emissions than coal. Natural gas also produces lower NO_x emissions due to its no fuel

bound-nitrogen content as well as reduced excess air requirement for combustion. Also, natural gas produces virtually no SO_2 and mercury emissions, eliminating the need for scrubbers and thus producing much less plant waste. In addition, the operational performance of the boiler, including its energy efficiency, can be improved by supplementing with natural gas. Because adding natural gas can compensate for the use of low grade fuel such as wet wood, it allows the other type of fuel to combust more quickly and completely.

To investigate the possibility and effect of co-firing natural gas in Unit 10, this comprehensive model was employed to simulate co-firing natural gas with coal in Unit 10. It was aimed to obtain the changes of the general combustion behavior inside the boiler and to collect the preliminary information on co-firing natural gas in Unit 10, which thereafter can be applied to co-firing natural gas with biomass fuel.

6.3.1 Co-firing plan for natural gas

In order to convert the existing unit to fire natural gas, a new wall fired low NO_x gas combustion system would have to be installed into the rear wall of the furnace. Fortunately, Unit 10 was originally built with two tube panel openings on the rear wall to accommodate future installation of natural gas burners. Therefore two nozzles were added in these corresponded locations (4.88 m from the center of nozzle to the boiler bottom) in Gambit mesh, shown as Fig. 6.9. A premixed injection of air and natural gas was assumed in this research, with equation (124) show the reaction. The higher heating value (HHV) of the mixed gas was calculated based on the relation shown in equation (125).

One thing needs to be made clear is that great simplification has been made in this simulation due to the lack of information regarding the burner's geometry and the amount of natural gas used. Therefore the result is focusing on predicting the qualitative trend of co-firing natural gas with coal.

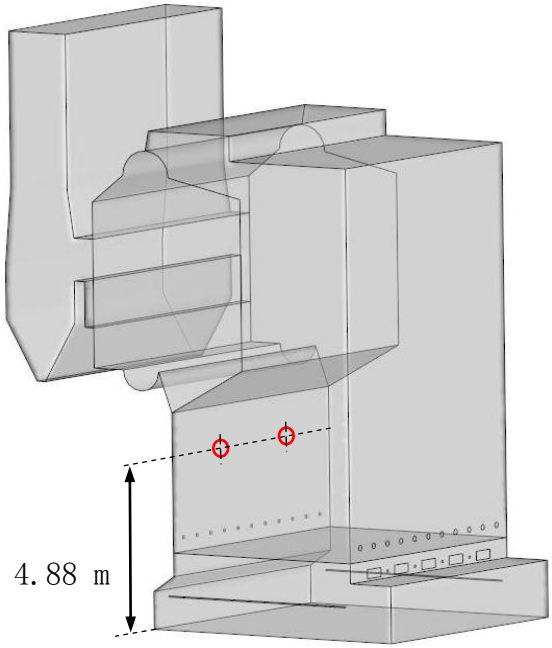

Figure 6.9 Natural gas nozzles

$$CH_4+2(O_2+3.76N_2)\rightarrow CO_2+2H_2O+7.52N_2 \quad (124)$$

$$\frac{HHV_{Natural\_gas}}{m_{Natural\_gas}+m_{Air}} \quad (125)$$

6.3.2 Results of co-firing natural gas in Unit 10

Fig. 6.10 showed the temperature contours on the middle plane of Unit10 with natural gas being co-fired at the ratio of 5%. Because the combustion of natural gas is quicker and more complete, and its location is in the main combustion zone above the coal bed, that temperature didn't drop significantly following the increase of co-firing ration. It was detected that the high temperature zone shifted to the back wall and moved close to the compulsory mixing wall, therefore the overall flame length got reduced. Therefore the turbulent and combustion mixing in this area should be the emphasis of consideration when designing the actual co-firing natural gas system in the future. On the other side, the flue gas temperature at the exit increased following the amount of co fired natural gas, caused by the higher injection location and better combustion of natural gas. Table 6.3 showed this trend, where the first data point (NO_x level of pure coal combustion) agreed very well with the measured flue gas temperature (463 K).

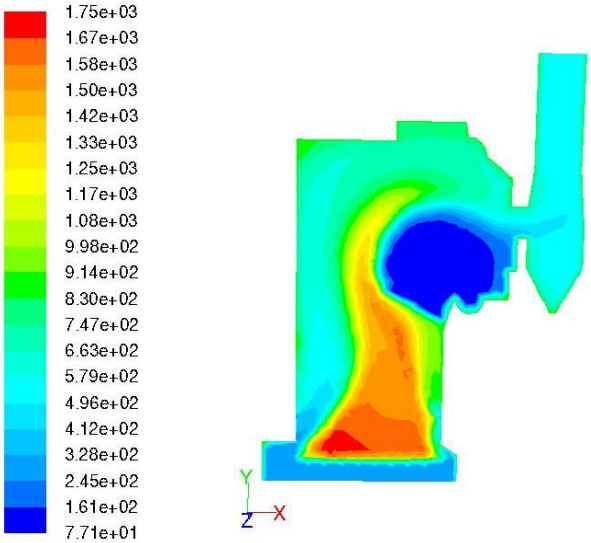

Figure 6.10 Temperature (1% natural gas, K)

Table 6.3 Flue gas temperatures

Ratio of natural gas	0	0.01	0.05
Temperature (K)	466	495	529

Fig. 6.11 showed the comparison of mass fractions of oxygen for both cases inside the boiler. Due to the combustion of natural gas, the temperature depletion zone (represented by the blue colored area) stayed under the mixing wall and was improved with the increase of natural gas co-firing ratio. It is because natural gas was injected as the premixed fuel with air, therefore caused no drop on the oxygen level, leaving its level increased inside the boiler.

Fig. 6.12 showed the mass fractions of CO_2 for each case. The overall CO_2 level inside the boiler was reduced after co-firing natural gas and is consistently decreased when the co-firing ratio was increased. Therefore, co-firing natural gas with coal and other type of fuels like biomass can mitigate the emission of green-house gas. The simulation results also showed the possible issues about poor turbulent mixing below the mixing wall.

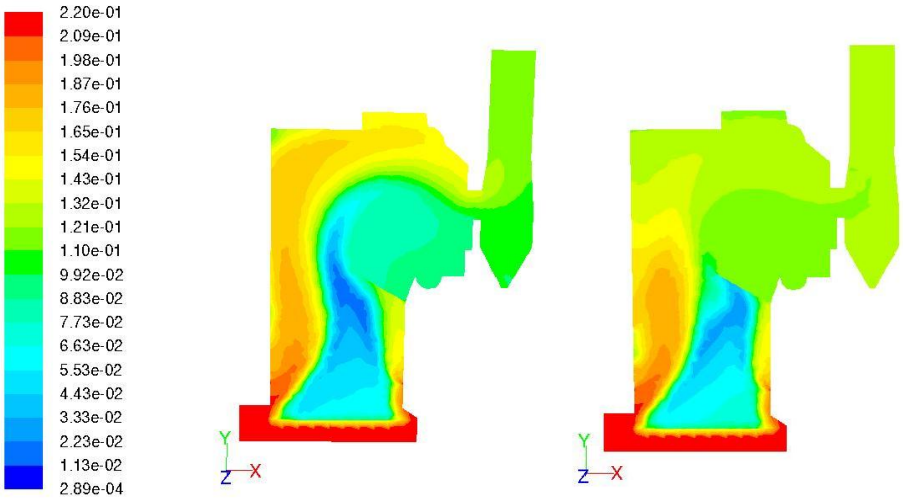

Figure 6.11 Mass fractions of oxygen at 1% and 5%

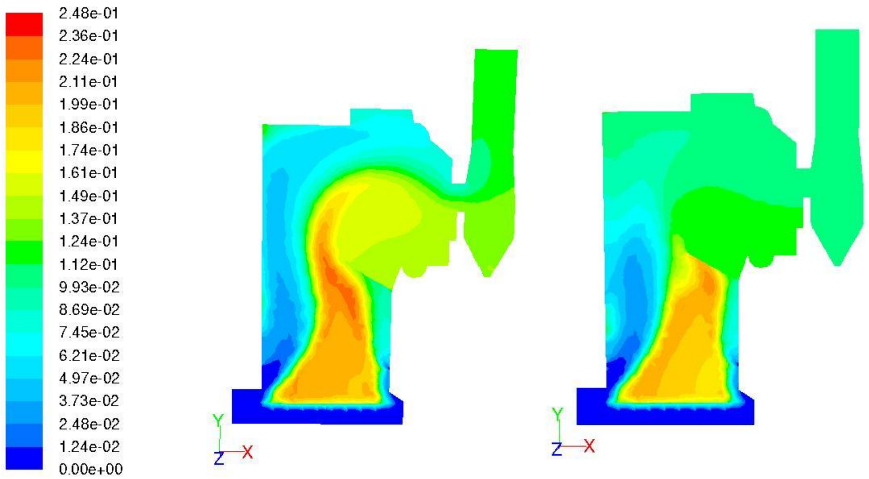

Figure 6.12 Mass fractions of CO_2 at 1% and 5%

CHAPTER 7: EFFECT OF PARTICLE INTERACTIONS

In nearly all of the previous works, fluid forces are considered as the dominant forces acting on a particle and are the only terms calculated to predict the trajectory of a particle. This assumption works well in most of the cases. However, it can turn to be untrue under certain conditions. For example, the interactions among particles will have a large effect in of the region near the point of particle injection. The forces can change the particle's movement and affect its combustion. With this motivation, this portion of the thesis work uses a numerical model to explore a more accurate calculation of particle's movement and combustion by accounting for the micro-scale forces between the particles.

The numerical model used in this research is a model connecting two independent solvers developed by the University of Iowa IIHR [90] and the MIE department [81] separately. A significant effort has been put forth to make these two solvers work together. Because of the scale and complexity of the problem, the results predicted in this chapter are based on a two dimensional model.

7.1 Numerical Model

As was mentioned at the beginning of this chapter, the numerical model used in this research is a model connecting two independent solvers. The first one, U^2RANS-2.6, is an Unsteady and Unstructured Reynolds Averaged Navier-Stokes solver that can be used to solve a variety of practical flow and thermal problems. It can be used to model fluid flow, heat transfer, multi-fluids transport. The code modeling the discrete phase is named Particles. It is a multiple-time step computational approach for efficient discrete element modeling. Further details for this code can be found in chapter 3.

7.1.1 Turbulent Model

U^2RANS-2.6 solves the Reynolds Averaged Navier-Stokes equations which use standard $k-\varepsilon$ model to model the fluid flow. The wall function is used at the boundary. A text-based interactive user interface is used to guide a user to set up the fluid flow problem. The values calculated by U^2RANS are all based on the absolute value.

7.1.2 Discrete Phase Model

An effective physical model of the discrete phase (particles) should be an accurate description of the physical forces present during collisions and fluid induced forces and torques acting on the particles. These forces include drag, lift, pressure gradients (or buoyancy), gravity, and any other added mass force, whose detailed expressions can be found in chapter 3. For small particles, the dominant fluid force is usually considered as drag force, hence the drag force is assumed to be the primary fluid force on an oat hull particle. Another fluid force taken into accounts is the gravitational force. It is know from previous work [31] that the gravitational force is important even for small particles when applied over sufficiently long time periods, unless the particle size is so small that the particles can be suspended indefinitely by Brownian motion.

The body force exerted by the particles on the fluid flow must be calculated in the case of injecting oat hulls into the boiler due to their large total mass. This body force term is computed by determining the fluid grid cell in which each particle lies and distributing the sum of the forces discussed above on the fluid (imposed by a particle onto the surrounding grid nodal points), as shown in Figure 7.1. For each grid cell, the value of the body force on this cell is obtained by summing over the contributions from all particles contained in the cells around it. Instead of computing particle concentration by counting the number of

particles in each fluid cell, which tends to be a highly variable indicator, a particle cloud approach is used [81] as an alternative method.

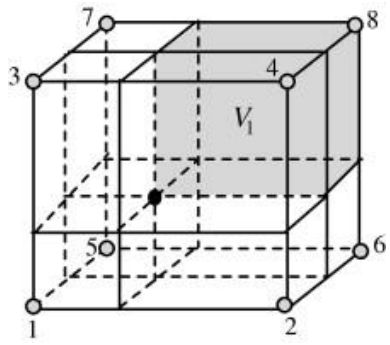

Figure 7.1 Schemes of distribution of forces

The particle interaction forces are decomposed into four parts: (1) those acting along the line normal to the particles centers, (2) sliding resistance, (3) twisting, and (4) rolling of one particle over another, as shown in chapter 3. These collision forces with no adhesion and with modification due to Van der Waals Adhesion force have been introduced in chapter 3 as well.

The computational algorithm structure of this model has been introduced in chapter 3. By applying this algorithm, the forces occurring at different time scale can be accurately modeled without causing a dramatic increase in the computational time.

7.1.3 Solver Connection

As shown in chapter 3, the calculations of these fluid forces require knowledge of the fluid velocity at the particle location. These values must be interpolated from the grid used for the fluid variables. Therefore, a Cartesian gird is created to overlay the U^2RANS grid and the fluid field values at each point of this Cartesian grid then can be obtained through a fast match method.

7.2 Grid and Post Processing

Gridgen was used to create the structured mesh and the Tecplot was used for post processing. Due to the limit resulting from the way that the interpretation between the U^2RANS and Cartesian grid was carried out, the Cartesian grid has to be square in 2D and a box in 3D. Therefore, the original grid for the Unit 10 boiler used in Fluent was recreated with a higher degree of geometrical simplification, shown in Figure 7.2 and 7.3, where the flow still enters from the bottom and leaves from the right side of the most upper block. Figure 7.2 shows the two dimensional grid of Unit 10 created in Gridgen. The grid is a structured mesh, with an interval of 5 centimeter. For this mesh, the air carrying the particles enters from the nozzle on the left and the primary air comes through the bottom. Then the air flow leaves from the outlet on the upper right of this mesh. In the 3D grid, the air/fuel injectors are modeled as five short square nozzles. The primary air comes through the bottom and the flue gas leaves the system through outlet in the same location as 2D grid. Some original geometrical features are neglected due to the degree to complexity, which therefore allow the research being conducted by addressing the issue of particle interaction forces.

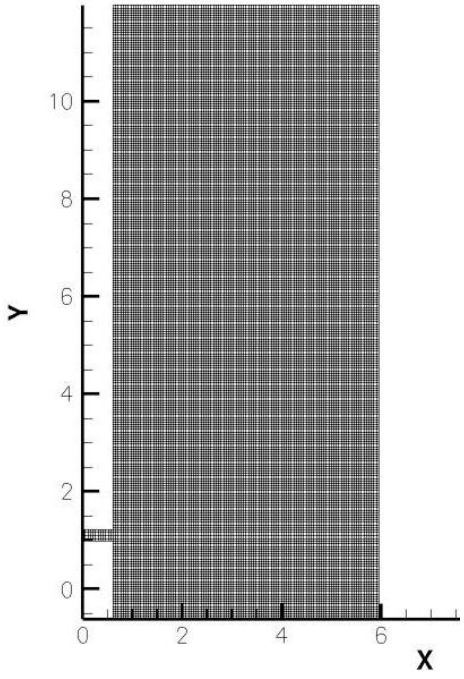

Figure 7.2 Two dimension grid (m)

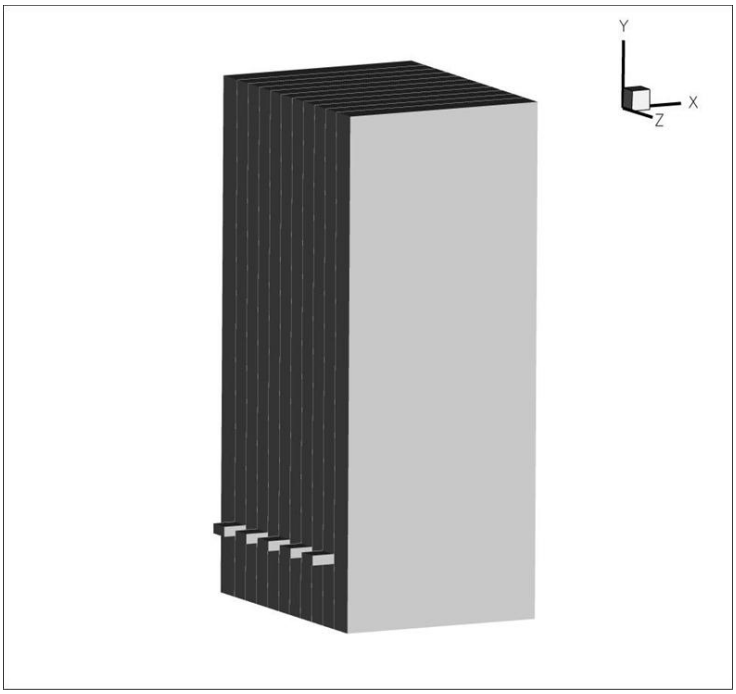

Figure 7.3 Three dimension grid of boiler

7.3 2D Flow With Particles' Movements

The combined model was first employed to simulate the cold flow inside the boiler. The air velocities in the nozzle and the air velocity at the bottom are kept the same as that in the comprehensive model. For the purpose of comparison, the case was also simulated in Fluent by computing it on the present mesh. Figure 7.4 shows the contours of temperature predicted both by Fluent and the combined model. It shows that they are both capable of describing that the hot air injection and subsequent mixing with the cold air coming up from the bottom. There is a small variation in the area around the nozzle, but it is fairly minor.

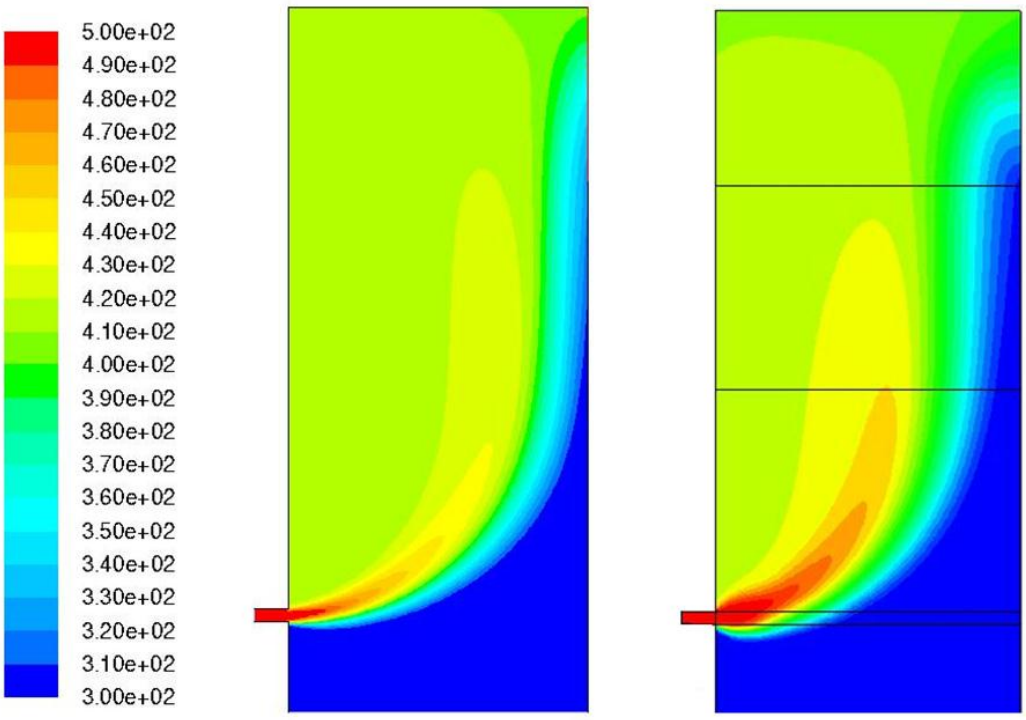

Figure 7.4 Temperature contour (left: Fluent, right: code, unit: K)

The next case studied was with particles injected into the domain, simulated with both Fluent and the combined code, and in both cases 2-way coupling between the particles and the fluid field were considered. Specifically in the code, a total number of five particles were injected per time-step through the nozzle. A random velocity perturbation was added to each particle at injection and the particles were tracked for the first three seconds. Fig. 7.5 shows the paths of particles in both cases, indicating that both programs computed consistent particle paths which showed the particles reached the back wall, bouncing off, and finally exiting at the upper left. The collisions and adhesion happened most often around the nozzle area. Fig. 7.6 shows the fraction of collisions that have occurred by a given distance downstream (from the injection location). It is evident that most collisions occur in the first 1 m, which is one quarter of the total boiler width.

The results confirmed that the particle interactions occur primarily in the near field of the injector due to a high volume fraction of particles, and quickly decreases inside the furnace. Since the area inside the furnace where no collisions are detected is much greater compared with the nozzle near field, the results indicate that it is reasonable to neglecting particle interactions in the case of simulating the particle combustion in a large combustion facility like this stoker boiler. One the other hand, simulating particle movement and combustion inside a smaller sized combustion facility clearly requires considering particles' interactions. In particle code, the particle interaction forces are expressed in a combined form. Therefore, this code could not predict the effect of each single force on particle's movement.

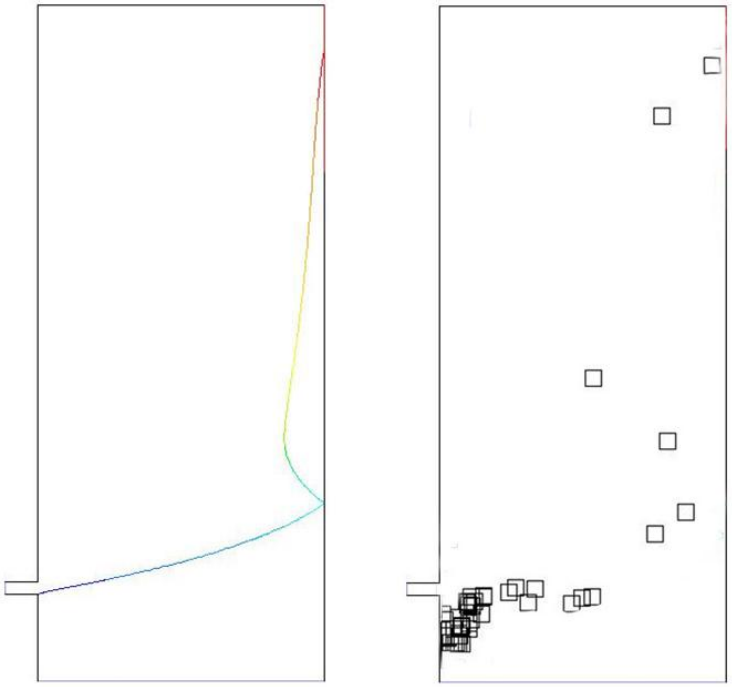

Figure 7.5 Comparison of particle path (left: Fluent, right: code)

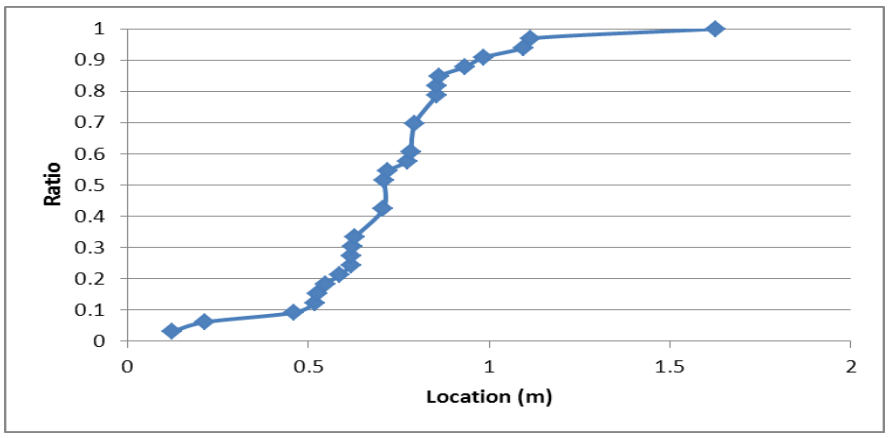

Figure 7.6 Number of collisions over the total collision number along at the points along injection direction

CHAPTER 8: CONCLUSIONS

8.1 Conclusions

In the first part of this work, a comprehensive model was developed to investigate co-firing of different kinds of biomass including oat hulls, wood chips and natural gas with coal in a stoker boiler. This model was also employed in the optimization of the air system and injecting plans for light weight biomass and NO_x reduction for the stoker boiler. Along with a standard realizable $k-\varepsilon$ turbulent model and an Eddy Dissipation reaction model, several sub-models were developed to describe the fuel bed, fuel particle's movement, and their gasification. To verify and fine-tune these sub-models, a series of experiments were conducted, including a temperature measurement campaign, a chemical lab analysis of oat hulls, an experiment measuring oat hull particles' physical properties, and a high heating rate gasification test of oat hull. The predictions of the temperatures of more than forty data points on the measurement plane agreed very well with the experimental data, with an averaged accuracy of 1.7%, compared with an experimental precision of 1.5%. The comparison showed the great capability of this comprehensive model of describing the combustion of this stoker boiler with a satisfying scientific accuracy.

For the co-firing of oat hulls with coal in the stoker boiler, it was found that the flame temperature decreased with increasing oat hull fraction and the high temperature zone became more elongated in the upper part of the boiler. The oat hull particles showed a pattern of flow following and were burned in suspension due to their light weight. The release of volatile species during oat hull heating/gasification occurred very quickly after the particles entered the boiler, leading to a high temperature combustion zone relatively close to the injection location. Due to oat hull's high oxygen content, the average oxygen level in the furnace was increased, creating a more oxygen rich environment and resulting in more complete combustion for co-firing cases. It was also observed that larger oat hull

particles tended to reach the opposing wall of the boiler, raising the possibility of coking/slagging/fouling on that wall.

As the air flow had the greatest impact on combustion efficiency, mixing, and particle distribution throughout the boiler, optimizing the air flow was selected as the tuning parameter and was utilized to enhance the turbulent mixing and combustion and to reduce the amount of oat-hull-induced fouling at the far wall. The first part of the optimization was finding an optimized injection velocity for oat hulls to keep the particles in the boiler long enough and with sufficient oxygen for them to complete burnout. Another aspect of the optimization was to reduce the peak temperature so as to reduce the NO_x level. Optimization also showed that increasing the injection air velocity could blow the oat hull particles above the oxygen depleted zone and contribute to full oat hull burnout. The second part of the optimization focused on increasing the number of oat hull injecting nozzles for more evenly distributed combustion. It was found that when applying a four nozzle injection plan on the stoker boiler, the combustion and turbulent mixing inside the boiler were greatly enhanced and the particles injected through the two middle nozzles created a higher local temperature and stayed longer inside the boiler.

In the simulation of wood chips co-firing with coal, the fuel bed was remodeled to describe the combined effect of combustion of wood chips and coal on the grate. The results showed that the flame temperature decreased with increasing wood chip fraction and the flame zone was much shorter because of the more oxygen rich environment, resulting from the high oxygen content of wood chips. It also noted that there is a significant improvement in combustion behavior with improved mixing of air above the grate.

In the numerical study of co-firing natural gas with coal in this stoker boiler, it was observed that the high temperature zone shifted to the back wall and moved close to the upper compulsory mixing wall, making the overall flame length shorter. Therefore the turbulent mixing and combustion in this compacted area should be the emphasis of future

system optimization. One the other side, the flue gas temperature at the exit increased with increasing natural gas fraction, most likely caused by the (higher) injection location.

In the investigation of NO_x production, the comprehensive model was at first applied to predict the NO_x level for pure coal combustion. The results agreed very well with the experimental data and benchmarked this model for the further studies involving injecting Urea into the furnace. The simulations showed that injecting Urea from the secondary air system on the front wall can greatly reduce the NO_x levels inside the boiler.

In the second part of the work which analyzed the effect of micro-scale forces on the oat hull particles, it was found that the particle interactions occur primarily in the near field of the injector due to a high volume fraction of particles and they quickly decreases inside the furnace. Therefore it is reasonable to neglect particle interactions in the case of simulating the particle combustion in a large combustion facility like this stoker boiler. However simulating particle movement and combustion inside a smaller sized combustion facility clearly requires considering particles' interactions.

8.2 Future Work

In the near future, the comprehensive model can be applied to simulate the combustion of other kinds of biomass such as paper sludge, core and wood pellet. For the biomass of small sized particles, more physical test should be conducted to provide some figuring parameters for the sub-models describing the movement and devolatilizaiton of them. For the biomass with bigger size, which is blown into the boiler through front wall coal feeders in Unit 10, the present coal bed model should be adjusted according to the changes on heat and mass fluxes resulted from the co-fired combustion on the bed.

This comprehensive model can also be used to optimize the overall air system of Unit 10, including primary air system, second air system and fuel injection system, for the

combustion of different types of biomass. Because their different volatiles will have different reaction kinetics and happen at varied locations above the coal bed, therefore there exists an optimized injection system for each biomass.

The flexibility of CFD method in solving different grids can also allow simulating the effect of installing different types of burner for biomass, NO_x reduction by injecting Urea at different locations and co-firing flue gas in Unit 10. These are all important issue related to biomass combustion and are difficult to achieve through traditional experimental research.

Finally, to study biomass combustion in other types of boilers, a new coal bed model should be at first developed using a similar method introduced in chapter 5. Then the comprehensive model can be applied on more boilers.

REFERENCES

[1] A. Demirbas. Global Renewable Energy Projections. *Energy Sources, Part B: Economics, Planning, and Policy*, 4(2):212-224, 2009.

[2] D.O. Hall. Biomass energy in industrialised countries-a view of the future. *Forest Ecology and Management*, 91(1):17-45, 1997.

[3] A. Demirbas. Combustion characteristics of different biomass fuels, *Progress in Energy and Combustion Science*, 30(2):219-230, 2004.

[4] A. Demirbas. Recent advances in biomass conversion technologies. *Energy Educatonal Science Technology*, 6:19-41, 2000.

[5] B.M Jenkinsa, L.L. Baxterb, T.R. Miles Jr., and T.R. Miles. Combustion properties of biomass. *Fuel Processing Technology*, 54:17-46, 1998.

[6] P. McKendry. Energy production from biomass (part 1): overview of biomass. *Bioresource Technology*, 83(1):37-46, 2002

[7] A. Demirbas. Calculation of higher heating values of biomass fuels. *Fuel*, 76(5):431-434, 1997.

[8] M. Sami, K. Annamalai , and M. Wooldridge. Co-firing of coal and biomass fuel blends. *Progress of Energy Combustion Science*,27(2):171-214, 2001.

[9] H. Spliethoff and K.R.G. Hein. Effect of co-combustion of biomass on emissions in pulverized fuel furnaces. *Fuel Processing Technology*, 54(1-3):189-205, 1998.

[10] B. Olanders and B.M. Steenari. Characterization of ashes from wood and straw. *Biomass Bioenergy*, 8(2):105-115, 1995.

[11] M. Blander and A. D. Pelton. The inorganic chemistry of the combustion of wheat straw. *Biomass Bioenergy*, 12(4):295-298, 1997.

[12] I. Obernberger. Decentralized biomass combustion: state of the art and future development. *Biomass and Bioenergy*, 14(1):33-56, 1998.

[13] D. A. Tillman. Biomass cofiring: the technology, the experience, the combustion consequences. *Biomass and Bioenergy*, 19(6):365-384, 2000.

[14] J. H. Allica, A. J. Mitre, J. A. G. Bustamanteb, C. Itoizc, F. Blancoa, I. Alkortad, and C. Garbisu. Straw quality for its combustion in a straw-fired power plant. *Biomass and Bioenergy*, 21(4):249-258, 2001.

[15] A. Demirbas. Heavy metal contents of fly ashes from selected biomass samples. *Energy Sources*, 27(13):1269-1276, 2005.

[16] I. Obernberger, T. Brunner, and G. Bärnthaler. Chemical properties of solid biofuels—significance and impact. *Biomass and Bioenergy*, 30(1):973-982, 2006.

[17] A. A. Tortosa Masia′, B.J.P. Buhre, R.P. Gupta, and T.F. Wall. Characterising ash of biomass and waste. *Fuel Processing Technology*, 88(11-12):1071-1081, 2007.

[18] J. Werther, M. Saenger, E.-U. Hartge, T. Ogada, and Z. Siagi. Combustion of agricultural residues. *Progress in Energy Combustion Science*, 26(1):1-27, 2000.

[19] A. Williams, M. Pourkashanian, and J.M. Jones. Combustion of pulverised coal and biomass. *Progress in Energy Combustion Science*, 27(6):587-610, 2001.

[20] C. D. Blasi, F. Buonanno, and C. Branca. Reactivities of some biomass chars in air. *Carbon*, 37(8):1227-1238, 1999.

[21] A. A. Boateng, K. B. Hicks, and K. P. Vogel. Pyrolysis of switchgrass (Panicum virgatum) harvested at several stages of maturity. *Journal of Analytical and Applied Pyrolysis*, 75(2):55-64, 2006.

[22] C. Yang, X. Lu, W. Lin, X. Yang, and J. Yao. TG-FTIR Study on Corn Straw Pyrolysis-influence of Minerals. *Chemical Research in Chinese Universities*, 22(4):524-532, 2006.

[23] I. De Bari, D. Barisano, M. Cardinale, D. Matera, F. Nanna, and D. Viggiano. Air Gasification of Biomass in a Downdraft Fixed Bed: A Comparative Study of the Inorganic and Organic Products Distribution. *Energy and Fuels*, 14(4):889-898, 2000.

[24] M. Dogru, C. R. Howarth, G. Akay, B. Keskinler, and A. A. Malik. Gasification of hazelnut shells in a downdraft gasifier. *Energy*, 27(5):415-427, 2002.

[25] C. Dupont, J. M. Commandre, P. Gauthier, G. Boissonnet, S. Salvador, and D. Schweich. Biomass pyrolysis experiments in an analytical entrained flow reactor between 1073 K and 1273 K. *Fuel*, 87(7):1155-1164, 2007.

[26] T. Hosoya, H. Kawamoto, and S. Saka. Pyrolysis behaviors of wood and its constituent polymers at gasification temperature. *Journal of Analytical and Applied Pyrolysis*, 78(2):328-336, 2007.

[27] M. Sami, K. Annamalai, S. Dhanapalan, and M. Wooldridge. Numerical simulation of blend combustion of coal and feedlot waste in a swirl burner, In: ASME conference, Nashville, TN, November 1999.

[28] R. Scharler, I. Obernberger, G. Längle, and J. Heinzle. CFD analysis of air staging and flue gas recirculation in biomass grate furnace, In: proceeding of the 1st world conference on biomass for energy and industry, Sevilla, Spain, June, 2000.

[29] R. Scharler and I. Obernberger. Numerical modeling of biomass grate furnaces, In: proceedings of the 5th European conference on industrial furnaces and boilers, Porto, Portugal, April, 2000.

[30] R. Scharler, R., M. Forstner, M. Braun, T. Brunner, and I. Obernberger. Advanced CFD analysis of large fixed bed biomass boilers with special focus on the convective section, In: 2nd world conference and exhibition on biomass for energy, industry and climate protection, Rome, Italy, May, 2004.

[31] Y. B.Yang, H. Yamauchi, V. Nasserzadeh, and J. Swithenbank. Effects of fuel devolatilisation on the combustion of wood chips and incineration of simulated municipal solid wastes in a packed bed. *Fuel*, 82(18):2205-2221, 2003.

[32] Y. B. Yang, V.N. Sharifi, and J. Swithenbank. Effects of air flow rate and fuel moisture on the burning behaviors of biomass and simulated municipal solid wastes in packed beds, *Fuel*, 83(11-12):1153-1562, 2004.

[33] Y. B. Yang, C. Ryu, A. Khor, V. N. Sharifi, and J. Swithenbank. Fuel size effect on pinewood combustion in a packed bed, *Fuel*, 84(16):2026-2038, 2005.

[34] Y. B. Yang, C Ryu, A Khor, N.E. Yates, V. N. Sharifi, and J. Swithenbank. Effect of fuel properties on biomass combustion Part II.: Modeling approach--identification of the controlling factors. *Fuel*, 84(16):2116-2130, 2005.

[35] Y. B. Yang, J. Goodfellow, V. N. Sharifi, and J. Swithenbank. Investigation of biomass combustion systems using CFD techniques: a parametric study of packed-bed burning characteristics. *Progress in computational fluid dynamics*, 6(4-5):262-271, 2006.

[36] C. Ryu, A. N. Phan, Y. Yang, V. N. Sharifi. and J. Swithenbank. Ignition and burning rates of segregated waste combustion in packed beds, *Waste management*, 27(6):802-810, 2007.

[37] Y. B. Yang, R. Newman, V. N. Sharifi, J. Swithenbank, and J. Ariss. Mathematical modelling of straw combustion in a 38 MWe power plant furnace and effect of operating conditions. *Fuel*, 86(1-2):129-142, 2007.

[38] Y. B. Yang, V. N. Sharifi, J. Swithenbank, L. Ma, L. I. Darvell, J. M. Jones, M. Pourkashanian, and A. Williams. Combustion of a Single Particle of Biomass. *Energy and Fuels*, 22(1):306-316, 2008

[39] C. Yin, L. Rosendahl, S. K. Kær, and H. Sørensen. Modeling the motion of cylindrical particles in a nonuniform flow. *Chemical Engineering Science*, 58():3489-3498, 2003.

[40] C. Yin, L. Rosendahl, and T. J. Condra. Further study of the gas temperature deviation in large-scale tangentially coal-fired boiler. *Fuel*, 82(9)1127-1137, 2003.

[41] C. Yin, L. Rosendahl, S. K. Kaer, and T. J. Condra. Use of numerical modeling in design for co-firing biomass in wall-fired burners. *Chemical Engineering Science*, 59(16)3281-3292, 2004.

[42] L. A. Rosendahl, C. Yin, S. K. Kær, K. Friborg, and P. Overgaard. Physical characterization of biomass fuels prepared for suspension firing in utility boilers for CFD modeling. *Biomass and Bioenergy*, 31(5):318-325, 2007.

[43] C. Yin, L. Rosendahl, and S. K. Kær. Grate-firing of biomass for heat and power production. *Progress in Energy and Combustion Science*, 34(6):725-754, 2008.

[44] C. Yin, L. Rosendahl, S. K. Kær, S. Clausen, S. L. Hvid, and T. Hille. Mathematical Modeling and Experimental Study of Biomass Combustion in a Thermal 108 MW Grate-Fired Boiler. *Energy and Fuels*, 22(2):1380-1390, 2008.

[45] S. K. Kær. Numerical modeling of a straw-fired grate boiler. *Fuel*, 83(9):1183-1190, 2004.

[46] S. K. Kær. Straw combustion on slow-moving grates—a comparison of model predictions with experimental data. *Biomass and Bioenergy*, 28(3):307-320, 2005.

[47] S. K. Kær, L.A. Rosendahl, and L. L. Baxter. Towards a CFD-based mechanistic deposit formation model for straw-fired boilers. *Fuel*, 85(5-6):833-848, 2006.

[48] S. K. Kær. Modeling deposit formation in straw fired grate boilers. From website: http://www.mendeley.com/research/modeling-deposit-formation-in-strawfired-grate-boilers/

[49] S. K. Kær. The impact of deposits on heat transfer during biomass combustion. In: Proceedings of the First Biennial Meeting of the Scandinavian-Nordic Section of Combustion Institute, Gothenburg, Sweden, April, 2001.

[50] S. K. Kær, L. Rosendahl, and P. Overgaard. Numerical analysis of co-firing coal and straw in utility boiler at MIDTKRAFT Energy Company. In Proceedings of the fourth European computational fluid dynamics conference, Athens, Greece, September, 1997.

[51] J. M. Jones, M. Pourkashanian, A. Williams, and D. Hainsworth. A comprehensive biomass combustion model. *Renewable Energy*, 19(1-2):229-234, 2000.

[52] R. I. Backreedy, J.M. Jones, M. Pourkashanian, and A. Williams. Burn-out of pulverized coal biomass chars. *Fuel*,82(15-17):2097-2105, 2003.

[53] R. I. Backreedy, L. Fletcher, J. Jones, L. Ma, M. Pourkashanian, and A. Williams. Co-firing pulverised coal and biomass: a modeling approach. *Proceedings of the Combustion Institute*, 30(2):2955-2964, 2005.

[54] L. Ma, J Jones, M. Pourkashanian, and A. Williams. Modeling the combustion of pulverized biomass in an industrial combustion test furnace. *Fuel*, 86(12-13):1959-1965, 2007.

[55] R. P. Van der Lans, L.T. Pedersen, A. Jensen, P. Glarborg, and K. Dam-Johansen. Modeling and experiments of straw combustion in a grate furnace. *Biomass and Bioenergy*, 19(3):199-208, 2000.

[56] D. Shin and S. Choi. The combustion of simulated waste particles in a bed. *Combustion and Flame*, 121:167-180, 2000.

[57] D. Wei and W. Blasiak. CFD modeling of ecotube system in coal and waste grate combustion. *Energy Conversion and Management*, 42(15-17):1887-1896, 2001.

[58] H. Zhou, A.D. Jensen, P. Glarborg, P.A. Jensen, and A. Kavaliauskas. Numerical modeling of straw combustion in a fixed bed. *Fuel*, 84(4):389-403, 2005.

[59] K. Goerner and T. Klasen. Modeling, simulation and validation of the solid biomass combustion in different plants. *Progress in computational fluid dynamics*, 6(4-5):225-234, 2006.

[60] T. Klasen and X. S. Bai. Combustion process in a biomass grate fired industry furnace: a CFD study. *Progress in computational fluid dynamics*, 6(4-5):278-286, 2006.

[61] Z. Yu, X. Ma, and Y. Liao.Mathematical modeling of combustion in a grate-fired boiler burning straw and effect of operating conditions under air- and oxygen-enriched atmospheres. *Renewable Energy*, 35(5):895-903, 2010.

[62] H. A. J. A. Van Kuijk, R. J. M. Bastiaans, J. A. Van Oijen, and L. P. H. De Goey. Grate furnace combustion: A submodel for the solid fuel layer. *International Journal for multiscale computational engineering*, 6(1):103-111, 2008.

[63] D. Gera, M. P. Mathur, M. C. Freeman, and Allen Robinson. Effect of large aspect ratio of biomass particles on carbon burnout in a utility boiler. *Energy and Fuels*, 16(6):1523-1532, 2002.

[64] T. F. Dixon, A.P. Mann, F. Plaza, and W.N. Gilfillan. Development of advanced technology for biomass combustion—CFD as an essential tool. *Fuel*, 84(10):1303-1311, 2005.

[65] H. Thunman and B Leckner. Influence of size and density of fuel on combustion in a packed bed. *Proceedings of the Combustion Institute*, 30(2):2939-2946, 2005.

[66] P. Venturini, D. Borello, C. Iossa, D. Lentini, and F. Rispoli. Modeling of multiphase combustion and deposit formation in a biomass fed furnace. *Energy*, 35(7):3008-3021, 2010.

[67] D. Mirka, N. P. Franka, T. J. Heindel, and F. Battaglia. CFD modeling and X-Ray imaging of biomass in a fluidized bed, *Journal of Fluid Engineering*, 131(11):111303-1-11, 2009.

[68] J. C. Wurzebverger, S. Wallner, H. Raupenstrauch, and J. G. Khinast. Thermal conversion of biomass: comprehensive reactor and particle modeling. *AIChE Journal*, 48(10):2398-2411, 2004.

[69] X. H. Liang and J.A. Kozinski. Numerical modeling of combustion and pyrolysis of cellulosic biomass in thermogravimetric systems. *Fuel*, 79(2):1477-1486, 2000.

[70] P. Grammelis and E. Kakaras. Biomass Combustion Modeling in Fluidized Beds. *Energy and Fuels*, 19(1):292-297, 2005.

[71] D. F. Fletcher, B. S. Haynes, F. C. Christo, and S. D. Joseph. A CFD based combustion model of an entrained flow biomass gasifier. *Applied Mathematical Modeling*, 24(3):165-182, 2000.

[72] F. Scala and P. Salatino. Modeling fluidized bed combustion of high-volatile solid fuels. *Chemical Engineering Science*, 57(7):1175-1196, 2002.

[73] F. Marias and B. Bruyères. Modeling of a biomass fired furnace for production of lime. *Chemical Engineering Science*, 64(15):3417-3426, 2009.

[74] J. Andersen, P. A. Jensen, K. E. Meyer, S. L. Hvid, and P. Glarborg. Experimental and numerical investigation of gas-phase freeboard combustion, part 2: main combustion process. *Energy and Fuels*, 23(12):5773-5782, 2009.

[75] K. C. Lo, K. Wu, C. Chyang, and K. Su. Modeling the woody biomass combustion in a vortexing fluidized-bed combustor. *Energy and Fuels*, 24(2):1316-1322, 2010.

[76] J. Pallarés, I. Arauzo, and A. Williams. Integration of CFD codes and advanced combustion models for quantitative burnout determination. *Fuel*, 86(15):2283-2290, 2007.

[77] J. Pallarés, A. Gil, C. Cortés, and C. Herce. Numerical study of co-firing coal and Cynara cardunculus in a 350 MWe utility boiler. *Fuel Processing Technology*, 90(10):1207-1213, 2009.

[78] C. Ghenai and I. Janajreh. CFD analysis of the effects of co-firing biomass with coal. *Energy conversion and management*, 51:1694-1701, 2010.

[79] C. S. B. Dixit, P. J. Paul, and H. S. Mukunda. Part 2: Computational studies on a pulverized fuel stove. *Biomass and Bioenergy*, 30(7):684-691, 2006.

[80] P.G. Saffman. The lift on a small sphere in a slow shear flow. *Journal of Fluid Mechanics*, 22(2):385-400, 1965.

[81] J. S. Marshall. Discrete-element modeling of particulate aerosol flows, *Journal of Computational Physics*, 228(5):154-1561, 2009.

[82] H. Hertz, Über die Berührung fester elastische Körper. *Journal of Reine und Angewandte Mathematik*, 92:156-171, 1881.

[83] P. A. Cundall and O. D. L. Strack. A discrete numerical model for granular assembles. *Géotechnique*, 29 (1):47-65, 1979.

[84] R. D. Mindlin. Compliance of elastic bodies in contact, *Journal of Applied Mechanics*, 16:259-268, 1949.

[85] Y. Tsuji, T. Tanaka, and T. Ishida. Lagrangian numerical simulation of plug flow of cohesionless particles in a horizontal pipe. *Powder Technology*, 71(3):239-250, 1992.

[86] C. Thornton. Interparticle sliding in the presence of adhesion. *Journal of Physics D: Applied Physics*, 24:1941-1946, 1991.

[87] The University of Iowa Biomass Fuel Project Supporting Materials, The University of Iowa, Iowa City, 2008

[88] A. G. Barneto, J. A. Carmona, A. Galvez, and J. A. Conesa. Effects of the composting and the heating rate on biomass gasification. *Energy and Fuels*, 23 (1):951-957, 2009.

[89] X. Zhang, Q. Chen, R. Bradford, V. Sharifi, and J. Swithenbank. Experimental investigation and mathematical modeling of wood combustion in a moving grate boiler. *Fuel Processing Technology*, 91(11):1491-1499, 2010.

[90] Y. G. Lai. U^2RANS-2.6 User's Manual, IIHR-Hydroscience and Engineering College of Engineering. The University of Iowa, Iowa City, 2001.